University of St Andrews

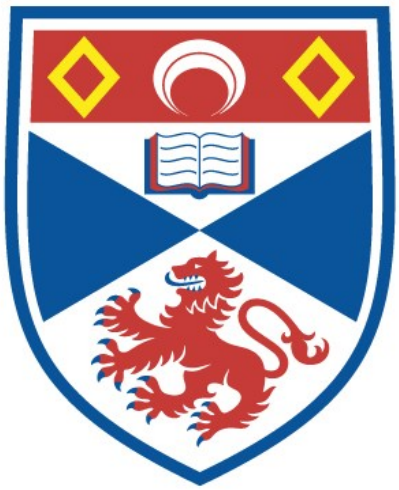

Full metadata for this thesis is available in
St Andrews Research Repository
at:
http://research-repository.st-andrews.ac.uk/

This thesis is protected by original copyright

ABSORPTION OF WHISTLER WAVES IN REVERSED FIELD PINCHES

by

Morag J. McMinn

ABSTRACT

In this thesis there is a discussion of some of the wave modes which can occur in cold plasmas, first in the absence of magnetic fields, and then in their presence. This is followed by short discussions of Landau damping and the origin of Alfven waves.

The next chapter discusses the general principle of toroidal confinement devices, and then looks in more detail at relaxation theory as it applies to RFPs. The last section gives brief theoretical and experimental details of current drive in tokamaks using Alfven and ion cyclotron waves and heating using lower hybrid and electron cyclotron waves.

In the conditions obtaining in a reversed field pinch only whistler waves, which have high momentum parallel to the magnetic field will propagate. An investigation was carried out to see if whistlers could be used to drive a poloidal current near the field reversal point and so sustain the toroidal reversal. A numerical experiment was carried out, in slab geometry, for waves with discrete values of the wave number in a plane perpendicular to the direction of propagation. The results suggest that the position where the bulk of the wave energy is deposited can be controlled by altering the magnitude of the wave number, and changing the angle that it makes with a fixed direction and by altering the frequency of the waves.

The final chapter suggests how the work could be made more accurate by either making changes to the model, or by solving Maxwell's equations as a set of coupled ODEs.

I, Morag J. McMinn, hereby certify that this thesis has been composed by myself, that it is a record of my own work, and that it has not been accepted in partial or complete fulfilment of any other degree or professional qualification.

Signed

Date 28th July 1988

In submitting this thesis to the University of St Andrews I understand that I am giving permission for it to be made available for use in accordance with the regulations of the University Library for the time being in force, subject to any copyright vested in the work not being affected thereby. I also understand that the title and abstract will be published, and that a copy of the work may be made and supplied to any bona fide library or research worker.

ACKNOWLEDGEMENTS

First of all I would like to thank my supervisor at St Andrews, Dr Alan Cairns, for his help; and the other members of the plasma physics group, past and present. Thanks are also due to my supervisor at Culham Laboratory, Dr Chris Lashmore-Davis, especially for the paper which he wrote, which is the basis of the work in chapter 4.

I would also like to express my thanks to a group of people who are often neglected in thesis acknowledgements - the people who listened when I was complaining about my work, and in paticular the members of the Cannongate house group.

I am also grateful to SERC and Culham Laboratory for financial support.

CONTENTS

CHAPTER 1 INTRODUCTION

A plasma is a gas which has been heated to such a high temperature that its molecules begin to ionise so that the gas is made up of a mixture of ions and electrons but remains electrically neutral overall. If the temperature is not too high the plasma will also contain neutral particles.

Much of the early work on plasmas was motivated by the need to understand the behaviour of radio signals, which are affected by the presence of ionised layers in the upper atmosphere. The basis of much of this work is the Appleton-Hartree dispersion relation, which is one form of the solution of the cold plasma dispersion relation.

The word plasma as a name for an ionised gas was introduced by Langmuir, who thought that the behaviour of gaseous plasmas was similar to that of blood plasma. Although he was mistaken the name has stuck.

Nowadays, the main motivation for much plasma physics research is to produce plentiful supplies of energy from the fusion of light elements. This requires temperatures of the order of 10^7 K, similar to that at the centre of the sun.

At temperatures of this magnitude it is not possible to confine plasmas using ordinary materials. The most successful method to date uses the fact that charged particles in magnetic fields gyrate about the field lines, so if the field lines are bent into a closed shape the particles can be trapped. However, in the presence of electric and magnetic fields the behaviour of the plasma becomes much more complicated, and some aspects of its behaviour are still

not fully understood.

The basis of fusion research is the well known Lawson criterion, which gives an estimate of the conditions necessary for a self sustaining fusion reaction to occur. This states that the plasma density multiplied by the time the energy is confined in the plasma must reach a certain value. One way to achieve this is to use comparatively low densities with long confinement times. This approach is the one described above which uses magnetic fields to confine the plasma for a long time.

The second method uses high densities which are achieved by illuminating a small pellet containing deuterium-tritium fuel with very intense laser light. This produces very dense plasmas and the confinement is supplied by the inertia of the plasma as it begins to fly apart.

Fusion research really took off with the success of the ZETA reversed field pinch at Harwell in the 1950s. (One of the reasons why work on ZETA was not continued was that several kinds of instability were found.)

In the 1960s there was great excitement when high temperatures were produced on Russian tokamaks. (The word tokamak is a Russian acronym for *toroidalnaya kamara i magnitnaya katushka* which means toroidal chamber and magnetic coil.) As a result of the success of these devices most of the world effort in fusion research has been concentrated on tokamaks.

Large strides have been made in raising the temperature and density of confined plasmas towards the levels required for fusion using tokamaks. This has required the development of new techniques to heat plasmas using the interactions of different forms of electromagnetic radiation with the plasma and

the injection of energetic beams of neutral particles.

Despite the success of tokamak experiments several other confinement devices are under investigation, such as the reversed field pinch, spheromak and stellarator. This is partly to provide knowledge of the behaviour of plasmas under different conditions and partly to provide alternatives if the tokamak approach to fusion should prove to be impracticable.

Chapter 2 mentions two models which are used to describe the behaviour of plasmas. The first model looks at the behaviour of a single particle in the plasma and how this information can be combined with Maxwell's equations to derive the dielectric tensor which describes the behaviour of the whole plasma in the cold plasma approximation. This means that the effects of temperature and pressure are neglected. This approximation is useful because when the behaviour of the dielectric tensor is investigated it shows what the basic wave motions in the plasma are, so the chapter goes on to investigate some of these modes and to find out under what conditions the wave can propagate. This leads on to a discussion of the CMA diagram, which is a useful way to classify the multitude of wave modes.

The consideration of the plasma temperature introduces new modes, but the basic wave modes are still those found in the cold plasma case. The main effect of temperature is to damp the wave modes, by a mechanism known as Landau damping. This is discussed in the next section of chapter 2.

The final section has a very brief introduction to magnetohydrodynamics (MHD). In this theory a plasma is treated as a fluid, but one which is electrically conducting, and so couples Maxwell's equations with the equations of fluid

dynamics. This introduces the Alfven wave modes of the plasma.

Chapter 3 discusses in more detail the way in which plasmas are confined in toroidal systems. The two systems discussed are the tokamak and the reversed field pinch.

After this general introduction the second section gives an introduction to Taylor's theory of the reversed field pinch, which assumes that the plasma relaxes to a near minimum energy state subject to the constraint that the total helicity remains constant. The theory is shown to agree with experimental results. Although it is not a complete explanation for the behaviour of the RFP it does provide a general mechanism to explain the results.

The last section describes the principles of current drive, and how some of the waves described in chapter 2 have been used for this purpose. Heating and current drive using radio waves have been demonstrated on several tokamaks.

Chapter 4 considers how current drive could be applied to RFPs. In the present experiments the toroidal reversal decays after a while, but if a poloidal current could be driven this would continue the toroidal reversal necessary for plasma confinement.

After the introduction the second section of the chapter considers the solution of the cold plasma dispersion relation in a cold plasma for the component of the refractive index which changes going into the plasma, the x-direction.

The first subsection describes the approximations made to find this refractive index component included using slab geometry, but with the

magnetic fields assumed to be Bessel functions. The plasma density was assumed to have a parabolic profile, in the x-direction, with maximum density at the centre of the plasma. It was also assumed that the component of the wave vector in the plane of the magnetic field was constant, but that its angle to the magnetic field could be varied.

The next subsection discusses the variation of the refractive index in the x-direction with various parameters, while the next subsection attempts to make simplifications to the expression for the x-component of the refractive index which would explain these results.

The fourth subsection discusses in more detail the positions where the square of the refractive index either passes through zero, or where the two branches of the square of the refractive index meet, which are important in determining where energy is absorbed in the plasma.

The third major section looks at where energy is deposited in the plasma. The first subsection examines the behaviour at the edge region of the plasma, where the waves are evanescent. The wave's behaviour here can be described by Airy's equation.

The second subsection reintroduces the warm plasma corrections to the cold plasma theory to determine the amount of absorption and the third subsection describes where the energy is deposited in the plasma. It also shows that the position of maximum absorption can be changed by changing the parameters the wave is launched with.

The fifth chapter then considers ways in which this work could be continued. One way would be to try and make the model more accurate so that

the effects of variations in the magnetic field could be considered more carefully. This would mean using cylindrical geometry instead of the the slab geometry used so far, and introducing more realistic density and especially temperature profiles. Another refinement is to look at methods of producing the waves which would be fired into the plasma. This would also mean considering a spectrum of waves, rather than the single value assumed in chapter 4. This is discussed in section 5.1.

A totally different approach is to reduce Maxwell's equations to a set of coupled ordinary differential equations and then solve them in the vacuum outside the plasma and in the plasma itself.

The appendix gives the program used to produce the results and a brief explanation of some of the major modules in the program.

CHAPTER 2 WAVES IN PLASMAS AND PLASMA HEATING

2.1 INTRODUCTION

One of the main requirements to understand the behaviour of a plasma is to know how electromagnetic waves interact with the plasma. The properties of these interactions can be used to devise schemes to transfer energy from the wave to the plasma to drive a current or to heat the plasma.

This chapter will consider some aspects of wave-plasma interactions and how these properties have been applied in various heating schemes.

2.2 WAVES IN COLD PLASMAS

Consider a fully ionised plasma, made up of electrons and singly charged ions. The electrons and ions will be identified by the subscripts e and i. The subscript s will be used to imply a sum over the electrons and ions. However, the rest of this section will deal with the properties of a single type of particle, but can be easily applied to the other kinds of particles and to behaviour of both kinds together.

The equation of motion for an electron in an electric field $\underline{\mathbf{E}}$ and a magnetic field $\mathbf{B}$ is

$$m\frac{\partial \mathbf{v}}{\partial t} = -e(\mathbf{E} + \mathbf{v} \times \mathbf{B}) \qquad (2.1)$$

If the time dependence of the variables is given by $\exp(-i\omega t)$ the previous

equation becomes

$$i\omega m\mathbf{v} = e(\mathbf{E} + \mathbf{v} \times \mathbf{B}) \qquad (2.2)$$

Writing equation (2) in Cartesian coordinates with the magnetic field in the z direction gives

$$\begin{aligned} i\omega m v_x &= eE_x + ev_yB \\ i\omega m v_y &= eE_y - ev_xB \\ i\omega m v_z &= eE_z \end{aligned} \qquad (2.3)$$

The electron cyclotron frequency, Ω, is given by $\Omega = eB / m$, and the ratio of the electron cyclotron frequency to the applied frequency is denoted by Y. Making this substitution and solving (3) for **v** gives

$$\begin{aligned} v_x &= \frac{e(E_x - iYE_y)}{i\omega m(1 - Y^2)} \\ v_y &= \frac{e(E_y + iYE_x)}{i\omega m(1 - Y^2)} \\ v_z &= \frac{eE_z}{i\omega m} \end{aligned} \qquad (2.4)$$

Now, the current density, **J**, is related to the velocity of the electrons by $\mathbf{J} = -ne\mathbf{v}$. But, since **v** is known in terms of **E** we can relate **J** to **E** via the conductivity tensor $\underline{\sigma}$ and $\mathbf{J} = \underline{\sigma}.\mathbf{E}$.

$$\underline{\sigma} = -\frac{ne^2}{i\omega m\,(1 - Y^2)} \begin{bmatrix} 1 & -iY & 0 \\ iY & 1 & 0 \\ 0 & 0 & 1 - Y^2 \end{bmatrix} \qquad (2.5)$$

Now consider Maxwell's equation relating the curl of **B** to the time derivative of **E**; making the substitution $\partial / \partial t = -i\omega t$ gives

$$\nabla \times \mathbf{B} = \mu_0 \mathbf{J} - \frac{i\omega E}{c^2} \qquad (2.6)$$

Substituting $1 / \varepsilon_0 c^2$ for μ_0 and $-ne\,\underline{\sigma}.\mathbf{E}$ for **J** gives

$$\nabla \times \mathbf{B} = -\frac{i\omega\,\underline{\varepsilon}\,.\,\mathbf{E}}{c^2} \qquad (2.7)$$

$\underline{\varepsilon}$ is the cold plasma dielectric tensor, for electrons only, but the ion terms can easily be added.

$$\underline{\varepsilon} = \begin{bmatrix} \varepsilon_\perp & i\varepsilon_{xy} & 0 \\ -i\varepsilon_{xy} & \varepsilon_\perp & 0 \\ 0 & 0 & \varepsilon_{\parallel} \end{bmatrix} \qquad (2.8)$$

with $\varepsilon_\perp = 1 - X / (1 - Y^2)$; $\varepsilon_{xy} = XY / (1 - Y^2)$; $\varepsilon_{\parallel} = 1 - X$. X is given by $ne^2 / \varepsilon_0 m \omega^2 = \omega_p^{\,2} / \omega^2$ and is proportional to the density of the plasma.

To find a solution to equation (7), use the equation $\nabla \times \mathbf{E} = -\partial \mathbf{B} / \partial t$ to find **B** in terms of **E** and then solve the equation by assuming spatial dependence of the form exp(i **k.r**), ie replace ∇ by (ik_x, ik_y, ik_z). Then instead of solving in terms of the propagation vector **k** solve the equation in terms of the refractive index vector **n**. So, (7) becomes

$$\underline{\varepsilon}.\mathbf{E} + \mathbf{n} \times (\mathbf{n} \times \mathbf{E}) = \mathbf{0} \qquad (2.9)$$

To proceed assume that the x-direction is given by the component of **n** perpendicular to **B**, and that the angle between **B** and **n** is given by θ. This means that $\mathbf{n} = (n \sin\theta,\ 0,\ n \cos\theta)$. Writing this out in Cartesian coordinates implies that there is only a solution when

$$\begin{bmatrix} \varepsilon_\perp - n^2 \cos^2\theta & i\varepsilon_{xy} & n^2 \sin\theta \cos\theta \\ -i\varepsilon_{xy} & \varepsilon_\perp - n^2 & 0 \\ n^2 \sin\theta \cos\theta & 0 & \varepsilon_{\parallel} - n^2 \sin^2\theta \end{bmatrix} \begin{bmatrix} E_x \\ E_y \\ E_z \end{bmatrix} = 0 \qquad (2.10)$$

2.2.1 **B = 0**

To see some of the waves which are possible in a plasma it is simplest to look at the case where there is no magnetic field. This means that there is no preferred direction in the plasma, so letting waves propagate in the z-direction does not result in any loss of generality.

With **B** = 0 and the waves propagating in the z-direction the dielectric

tensor components become

$$\varepsilon_{\perp} = \varepsilon_{\parallel} = \varepsilon = 1 - \omega_p^2 / \omega^2 \qquad \varepsilon_{xy} = 0 \qquad (2.11)$$

and equation (10) becomes

$$\begin{bmatrix} \varepsilon - n^2 & 0 & 0 \\ 0 & \varepsilon - n^2 & 0 \\ 0 & 0 & \varepsilon \end{bmatrix} \begin{bmatrix} E_x \\ E_y \\ E_z \end{bmatrix} = 0 \qquad (2.12)$$

There are two distinct solutions to this equation. In the first $E_z \neq 0$, which implies that

$$\varepsilon = 1 - \frac{\omega_p^2}{\omega^2} = 0 \quad \Rightarrow \quad \omega^2 = \omega_p^2 \qquad (2.13)$$

Looking again at equation (12), since $E_z \neq 0$ (and $E_x = E_y = 0$), **k** is parallel to **E** giving a longitudinal wave. However $\omega \neq \omega(\mathbf{k})$ so the group velocity is zero, and hence the wave does not travel through the plasma, but any disturbance remains localised. This type of oscillation occurs when some electrons are displaced and then oscillate about their equilibrium position at the electron plasma frequency.

The second type of solution has E_x or $E_y \neq 0$. This gives two mutually perpendicular solutions which have the same characteristics, given by the dispersion relation

$$\varepsilon - n^2 = 0 \quad \Rightarrow \quad \omega^2 = \omega_p{}^2 + (kc)^2 \qquad (2.14)$$

This is similar to the dispersion relation for an electromagnetic wave in vacuum, but it is modified by the factor $\omega_p{}^2$ which is caused by the plasma. Equation (14) implies that this wave cannot propagate unless $\omega \geq \omega_p$. As a consequence of this it can also be seen that the wave will only propagate in the plasma if the plasma density is below a critical value. When the density exceeds this value the wave is reflected and the plasma is said to be overdense.

2.2.2 $\mathbf{B} \neq 0$

The addition of a magnetic field introduces a preferred direction to the plasma. Going back to the previous coordinate system shows that equation (10) is the correct one to describe wave propagation. (10) only has a solution if the determinant of the matrix is zero, ie if

$$A\, n^4 - B\, n^2 + C = 0 \qquad (2.15)$$

with

$$A = \varepsilon_{\parallel} \cos^2\theta + \varepsilon_{\perp} \sin^2\theta$$

$$B = \varepsilon_{\parallel}\, \varepsilon_{\perp} (1 + \cos^2\theta) + RL \sin^2\theta \qquad (2.16)$$

$$C = \varepsilon_{\parallel} RL$$

where R and L stand for right and left circular polarisation and are also introduced to simplify some later expressions. They are given by

$$R = 1 - \frac{\omega_p^2}{\omega^2}\frac{\omega}{\omega + \Omega} \qquad L = 1 - \frac{\omega_p^2}{\omega^2}\frac{\omega}{\omega - \Omega} \tag{2.17}$$

$$\text{and} \quad \varepsilon_\perp = \frac{R + L}{2} \qquad \varepsilon_\parallel = \frac{R - L}{2} \tag{2.18}$$

Making these substitutions shows that the solution of (15) is

$$n^2 = \frac{B \pm ((\varepsilon_\parallel \varepsilon_\perp - RL)^2 \sin^4\theta + 4\varepsilon_\parallel^2 \varepsilon_{xy}^2 \cos^2\theta)^{1/2}}{2A} \tag{2.19}$$

When $n^2 = 0$ the wave is said to have a cutoff. Going back to equation (16) this is true when $\varepsilon_\parallel = 0$, $R = 0$ or $L = 0$.

Resonances

A resonance occurs when $n^2 \to \infty$, which is true when $A = 0$. From (16) this is true when

$$\tan^2\theta = \frac{\varepsilon_\parallel}{\varepsilon_\perp} \tag{2.20}$$

At $\theta = 0$ this implies that $\varepsilon_\perp \to \infty$, or alternatively that $R + L \to \infty$. R

tends to infinity when $\omega = \Omega_i$, so there is a resonance at the ion cyclotron frequency. Similarly $L \rightarrow \infty$ at the electron cyclotron frequency.

<u>At $\theta = \pi/2$</u> resonance occurs for $\varepsilon_\perp = 0$, or explicitly when

$$1 - \frac{\omega_{pe}^2}{\omega^2 - \Omega_e^2} - \frac{\omega_{pi}^2}{\omega^2 - \Omega_i^2} = 0 \qquad (2.21)$$

Equating the first two terms to zero and substituting into the third term shows that this is very small, so

$$\omega^2 = \omega_{pe}^2 + \Omega_e^2 \qquad (2.22)$$

is a good approximation to one of the roots.

Rewriting (21) to give an explicit equation for ω^4 gives

$$\omega_{pe}^2 \Omega_i^2 + \omega_{pi}^2 \Omega_e^2 + \Omega_e^2 \Omega_i^2 \approx \Omega_e^2 \Omega_i^2 + \omega_{pi}^2 \Omega_e^2 \qquad (2.23)$$

as the constant in the equation, which is the product of the roots. Using this gives the second root of equation (21) as (approximately)

$$\omega^2 = \frac{\Omega_e^2 \Omega_i^2 + \omega_{pi}^2 \Omega_e^2}{\omega_{pe}^2 + \Omega_e^2} \qquad (2.24)$$

The first root is greater than the electron cyclotron and electron plasma frequencies and is called the upper hybrid frequency. The second root lies

between the ion and electron cyclotron frequencies and is called the lower hybrid frequency.

If instead of looking for infinities of the refractive index we look for the zeros, using the determinant of equation (10), the condition for n^2 to equal 0 is

$$\varepsilon_{\parallel} (\varepsilon_{\perp}^2 - 1) = 0 \qquad (2.25)$$

Solving this equation for ω gives two approximate solutions

$$\omega_1 \approx -\frac{\Omega_e}{2} + \left[\frac{\Omega_e^2}{4} + \omega_p^2 \right]^{1/2} \qquad (2.26)$$

$$\omega_2 \approx -\frac{\Omega_e}{2} + \left[\frac{\Omega_e^4}{4} + \omega_p^2 \right]^{1/2} \qquad (2.27)$$

Plotting the dispersion curve in this case gives a mode with two branches - the extraordinary or X mode, see figure 2.1.

Going back to equation (10) there is also a solution when $E_z \neq 0$, ie when $\varepsilon_{\parallel} - n^2 = 0$ which gives the dispersion relation $\omega^2 = \omega_p^2 + k^2c^2$. Since this wave propagates in the x-direction and has its electric vector in the z-direction it is a transverse wave. The particle motions caused by the electric field are also in the z-direction, so the particles gyrate about the magnetic field, but are otherwise unaffected by it. This is called the ordinary or O mode.

Cutoffs and resonances

At a cutoff the refractive index of the plasma equals zero. The behaviour of the wave depends on whether it approaches the cutoff from the evanescent side or from the side with $n > 0$.

If the wave approaches from the evanescent side it passes through the cutoff into the region where it can propagate. If the wave approaches the cutoff from the propagating side it is reflected from the cutoff. The exception is if there is a very thin evanescent layer followed by another propagating region. In this case some of the wave energy can tunnel through to the second propagating region.

At a resonance the refractive index goes to infinity and the phase velocity falls to zero. Resonances can be found by examining the cold plasma dispersion relation and occur at the ion and electron cyclotron frequencies and their harmonics and at the various hybrid frequencies.

Whether a wave is absorbed or reflected at a refractive index infinity depends on the strength of the damping mechanism in the surrounding region. The weaker the damping mechanism the thinner the absorbing layer becomes. However, if the damping mechanism becomes too weak the wave becomes evanescent at the refractive index maximum and is reflected.

Evanescence arises because the finite temperature of the plasma means that there is a minimum wavelength which in turn means that the refractive index cannot go to infinity. Damping can only occur when the refractive index is bounded if there is a large imaginary refractive index component.

The results of the previous sections can be summarised in the Clemmow-Mullaly-Allis (CMA) diagram. For a plasma composed of electrons and one ion species the diagram maps a two dimensional parameter space. The axes of the graphs in figure 2.2 are plotted in units of $\beta^2 = | \Omega_e \Omega_i | / \omega^2$ and $\alpha^2 = (\omega_{pe}^2 + \omega_{pi}^2) / \omega^2$. **B** increases with increasing β^2, or for fixed **B** the frequency decreases. α^2 is a measure of increasing density, or for fixed density the frequency decreases as α^2 increases.

The CMA diagram can also include information about the wave-normal surfaces of waves in the plasma. The wave-normal surface is a plot of the phase velocity of a wave against θ, so the shape of the surface is determined by the anisotropy of the plasma. The surface sketched out is given by the tip of a vector in the same direction as the propagation vector, but whose magnitude is given by the phase velocity of the wave.

The topological properties of the wave-normal surfaces remain constant within each bounded region of parameter space in the CMA diagram. This provides a good way to label the various wave modes.

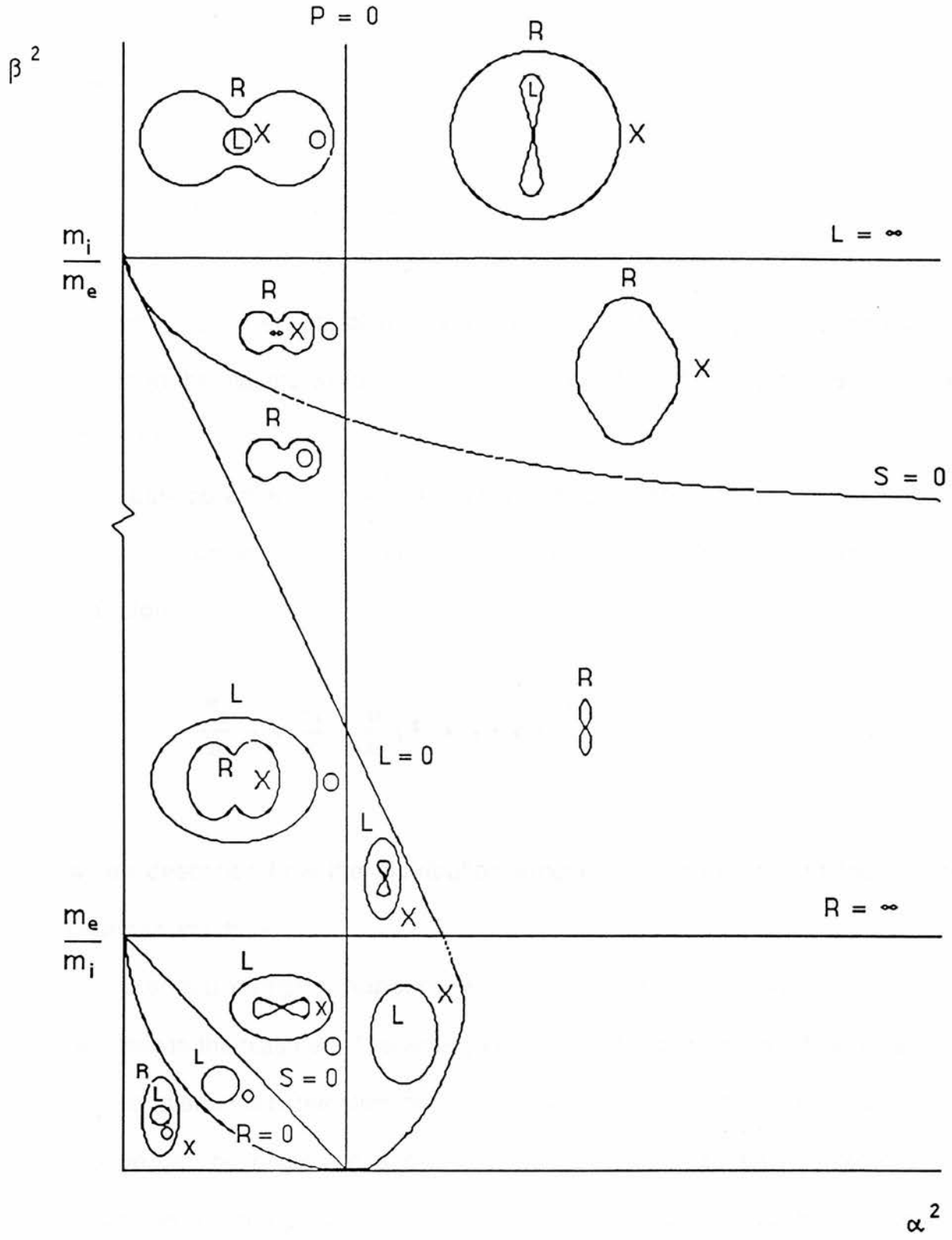

Fig 2.1 CMA diagram for a cold plasma, with one ion species, showing the wave-normal surfaces.

perturbations in the electric and magnetic fields in the plasma.

(i) No Magnetic Field

Initially consider the case where there is no magnetic field and assume that the electric field is zero in the unperturbed case, so that when **E** appears it is a first order quantity. Making these substitutions in (28) and linearising gives

$$\frac{\partial f_1}{\partial t} + \mathbf{v} \cdot \frac{\partial f_1}{\partial \mathbf{r}} - \frac{e}{m} \mathbf{E} \cdot \frac{\partial f_0}{\partial \mathbf{v}} = 0 \qquad (2.29)$$

Then use the fact that the charge density in the plasma is given by the first moment of the distribution function to get an expression for the electric field in the plasma from Poisson's equation, using the perturbation of the electron distribution function.

$$\nabla^2 \phi = -\frac{\rho}{\varepsilon_0} = \frac{e}{\varepsilon_0} \int f_1(\mathbf{v})\, d^3v \qquad (2.30)$$

Again assume that quantities vary as $\exp i(\underline{k}.\underline{r} - \omega t)$, so that with $\mathbf{E} = -\nabla\phi$ equations (29) and (30) become

$$-i\omega f_1 + i\mathbf{k}.\mathbf{v} f_1 + \frac{e}{m} i\phi \mathbf{k}.\frac{\partial f_0}{\partial \mathbf{v}} = 0 \qquad (2.31)$$

$$k^2 \phi = -\frac{e}{\varepsilon_0} \int f_1\, d^3v \qquad (2.32)$$

Using (31) to substitute for f_1 in (32) and cancelling the potential, ϕ, on both sides gives

$$1 + \frac{e^2}{\varepsilon_0 m k^2} \int \frac{\mathbf{k} \cdot \partial f_0/\partial v}{\omega - \mathbf{k}.\mathbf{v}} d^3v = 0 \qquad (2.33)$$

The singularity at $\omega = \underline{k}.\underline{v}$ means that the integral in equation (33) is undefined and so it is not possible to proceed with this method. Instead go back to the original differential equation and treat it as an initial value problem, where the value of f_1 is given at time $t = 0$, but its behaviour is not assumed to vary as $\exp(-i\,\omega t)$ but has to be found. This means that equation (28) has to be Laplace transformed in time. However, it is still assumed that the spatial variation is harmonic, so f_1 can be Fourier transformed and rewritten as

$$f_1(\mathbf{r},\mathbf{v},t) = f_1(\mathbf{v},t) \exp i\mathbf{k}.\mathbf{r} \qquad (2.34)$$

Also, it is only the component of velocity parallel to the propagation vector which contributes to Landau damping. Call this velocity $u = \mathbf{k}.\mathbf{v}/k$. Let $F_0(u)$ and $F_1(u,t)$ be the integrals of $f_0(\mathbf{v})$ and $f_1(\mathbf{v},t)$ over the two velocity components perpendicular to $\mathbf{k}$. Then, integrating (31) and (32) wrt the perpendicular components of velocity and using $\mathbf{E} = -\nabla\phi$ in (32) gives

$$\frac{\partial F_1}{\partial t} + ikuF_1 - \frac{e}{m} E \frac{\partial F_0}{\partial u} = 0 \qquad (2.35)$$

$$ikE = \frac{e}{\varepsilon_0} \int_{-\infty}^{\infty} F_1(u)\, du \qquad (2.36)$$

To solve (35) and (36) as an initial value problem use the Laplace transform method. The Laplace transform of a function is defined by

$$F_1(u,p) = \int_0^{\infty} F_1(u,t)\, e^{-pt}\, dt \qquad (2.37)$$

and the inverse Laplace transform is defined by

$$F_1(u,t) = \frac{1}{2\pi i} \int_c F_1(u,p)\, e^{pt}\, dp \qquad (2.38)$$

The contour C will be described later. The Laplace transform of the derivative of a function is given by

$$\frac{dF_1(u,t)}{dt} = \int_0^{\infty} \frac{dF_1(u,t)}{dt}\, e^{-pt}\, dt = pF_1(u,t) - F_0(u,0) \qquad (2.39)$$

Applying (37) and (38) to (35) and (36) gives

$$pF_1 + ikuF_1 = -\frac{e}{m} E \frac{\partial F_0}{\partial u} + F_1(t=0) \qquad (2.40)$$

$$ikE = -\frac{e}{m} \int_{-\infty}^{\infty} F_1(u)\, du \qquad (2.41)$$

Substituing for F_1 from (40) into (41) gives

$$ikE = -\frac{e}{\varepsilon_0} \int_{-\infty}^{\infty} \left\{ \frac{-\frac{e}{m} E \frac{\partial F_0}{\partial u}}{p + iku} + \frac{F_1(u, t=0)}{p + iku} \right\} du \qquad (2.42)$$

and solving for E gives

$$E = \frac{ie}{\varepsilon_0 k \varepsilon(k,p)} \int_{-\infty}^{\infty} \frac{F_1(t=0)}{p + iku}\, du \qquad (2.43)$$

$\varepsilon(k,p)$ is the plasma dielectric constant and is given by

$$\varepsilon(k,p) = 1 + \frac{e^2}{\varepsilon_0 m k} \int_{-\infty}^{\infty} \frac{\partial F_0 / \partial u}{ip - ku}\, du \qquad (2.44)$$

Comparing (44) and the previous expression (33) shows that if p is

replaced by -iω the two formulations are equivalent. ((44) does not have a singularity because the real part of p is positive.)

Now substitute the value of E found in equation (43) back into equation (40) to find an expression for the Laplace transform of the distribution function.

$$F_1 = \frac{-ie^2}{(p + iku)\,\varepsilon_0\, mk\, \varepsilon(k,p)} \frac{\partial F_0}{\partial u} \int_{-\infty}^{\infty} \frac{F_1(t=0)}{p + iku}\, du + \frac{F_1(t=0)}{p + iku} \qquad (2.45)$$

Any poles in equations (43) and (45) occur when the dispersion relationship equals zero.

To find the values of the electric field and the perturbations in the distribution function equations (43) and (45) have to be inverted using equation (38). The contour of integration to invert a Laplace transform is an infinite vertical line on the complex p-plane, lying to the right of all singularities in the plane. This is shown in the first part of figure 2.

Now deform the original contour C to C' as shown in the second part of the diagram. The value of σ is chosen so that all the poles lie to the left of the vertical dashed line passing through σ. If C' is sufficiently close to σ the integral along that part of the contour behaves as $\exp(-\sigma t)$ and tends to zero for large enough time. Similarly the contribution from the pole furthest to the right will be the largest for sufficient large values for t. This means that it is possible to find an asymptotic value for the integral.

However, to be able to deform contour C into C' in the complex p-plane

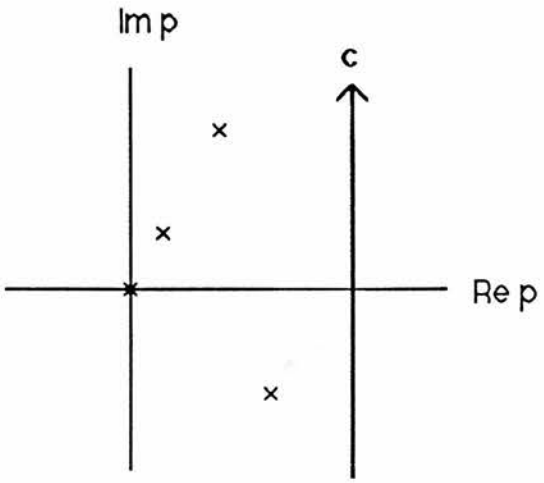

Original contour C to invert a Laplace transform.

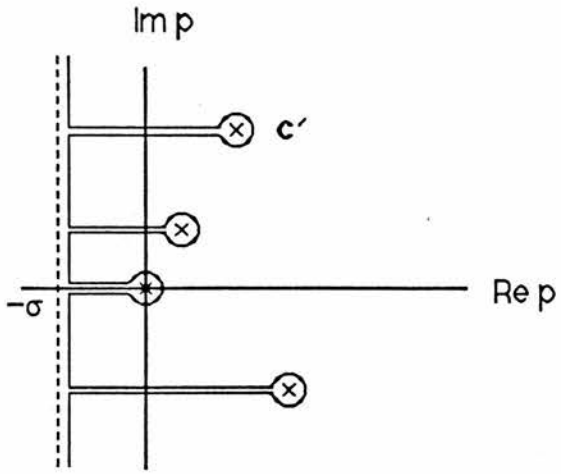

Modified contour C'

Figure 2.2

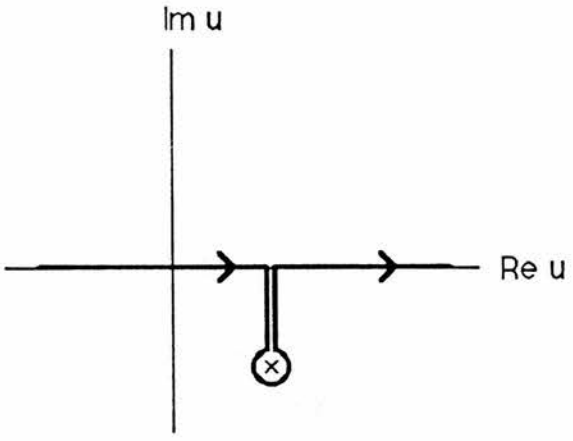

Contour for integration wrt u

Figure 2.3

implies that there have to be conditions on the integrals of the form

$$G(\frac{ip}{k}) = \int_{-\infty}^{\infty} \frac{g(u)}{u - ip/k}\, du \qquad (2.46)$$

which are part of the expressions for E, F_1 and $\varepsilon(k,p)$.

These integrals are integrated from $-\infty$ to ∞ along the real axis. However, there is a singularity at $u = ip/k$ which has to be treated correctly. Looking again at figure 2.2 the contour of integration runs to the right of all the singularities, so since u is proportional to i times p the contour of integration has to pass below the pole, as shown in figure 2.3, which shows the complex u-plane. But to be able to deform this contour in this way implies additional constraints on the function G(u). The constraints are that the initial velocity distribution and the perturbed velocity distribution functions have to be sufficiently smooth.

The work which will be described in chapter 4 only deals with the magnitude of the Landau damping, and is not concerned to find the velocity perturbation or the electric field, so here solve the plasma dispersion relation, equation (44), to find the Landau damping decrement.

Solve this equation asymptotically for large values of t in terms of the wave frequency ω rather than the Laplace transform variable p, ie solve

$$\varepsilon(k,\omega) = 1 + \frac{e^2}{\varepsilon_0 mk} \int_{-\infty}^{\infty} \frac{\frac{\partial F_0}{\partial u}}{\omega - ku} du = 0 \qquad (2.47)$$

with a Maxwellian distribution function

$$F_0(u) = \frac{n_0}{(2\pi\kappa T/m)^{1/2}} e^{-mu^2/2\kappa T} \qquad (2.48)$$

If ω is assumed to be real to a first approximation there is a pole at $\omega = ku$, ie on the contour of integration. But from the argument above the imaginary part of ω must be greater than zero if the contour is always to lie below the poles. So the imaginary part of ω has to tend to zero from above. The correct way to treat integrals of this form is to use the Plemelj formula, and in this case the answer is

$$-\frac{1}{2\pi ik} P\int_{-\infty}^{\infty} \frac{\partial F_0 / \partial u}{u - \omega k} du - \frac{1}{2k} \frac{\partial F_0}{\partial u}_{u = \omega/k} \qquad (2.49)$$

The principal value of an integral is found by removing a region of width r on each side of the point where the integrand is singular and then letting r tend to zero. If the contour had been above the pole the sign of the second term would have been positive.

If k is then assumed to be small in the region where the value of $\partial F_0/\partial u$ is

significant $\omega \gg ku$ then $(\omega - ku)^{-1}$ can be expanded in a Taylor series and the integrand integrated term by term. For a Maxwellian plasma $\partial F_0/\partial u$ is odd, thus 'knocking out' some of the terms in the Taylor series. Integrating gives

$$1 - \frac{\omega_p^2}{\omega^2} - 3k^2 \frac{\kappa T \omega_p^2}{m\omega^4} - \frac{e^2}{\varepsilon_0 m} \frac{i\pi}{k^2} \frac{\partial F_0}{\partial u}_{u = \omega/k} \qquad (2.50)$$

and equating the real parts gives

$$\omega^2 \approx \omega_p^2 (1 + 3k^2\lambda_D^2) \qquad (2.51)$$

λ_D $(= [\kappa T/m\omega_p^2]^{1/2})$ is the Debye length and the further assumption that $k\lambda_D \ll 1$ is made. Then, in line with the assumptions made so far, the imaginary part of the frequency is assumed to introduce a small perturbation. Letting $\omega = \omega_0 + \delta\omega$ where ω_0 is the solution of equation (51) gives

$$\delta\omega \approx \frac{i}{2} \frac{\pi}{\omega_p k^2} \frac{e^2}{\varepsilon_0 m} \frac{\partial F_0}{\partial u}_{u = \omega/k} \qquad (2.52)$$

and, using equation (51), for a Maxwellian plasma this becomes

$$\delta\omega \approx -\frac{i}{2}\sqrt{\frac{\pi}{2}}\ \omega_p \frac{1}{k^3\lambda_D^3} \exp\left(-\frac{1}{2k^2\lambda_D^2} - \frac{3}{2}\right) \qquad (2.53)$$

This is true for electrostatic waves in a plasma with no applied magnetic field. The result used in chapter 4 is for a plasma in a magnetic field. This introduces some changes, but these will be discussed after the next section on the physical mechanism of Landau damping.

(ii) Physical Mechanism for Landau Damping

From equation (52) the amount of Landau damping is proportional to the slope of the distribution function at $u = \omega / k$, ie where the parallel thermal velocity of the electrons equals the group velocity of the plasma. This suggests that the damping is caused by some sort of resonant interaction.

In a Maxwellian plasma the slope of the distribution function at the phase velocity is negative, so there are more particles with velocities a little lower than the group velocity than there are particles with velocities a little higher than the group velocity. Exactly how a particle interacts with the wave depends on its phase wrt the wave as well as its velocity. Particles which are not nearly in resonance with the wave oscillate in the field and so are not relevant for Landau damping.

When the particles with velocity slightly lower than the wave gain energy their velocity increases and so they approach the resonant velocity more closely and hence can gain more energy from the wave. Conversely, if a particle gives energy to the wave its velocity decreases and so it interacts less

efficiently with the wave.

The opposite is true for particles which start with velocities slightly higher than the phase velocity. If they lose energy they interact more efficiently with the wave and if they gain energy they move out of resonance.

Since in a Maxwellian plasma there are more slightly slower particles than slightly warmer particles on balance the wave gives energy to the plasma and is damped.

(iii) Landau Damping in a Magnetic Field

The addition of a magnetic field to a plasma does not change the mechanism of Landau damping. The spiralling of the electrons round the magnetic field lines does not change their energy, but their motion parallel to the magnetic field does allow for the possibility of Landau damping in this direction.

The magnetic field is eliminated in the Vlasov equation by using Maxwell's equation

$$\nabla \times \mathbf{E} = - \frac{\partial \mathbf{B}}{\partial t} \qquad (2.54)$$

The calculation then follows through in a similar way to the previous case with only an electric field present. For waves propagating purely along the magnetic field the only component of the wave vector present is $k_{||}$, and the imaginary part of the dielectric tensor is given by

$$\sqrt{\frac{\pi}{2}}\ \frac{\omega_p^2\,\omega}{k_{||}^3 u^3}\ \exp\left(-\frac{\omega^2}{2k_{||}^2 u^2}\right) \qquad (2.55)$$

2.4 ALFVEN WAVES

Another set of waves arise from consideration of magnetohydrodynamics (MHD). The MHD approach to plasmas arises from consideration of the equations of fluid dynamics with the additional assumption that the fluid is electrically conducting. The conductivity of the fluid is assumed to be high enough that any electric charge is dissipated in a shorter time than the time scale being considered. This means that the fluid is electrically neutral and any electric fields present are only caused by changing magnetic fields.

The Alfven waves can be found by considering the linearised MHD equations :-

$$\frac{\partial \rho_1}{\partial t} + \nabla . (\rho \mathbf{v}_1) = 0 \qquad (2.56)$$

$$\rho \frac{\partial \mathbf{v}_1}{\partial t} + \nabla p_1 = \mathbf{J} \times \mathbf{B}_1 + \mathbf{J}_1 \times \mathbf{B} \qquad (2.57)$$

$$\frac{\partial p_1}{\partial t} + (\mathbf{v}_1 . \nabla) p + \gamma p \nabla . \mathbf{v}_1 = 0 \qquad (2.58)$$

$$\frac{\partial \mathbf{B}_1}{\partial t} = \nabla \times (\mathbf{v}_1 \times \mathbf{B}) \qquad (2.59)$$

The unsubscripted quantities are the equilibrium states and the subscript 1 on a quantity means that it is a perturbation. **B** is the magnetic field, **J** the

current density, p the plasma pressure, ρ the plasma density and γ the ratio of specific heats.

In equilibrium assume that p and **B** are uniform and that the current is zero. Letting $\xi = \xi(\mathbf{r},t)$ be the displacement of the plasma from equilibrium gives

$$\rho \frac{\partial^2 \xi}{\partial t^2} = \nabla(\gamma p \nabla.\xi) + \frac{1}{\mu_0} (\nabla \times \mathbf{B}_1) \times \mathbf{B} \qquad (2.60)$$

with

$$\mathbf{B}_1 = \nabla \times (\xi \times \mathbf{B}) \qquad (2.61)$$

Continue to use the coordinate system with **B** along the z-axis and the angle between **B** and **k** being θ. Then taking the scalar product of (**k** x **z**) with equation (60) gives

$$(\omega^2 - c_A^2 k^2 \cos^2\theta)(\mathbf{k} \times \mathbf{z}).\xi = 0 \qquad (5.62)$$

which shows that there is a mode with the dispersion relation

$$\omega^2 = c_A^2 k^2 \cos^2\theta = c_A^2 k_z^2 \qquad (5.63)$$

The mode is known as the Alfven mode and $c_A^2 = B^2 / \mu_0 \rho$ is the square of the Alfven speed. In this mode ξ is along **k** x **z** and so is perpendicular to

both the magnetic field and the wave vector. But, equation (63) shows that ω only depends on k_z, so the group velocity and hence the wave energy are parallel to the magnetic field.

Taking the scalar product of equation (60) with **k** and **z** and making the substitution $c_s^2 = \gamma p / \rho$ (where c_s is the speed of sound in the gas) gives the two coupled equations

$$\omega^2 (\xi.\mathbf{k}) = c_s^2 k^2 (\xi.\mathbf{k}) - c_A^2 \cos\theta \, \xi_z k^3 + c_A^2 k^2 (\xi.\mathbf{k}) \qquad (2.64)$$

$$\omega^2 \xi_z = c_s^2 k \cos\theta (\xi.\mathbf{k}) \qquad (2.65)$$

Eliminating k_z and $(\mathbf{k}.\xi)$ between (64) and (65) gives the dispersion relation

$$\omega^4 - k^2 \omega^2 (c_s^2 + c_A^2) + k^4 c_s^2 c_A^2 \cos^2\theta = 0 \qquad (2.66)$$

with solution

$$\frac{\omega^2}{k^2} = \frac{1}{2}\left(c_s^2 + c_A^2 \pm \{(c_s^2 + c_A^2)^2 - 4c_s^2 c_A^2 \cos^2\theta\}^{1/2} \right) \qquad (2.67)$$

The two solutions to equation (66) given in (67) are known as the fast (+ sign) and slow (- sign) magnetosonic waves. In general both waves have k_z and $\mathbf{k}.\xi$ non-zero.

CHAPTER 3 TOKAMAKS AND RFPS

3.1 TOROIDAL CONFINEMENT SYSTEMS

One way to confine plasmas is to use the fact that charged particles spiral round magnetic field lines. If the magnetic field lines are closed the particles will then be trapped. The simplest way to close the field lines is to bend them into a circle. This is the basis of toroidal confinement systems, in which the magnetic field lines form closed loops which are enclosed in a torus (ring doughnut).

The two main directions in a torus are the toroidal and the poloidal directions. The toroidal direction corresponds to travelling along the major circumference of the torus and the poloidal direction to going along the minor circumference. Figure 3.1 illustrates this geometry.

To see how a plasma is confined in a torus first consider setting up a toroidal field in the torus using a set of poloidal field coils. The particles are then constrained to travel round the torus following the field lines. However, the coils produce a field which is higher at the inner sided of the torus (the hole) than the outside. This field gradient produces a transverse drift of electrons in one direction and a drift of ions in the opposite direction. The separation of ions and electrons produces an electric field, which then interacts with the toroidal magnetic field to produce an **E** x **B** drift of ions and electrons radially outwards.

However, the drifting will not occur if the electric field can be neutralised or short circuited. This is achieved by passing an electric current through the

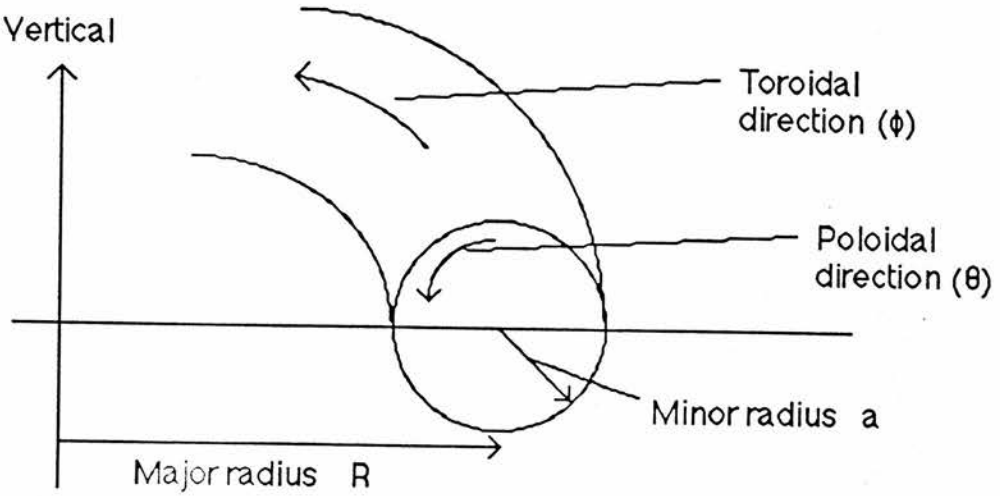

3.1 Toroidal and poloidal directions in a torus.

plasma. The effect of this toroidal current is to produce a poloidal magnetic field. The combination of the toroidal and poloidal magnetic fields produces field lines which spiral round the torus. This twisting means that the particles which spiral round the field lines pass through opposite polarities of the electric field and hence short it out.

The poloidal field is important in determining the stability of the system - leading to q, rotational transform.

The toroidal current also tends to make the plasma expand radially. To counteract this it is possible to surround the plasma with a conducting shell, or to use more coils to apply a vertical magnetic field, B_z. Some toroidal devices have no conducting shell, which means that an additional quadrupole magnetic field has to be applied vertically to avoid an instability which arises when $\partial B/\partial r < 0$.

The basic method of confining a plasma is the same in the two main classes of toroidal confinement device, the tokamak and the reversed field pinch. The main differences between the two arise in the magnetic field structure, which is shown schematically in figure 2. In the tokamak the toroidal field is greater on the inside than the outside and decreases approximately as $1/r$. The toroidal field is also considerably greater than the poloidal field.

In the RFP, as the name suggests, the toroidal field is reversed in the outside of the plasma. The toroidal and poloidal fields have approximately the same magnitude. One of the other differences between the tokamak and the RFP is that the fields are usually much lower in RFPs than in tokamaks.

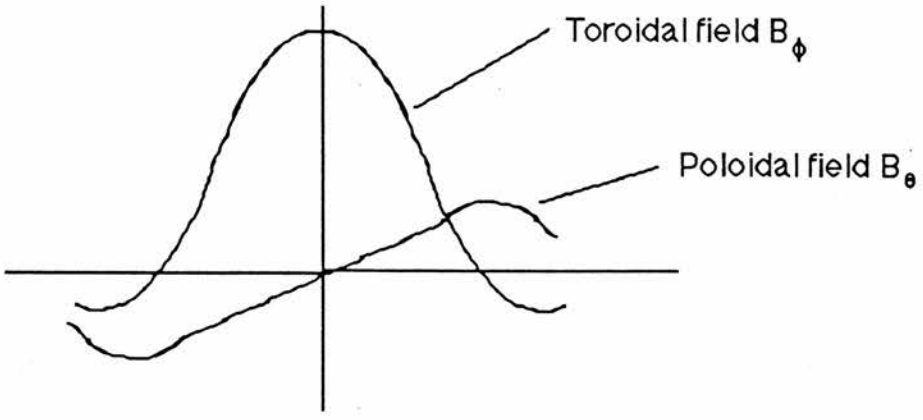

Fig 3.2a Radial variation of magnetic fields in RFP

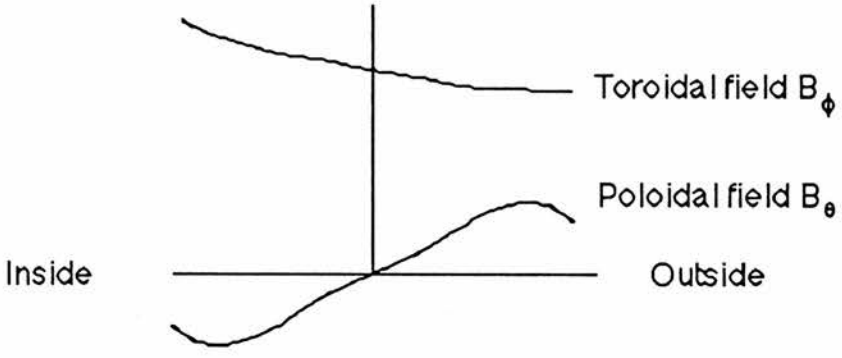

Fig 3.2b Radial variation of magnetic fields in a tokamak.

Magnetic pressure. Consideration of the equations of motion of a charged particle in a magnetic field or of the MHD equations in a plasma show that the magnetic field in a plasma behaves as if it exerts a pressure $B^2 / 2\mu_0$. This magnetic pressure plays an important role in the physics of tokamaks and RFPs.

The ratio of the plasma pressure to the magnetic pressure β ($=p / [B^2/2\mu_0]$) is an important parameter in determining the stability of any particular discharge. β is also a measure of the amount of magnetic energy stored in the plasma. Typical values for β in RFPs lie in the range 5 - 10 %, which is higher than in tokamaks.

3.2 RELAXATION THEORY AND RFPS

One of the most interesting features of RFPs is how the toroidal field reversal arises. Initially, when experiments are set up to generate a reversed field configuration, once the plasma has been formed it becomes spontaneously unstable and very turbulent. After this turbulent phase the plasma enters a stable state which is independent of the initial conditions of the experiment.

This state can be described by two parameters; the field reversal ratio $F = B_{\phi wall} / B_{\phi ave}$ and the plasma pinch ratio $\theta = 2I / aB_{\phi}$. The main features of the

F- θ diagram shown in fig 3 are that the field reversal (F<0) does not occur until some critical value of θ (~1.2) is exceeded and that there is a change in behaviour for values of θ greater than ≈ 1.6. For values of θ greater than this in some experiments the field reversal disappears while on others the plasma becomes more turbulent..

An explanation for this behaviour was put forward by J.B. Taylor, who suggested that the behaviour of RFPs could be explained by saying that they relax to a state which is a near minimum of magnetic energy subject to the constraint that the total helicity of the plasma remains constant.

The initial assumptions made are that the plasma is a perfectly conducting, viscous fluid surrounded by a perfectly conducting toroidal shell. In this case Maxwell's equations for a perfectly conducting fluid with velocity **v** can be reduced to

$$\frac{\partial \mathbf{B}}{\partial t} = \nabla \times (\mathbf{v} \times \mathbf{B}) \qquad (3.1)$$

which implies that the magnetic field moves along with the fluid, ie it is 'frozen in.' This means that the topological properties of the magnetic field are determined by the fluid behaviour. Since the velocity of the fluid is continuous the magnetic field lines cannot break and rejoin, so in a perfectly conducting fluid the topological properties of the magnetic field are conserved. These constraints can be expressed through the magnetic vector potential **A**, where **B** $= \nabla \times \mathbf{A}$.

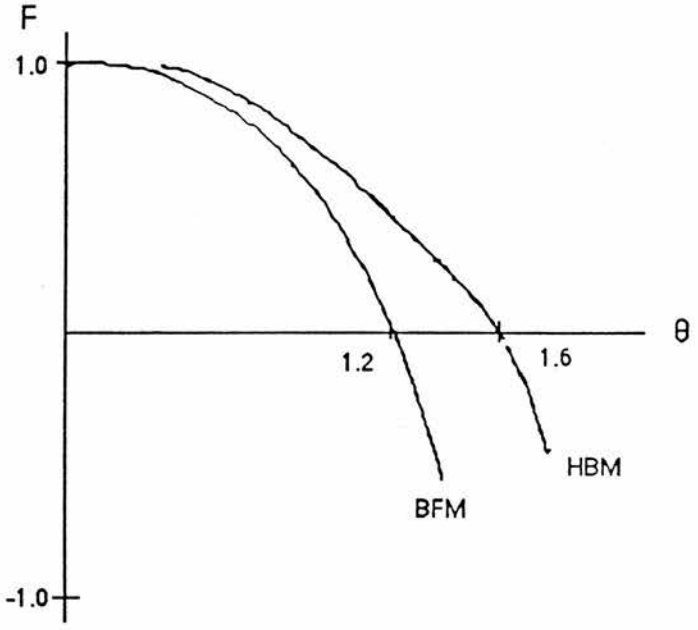

Fig 3.3 Schematic F-θ diagram showing two theoretical curves derived from relaxation theory. BFM stands for Bessel function model and HBM for high beta model. The experimental results lie between the two curves.

Rewriting equation (1) and integrating gives

$$\frac{\partial \mathbf{A}}{\partial t} = \mathbf{v} \times \mathbf{B} + \nabla\chi \qquad (3.2)$$

where χ is an arbitrary gauge. Since χ is arbitrary equation (2) does not impose any condition on the component of $\partial\mathbf{A}/\partial t$ perpendicular to **B**. However, multiplying (3.2) by **B.** gives an equation for $\nabla\chi$

$$\mathbf{B} \cdot \nabla\chi = \mathbf{B} \cdot \frac{\partial \mathbf{A}}{\partial t} \qquad (3.3)$$

which in turn imposes conditions on $\partial\mathbf{A}/\partial t$ if $\nabla\chi$ is to be single valued. These constraints are given below, where Ψ is the toroidal flux.

$$\int \frac{\mathbf{B}}{B} \cdot \frac{\partial \mathbf{A}}{\partial t}\, dl = 0 \qquad \int \frac{\mathbf{B}}{\nabla\Psi} \cdot \frac{\partial \mathbf{A}}{\partial t}\, dS = 0 \qquad (3.4)$$

In any volume V these constraints can be summarised by the equation

$$K \equiv \int_V \mathbf{A}.\mathbf{B}\, dV = \text{constant} \qquad (3.5)$$

where K is the helicity.

In a perfectly conducting plasma there is a value of K for each infinitesimal flux tube in the plasma. However, in the turbulent setting up phase of the RFP it is not possible to assume that the plasma is perfectly conducting. This means that flux tubes are free to break and rejoin, but although helicity is no longer conserved for each individual flux tube it is possible to assume that it is a

conserved quantity in the whole volume of the plasma.

To investigate what is happening in the RFP minimise the magnetic energy of the plasma, given by $W_m = \int B^2/2 \, dV$ subject to the constraint that the total helicity remains constant.

Going back to equation (2) and choosing a gauge such that $\nabla\chi = 0$ we find that

$$\mathbf{B} \cdot \frac{\partial \mathbf{A}}{\partial t} = 0 \qquad (3.6)$$

Using this to determine the next integral gives

$$\frac{\partial}{\partial t} \int_V \mathbf{A} \cdot \nabla \times \mathbf{A} \, dV = \int_V \mathbf{A} \cdot \nabla \times \frac{\partial \mathbf{A}}{\partial t} \, dV \qquad (3.7)$$

Integrating the RHS of equation (7) by parts gives

$$\int_V \mathbf{A} \cdot \nabla \times \frac{\partial \mathbf{A}}{\partial t} \, dV = \int_V \nabla \times \mathbf{A} \cdot \frac{\partial \mathbf{A}}{\partial t} \, dV + \int_S \mathbf{A} \times \frac{\partial \mathbf{A}}{\partial t} \, dS = 0 \qquad (3.8)$$

In a closed system the surface integral vanishes. Integrating the LHS of equation (7) wrt time implies that the helicity remains constant, so minimising the magnetic energy subject to that constraint using a Lagrange multiplier μ gives

$$\int_V [2 \nabla \times \mathbf{A} \cdot \nabla \times \delta\mathbf{A} - \mu(\delta\mathbf{A} \cdot \nabla \times \mathbf{A} + \mathbf{A} \cdot \nabla \times \delta\mathbf{A})] \, dV = 0 \qquad (3.9)$$

When equation (9) is integrated by parts, using the fact that $\delta\mathbf{A}$ equals zero on the surface gives

$$\int_V [\nabla \times \nabla \times \mathbf{A} - \mu \nabla \times \mathbf{A}] . \delta\mathbf{A} \, dV = 0 \qquad (3.10)$$

and since $\delta\mathbf{A}$ is arbitrary

$$\nabla \times \nabla \times \mathbf{A} - \mu \nabla \times \mathbf{A} \equiv 0 \qquad (3.11) \text{ or}$$

$$\nabla \times \mathbf{B} = \mu\mathbf{B} \qquad (3.12)$$

where μ is constant. This shows that the minimum energy state subject to the constraint that the total helicity is constant is the force-free configuration given in equation (12).

If equation (12) is solved in cylindrical coordinates (r,θ,z), which implies that the solutions neglect the toroidal effects and is axisymmetric, the magnetic field components are given by

$$B_z = B_0 J_0(\mu r) \qquad B_\theta = B_0 J_1(\mu r) \quad B_r = 0 \qquad (3.13)$$

where J_0 and J_1 are Bessel functions.

Consideration of the B_z component shows that field reversal will occur when $\mu a > 2.404$, or when $\theta > 1.202$. Experimental results show that field reversal occurs when $\theta \approx 1.4$, so the theory is in fair agreement, especially since the plasma is not in a fully relaxed state. However, the axisymmetric state ceases to be the lowest energy state when $\mu a = 3.11$, or $\theta \approx 1.6$, and

becomes a helically deformed state. Experimentally, when $\theta \approx 1.6$ the axisymmetric state becomes unstable to the resistive instability, which again suggests that the theory is on the right lines.

The simple picture presented above which results in a Bessel function model for the magnetic fields is not complete because it predicts that μ, which is the ratio of the current density to the magnetic field, will remain constant across the plasma. In practice it is found that the current density falls smoothly in the outer regions of the plasma to zero at the wall. It is thought that this is because the plasma resistivity is higher in the outer regions of the plasma and that the reversal mechanism is not strong enough to overcome this.

One way to get round this problem is to include the effects of the finite plasma pressure in the model. Figure 3 is based on figure 17 from Robinson's chapter in Plasma Physics and Nuclear Fusion Research. Experimentally it is found that the results from different RFP experiments do lie on a universal F-θ curve, but that the curve lies between that predicted by Taylor's theory and the high beta model, which does include the effects of pressure.

Experimental Results

Section 3.3 deals with current drive experiments on tokamaks. A considerable amount of work has also been carried out on ways to heat tokamaks noninductively. However, in the case of RFPs experimental work is still at the stage of exploring the properties of the plasma rather than carrying out experiments on current drive or heating per se. As a result this section will

give a brief view of some results in this field.

In the discussion on the generation of the reversed field configuration by self-reversal it was mentioned that the plasma is turbulent and has large fluctuations in the values of various parameters. This is particularly true in the case of magnetic fluctuations, measured as $\delta B / B$.

The behaviour of the plasma torus can be described by using the poloidal and toroidal mode numbers m and n, where $x = x_0 \exp i(m\theta + n\phi)$.

Experiments to measure these fluctuations show that they are caused by the presence of large scale MHD modes in the plasma. Analysis of data for HBTX1A by Hutchinson et al and Brotherton-Ratcliffe et al using statistical methods to separate out the various components of the fluctuations show that many of the fluctuations are due to low poloidal mode number, m=0 and m=1 modes with a mixture of toroidal mode numbers.

By contrast in a RFP without a conducting shell Robertson and Schmid find that the length of the discharge is limited by the presence of n=1 and n=2 toroidal kink modes. The reason for considering a RFP without using a stabilising conducting shell is that in many experiments the discharge lasts for longer that the magnetic diffusion time of the shell and so the shell is effectively not present. In addition the absence of a conducting shell means that stability has to be ensured by means of a vertical electric field, which would allow greater control over the position and shape of the plasma. Although since the length of the discharge is reduced by the toroidal kink modes sets of external coils would be needed to guard against them.

3.3 CURRENT DRIVE IN TOKAMAKS

Most of the effort in plasma fusion research is expended on tokamaks, so this section will discuss plasma heating mainly with respect to tokamaks, although the techniques mentioned could be applied more widely.

The ultimate aim of auxiliary heating schemes is to enable a fusion reactor to operate in a steady state, which will increase the lifetime of the reactor by reducing the stress caused by continued heating and cooling of the structure. Another advantage of continuous operation is that there will not be frequent changes in the parameter regime, which means that the plasma will spend less time in regimes where disruptions are likely.

On JET it is not possible to heat a plasma using ohmic heating above about 4 keV. Similar results are true for other devices, so ignition temperatures cannot be reached using ohmic heating alone. This is because the resistivity of a plasma goes as $T^{-3/2}$, and so falls steeply as the temperature increases. The two main ways to heat the plasma further are to inject energetic beams of neutral particles or radio frequency waves which exploit the resonances in the plasma.

In neutral beam injection molecules are first ionised and accelerated to high energies before being neutralised by passing through a gas cell. The beam of neutral particles can then pass through the magnetic fields surrounding the plasma, before being ionised and giving its energy to the plasma by collisional processes. The matter is more complicated but further discussion is beyond the scope of this thesis.

To maintain steady state operation in a tokamak current drive is used to sustain a toroidal current, which then produces the poloidal magnetic field which is necessary for stability. The current is produced by injecting waves with a toroidal asymmetry. Alfven and lower hybrid waves transfer parallel momentum from the wave to the plasma, while schemes using the cyclotron waves decrease the collisionality of the plasma in the perpendicular direction to decrease the plasma resistivity.

The two main kinds of resonance are the Landau resonance, where $\omega = \mathbf{k}.\mathbf{v}$; and the cyclotron resonance in the presence of a magnetic field, which occurs when $\omega - k_{\|}v_{\|} - n\Omega = 0$.

Low and high phase velocity electrons

Current drive is most efficient when momentum is transferred to low or high parallel velocity electrons. (Parallel means parallel to the direction of the magnetic field and high and low velocities are referred to the thermal velocity of the electrons.)

To see this find the ratio of current produced to energy absorbed. Consider an electron of mass m and charge q and let **i** be a unit vector parallel to the magnetic field. If the electron is accelerated from a velocity $\mathbf{v} = v_{\|}\mathbf{i} + \mathbf{v}_{\perp}$ to a velocity $\mathbf{v} + \Delta v_{\|}\mathbf{i}$ it gains energy $\Delta\varepsilon = m\, v_{\|}\, \Delta v_{\|}$ and carries an extra current $\Delta j = q\, \Delta v_{\|}$. So the ratio $\Delta\varepsilon / \Delta j$ is proportional to $v_{\|}$, so it is more energetically favourable to accelerate slow electrons than fast electrons. This is the basis of neutral beam heating which accelerates slow electrons and of Alfven heating,

where the waves have a low phase velocity.

However, an electron with parallel velocity much greater than the thermal velocity collides less often than electrons with the thermal phase velocity so if energy is given to fast electrons the current that is produced will last longer than the current carried by slow electrons. This may mean that the energy required to drive a given current may be smaller for the fast electrons than the slow electrons.

To see how this can happen use the expressions for the incremental current and energy to get the relation

$$\Delta j = \Delta\varepsilon \frac{q}{m v_{||}} \tag{3.14}$$

If the collision frequency of the electrons is ν, the power required to drive the current is $P = \nu \Delta\varepsilon$. Assuming that the current is due to this power alone, Δj can be replaced by J and the steady state efficiency is given by

$$\frac{J}{P} = \frac{q}{m v_{||} \nu(v)} \tag{3.15}$$

This can be maximised if $v_{||}\, \nu(v)$ is minimised. First consider the case $v_{||} \rightarrow 0$ and $v_{\perp} \approx v_{thermal}$ and $\nu \sim$ constant, which corresponds to using Alfven waves. The efficiency is high because $J / P \propto 1 / v_{||}$ and $v_{||}$ is small.

For high parallel velocity waves, ie $v_{||} \gg v_{thermal}$, $\nu \propto 1 / v_{||}^3$ the efficiency is

therefore proportional to $v_{||}^2$ and since $v_{||}$ is large this gives large efficiency. This suggests the use of lower hybrid (or even whistler) waves which have a high parallel velocity.

Four main schemes

There are four types of scheme utilising the properties of electromagnetic radiation. At the lowest frequencies Alfven waves are used. The next class of scheme is ion cyclotron resonance heating (ICRH) which exploits the properties of the ion resonances in a plasma with at least two species of ion and their harmonics in the frequency range 20 - 100 MHz. The waves are excited by arrays of antenna loops in the poloidal direction which are excited with different phases.

The lower hybrid resonance occurs near the centre of the plasma in the frequency range 1 - 5 GHz. The required wave spectrum is excited by an array of phased waveguides called the 'grill'. The highest frequency waves exploit the properties of waves at the electron cyclotron frequency between 100 - 200 GHz in tokamaks. The difficulty of producing high power at these high frequencies has only been overcome recently with the development of the gyrotron.

3.3.1 Alfven waves

It has been shown in an earlier section that the Alfven wave could be used to accelerate low parallel velocity electrons efficiently. However, this expectation overlooks the phenomenon of trapped particles in a magnetic field.

In a tokamak particles with a low parallel velocity and a high perpendicular velocity can be trapped in magnetic wells, which means that they are not free to carry current.

In a large aspect ratio tokamak Wort (1971) showed that it was possible to drive current using Alfven waves, but it was later found that this was not the case in plasmas with realistic aspect ratios.

However, Alfven waves could drive current in regimes without trapped electrons, such as occur near the magnetic axis of a tokamak.

Alfven wave current drive was first proposed by Wort and further theoretical work was carried out by Hasegawa. A description of experiments using Alfven waves on the TCA tokamak is given by Behn et al. The results of these experiments were that it was possible to inject up to 206 kW of Alfven wave power into the tokamak, which is roughly comparable with the ohmic heating supplied. The power went into raising the temperature of the ions and electrons in the plasma. However the electron density was found to increase and the radiated power loss increased, both of which limit the amount of power which can be supplied before the plasma becomes unstable and there is a disruption.

3.3.2 Ion cyclotron waves and minority ion heating schemes.

As the frequency of the Alfven wave increases and tends towards Ω_i the phase velocity decreases and the wave is renamed the ion cyclotron wave. This wave has two branches named the fast and the slow and a resonance at

$\omega = \Omega_i$.

In a deuterium plasma at 3T the resonance frequency is ≈ 25 MHz, which corresponds to a vacuum wavelength of 10m. As a result the wave has to be launched using large coils wrapped around the tokamak in the poloidal direction.

The slow wave (ion cyclotron wave) is evanescent for $\omega > \Omega_i$ and is mode converted at the edge of the plasma to an outbound warm plasma wave so it cannot be used for ICRH. The fast wave can propagate across the magnetic field, if the density is greater than the cutoff density.

The propagation of the wave can be described by the cold plasma dispersion relation using the fact that $\varepsilon_{||} \gg n_{\perp}^2$. This means that $E_{||}$ is negligible compared to $E_{\perp}$ which is true provided $\omega_{pe} \gg \omega$.

In a single ion species plasma the absorption is very small at the fundamental frequency because the wave electric field vector rotates in the opposite sense to the ions. This is no longer true at the second harmonic resonance $\omega = 2\,\Omega_i$ or when there is a second ion species because the electric field then has the necessary perpendicular electric field to couple to the ions.

Minority heating schemes

Minority ion heating schemes rely on having two species of ion with different charge states in a plasma. This could be achieved by using a D - ^{3}He plasma or in a D-T plasma with some of the ^{4}He produced by the reaction left to

provide minority ion concentration.

For minority ion concentrations of less than 5% energy is absorbed by the cyclotron damping of the minority species. Cyclotron damping is most efficient with higher velocity particles so a high energy tail of ions is produced.

At larger minority ion concentrations the energy is absorbed at the ion-ion hybrid resonance frequency. The incident wave mode converts to a slow wave which is damped by the bulk of the ions.

It is also possible to use lower hybrid waves in a current drive scheme by accelerating minority ions preferentially in one direction. To see what is happening consider a uniform distribution of minority ions and heat those moving to the right (say) using the perpendicular momentum in the waves. Because these ions are moving faster than the ions moving to the left they collide less often with the majority ions than the minority ions moving left. The net result is that the majority ions are on average dragged to the left.

To ensure this happy outcome, the effect of minority-majority ion collisions and electron-minority ion collisions must be approximately equal.

The velocity difference between the minority ions and the electrons is so great that there is not much difference between the left and right moving ion collision rates with the electrons, so if there are too many minority ion-electron collisions there would not be an asymmetric slowing down of electrons.

If the two kinds of ions collide more frequently than the minority ions collide with the electrons more energy is given to the majority ions than to the electrons which carry the current, so again there is not efficient current drive.

There are two regimes of minority heating scheme depending on the

concentration of minority ions.

Heating experiments on JET using ICRH antennae have successfully delivered 6 MW of power to the plasma (Bickerton et al 1986). As far as current drive is concerned, there have been many theoretical studies to investigate how to couple ion cyclotron waves to the plasma and some coupling experiments have been carried out, but no current has yet been driven.

3.3.3 Lower Hybrid Resonance Heating (LHRH)

The next frequency range for heating tokamak plasmas is in the low GHz range. Lower hybrid resonance heating is one of the schemes which heats high velocity electrons to exploit the persistence of this current. (See the earlier section where it was shown that the efficiency is proportional to $v_{||}^2$.)

[To trace the effect of LH waves on the plasma it is necessary to balance the effects of collisions, which tend to drive the electrons to thermal equilibrium, and the effect of the waves, which is to inject toroidal momentum. This is done by solving the Fokker-Planck equation. Unfortunately, this equation is so complicated that this is difficult, and various approximations have to be made. The equation includes so many effects that it is difficult to be unambiguously sure what the results of injecting a wave into the system are. It is also difficult to solve this equation numerically, partly because of its complication and partly because it is not easy to investigate a large enough parameter regime numerically.]

One advantage of the LH range of frequencies is that powerful sources

are already available and power can be easily delivered to the tokamak via waveguides. One convenient method of doing this is to used an array of phased waveguides, called the grill (Brambilla 1976), which allows control over the $k_{||}$ spectrum of the waves.

Plotting the square of the perpendicular refractive index of the wave against the density (which is proportional to the square of the plasma frequency) shows that there are two regimes for the wave - see figure 4.

For $n_{||}$ below a critical value given by the Stix-Golant accessibility criterion

$$n_{||}^2 > 1 + \frac{\omega_{pe}^2}{\Omega_e^2} \Big|_{res}$$

there is an evanescent layer before the LH resonance is reached.

This means that $n_{||} > 1$ when the wave is launched and hence that it is evanescent at the edge of the plasma.

It can also be seen that it is necessary to excite the slow LH wave in the plasma because the fast wave does not have a resonance at the LH frequency. To do this it is only necessary to align the grill with the short side of the wave guides along the magnetic field and to excite a TE mode.

As the slow wave approaches the LH resonance its perpendicular wave number increases and it mode converts to the ion Bernstein mode, which then heats the ions. Both modes are evanescent on the high density side of the resonance. This evanescent region can be moved closer to the edge of the plasma by increasing the value of $n_{||}$ or increasing the ion or electron temperatures.

In addition, because the slow wave has a large component of its electric

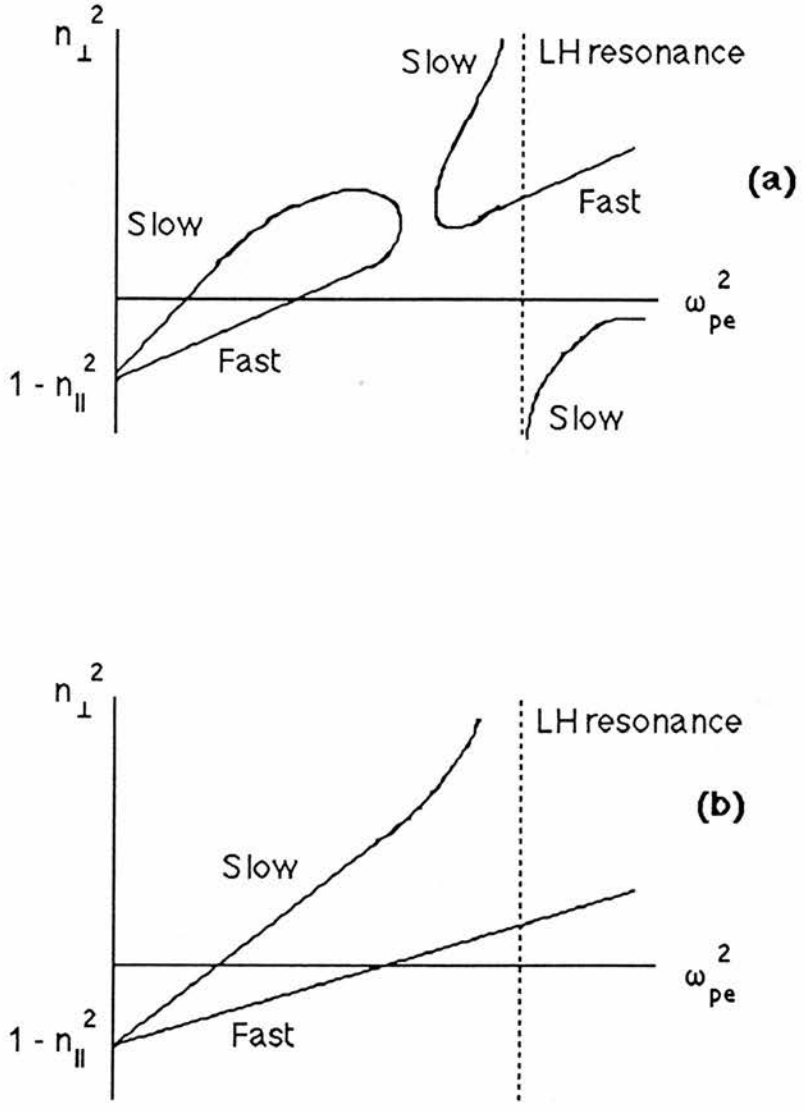

Fig 3.4 Plot of perpendicular refractive index against plasma density. (a) shows the evanescent layer which is present when the Stix-Golant condition is not met, while (b) shows that the lower hybrid resonance is accessible when this condition is met.

field parallel to the magnetic field it can also heat electrons by Landau damping. The disadvantage of this is that the heating is not confined to any particular region and so can heat the edge of the plasma.

At low enough densities, and with a suitable $k_{||}$ spectrum, achieved by adjusting the phase of the wave guide elements, Landau damping provides an efficient current drive mechanism.

At high enough plasma density the LH waves interact with ions rather than electrons. Numerically the lower hybrid frequency corresponds to high harmonics of the ion cyclotron frequency and the region where damping occurs can span several of the ion harmonics which results in effective stochastic heating of the ions.

Jobes et al describe an experiment on the PLT tokamak which demonstrated current drive using LH waves alone. With the ohmic heating reduced or not applied the current in the tokamak was first sustained and then ramped up using LH waves alone.

3.3.4 Electron Cyclotron Resonance Heating (ECRH)

Electron cyclotron resonance heating operates at the highest frequency range of the heating schemes. Despite the drawbacks of high frequency its advantage over other radio frequency schemes is that the waves launched are not evanescent and there is no matching problem so the waveguide can be set back from the plasma to avoid damage to itself and contamination of the plasma.

In the cold plasma approximation only the X-mode has a resonance in the plasma at the upper hybrid frequency. However, this resonance cannot be approached from the outside of the torus because the wave is reflected at the low density cutoff. This means that the wave has to be launched from the inside of the plasma to reach the upper hybrid resonance, which means that the antennae have to be put in the inside of the torus. This is in turn assumes that the conditions in the torus are such that the upper density cutoff is not present.

This is illustrated in figure 5, which is the high frequency part of the CMA diagram. If the wave is launched along the path 1 it is reflected at the cutoff, but if it follows path 2 on the high magnetic field side it can penetrate to the UH resonance.

Figure 5 also shows that in the cold plasma approximation the O-mode propagates into the plasma until it reaches its cutoff at $\omega = \omega_{pe}$ where it is reflected.

Consideration of the warm plasma terms shows that both modes are absorbed at the electron cyclotron frequency and its harmonics. Ie when

$$\omega - n\,\Omega_e - k_{\parallel} v_{th\,e} \approx 0 \qquad (3.16)$$

This means that in a tokamak where **B** depends on the major radius waves can be absorbed over a width

$$\Delta R \sim 2R \frac{k_{\parallel} v_{th\,e}}{n\,\Omega_e} \qquad (3.17)$$

In addition the position of the absorption layer can be changed by controlling the density of the plasma.

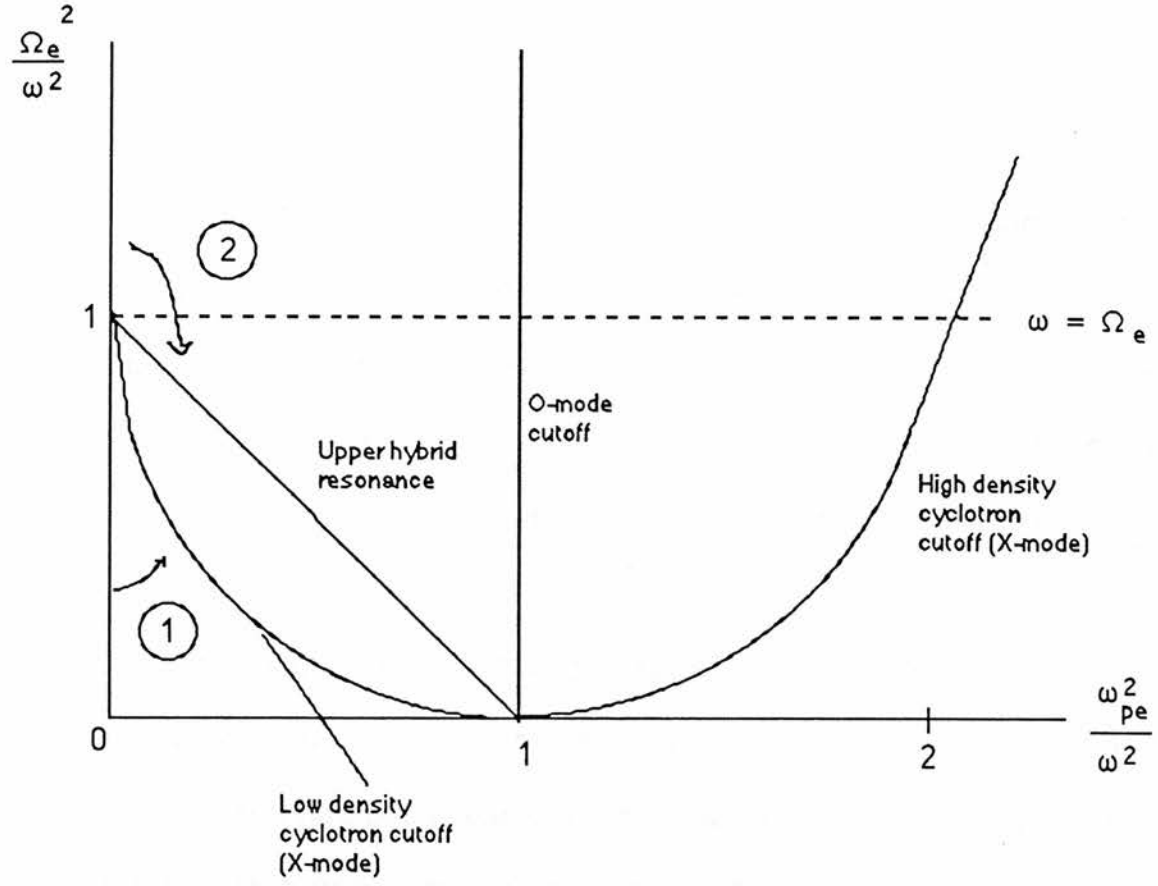

Fig 3.5 The high frequency part of the CMA diagram, showing upper hybrid resonance and the high and low cyclotron cutoffs. An X-mode wave launched along path 1 is reflected at the low density cutoff before it reaches the UH resonance. When launched along path 2 the X-mode can reach the UH resonance.

Only the fundamental and the first harmonic are likely to be used since the fraction of energy absorbed is less at the higher harmonics and more development of higher frequency sources would have to be carried out.

More details of the physics of the electron cyclotron resonance, although in the weakly relativistic case are given by Bornatici.

Experiments carried out on the WT-2 tokamak (Ando et al) show that it is possible to drive a current using electron cyclotron waves in tokamaks. The experiments showed that EC waves could sustain and ramp up the current in the tokamak when the ohmic heating had been switched off. These experiments were similar to the LH experiments reported in an earlier section. The EC waves gave their energy to a tail of high velocity electrons which had been formed during the ohmic heating phase of the discharge.

In addition experiments were carried out when EC waves were fed into the plasma after it had been heated using LH waves. In this case it was found that the rate of current ramp up was increased because the LH heating had produced a tail of weakly relativistic electrons which interact more efficiently with the EC waves.

CHAPTER 4 ABSORPTION OF WHISTLER WAVES IN A RFP

4.1 INTRODUCTION

As described in a previous chapter the reversed field pinch configuration persists as long as the reversal of the toroidal field in the the outer part of the plasma is sustained. This chapter investigates whether or not it is possible to extend the life of the configuration by using a poloidal current to increase the time the toroidal reversal exists.

The poloidal current is to be driven using radio frequency waves. The high frequencies used and the various plasma parameters show that the only wave which can propagate in an RFP is the whistler.

The RFP is modelled in slab geometry, using the cold plasma approximation, which is described in section 2.2. The damping of the waves is accounted for by the addition of the warm plasma corrections and the resultant Landau damping (section 2.3).

If the toroidal reversal is to be sustained successfully it would be best if the energy could be deposited only near the field reversal point. The results show that it is possible to deposit energy in a well defined region of the plasma, which can be varied by changing the plasma parameters.

4.2 SOLUTION OF COLD PLASMA DISPERSION RELATION

4.2.1 The model used and details of the parameters

The aim of this work is to see if it possible to sustain the toroidal field reversal in a reversed field pinch by driving a current in the poloidal direction and hence increase the length of the discharge.

To do this means solving the cold plasma dispersion relation, which has already been done in chapter 2, but it is easier to use a different notation. Solve the equation

$$n_x^4 - n_x^2 (A - 2 n_y^2) + n_y^4 - n_y^2 A + B = 0 \qquad (4.1)$$

where

$$A = \frac{[(\varepsilon_\perp - n_z^2) (\varepsilon_\perp + \varepsilon_{||}) - \varepsilon_{xy}^2]}{\varepsilon_{||}} \qquad (4.2a)$$

$$B = \frac{\varepsilon_\perp [(\varepsilon_\perp - n_z^2)^2 - \varepsilon_{xy}^2]}{\varepsilon_{||}} \qquad (4.2b)$$

The other symbols have the same meaning as in chapter 2.

With this combination of variables in A and B the solution to the biquadratic (1) is the simple form

$$n_x^2 = 0.5 A - n_y^2 \pm 0.5\sqrt{(A^2 - 4B)} \qquad (4.3)$$

To discover what the solutions of equation (3) look like in this context it helps to make some simplifying assumptions about the system. Consider the RFP in slab geometry rather than cylindrical geometry, with the x axis pointing towards the centre of the torus, y along what would be the toroidal direction and z along the poloidal direction as shown.

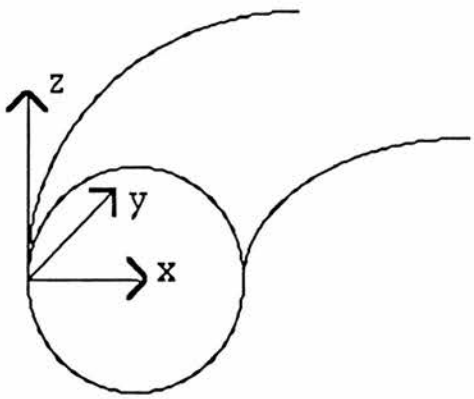

The diagram shows a cross section through part of a torus. Superimposed on this is the Cartesian coordinate system used when the torus is model in slab geometry.

Fig 4.1 Coordinate system applied to RFP.

However, in an RFP the magnetic field is not purely along the z-axis, but in the coordinate system used here is in the y-z plane. In addition the relative sizes of the toroidal and poloidal components of the magnetic field vary with x, which means that the magnetic field rotates in the y-z plane. Assume that the toroidal and poloidal fields are given by the J_0 and the J_1 Bessel functions.

(J_0 and J_1 Bessel functions of the first kind.)

The arguments of the Bessel functions can be changed to produce fields similar to those on a particular RFP. In this case the toroidal field is given by $J_0(3.8*(1-x/R))$ and the poloidal field by $J_1(2.4*(1-x/R))$. J_0 and J_1 are then multiplied by a scaling factor B, which gives the magnitude of the magnetic field at the centre of the plasma where the J_1 Bessel function (the poloidal field) is zero. (Typical values of B in an RFP are of the order of 0.15 tesla. However, many of the graphs shown later were plotted with a multiplying factor of 0.3 T, because at the time the program was being written it could only be made to work with this larger value of the magnetic field.)

Figure 2 shows how the magnetic field behaves. It rotates in the y-z plane and makes a varying angle $\theta(x) = \arctan(J_1 / J_0)$ with the z-axis. Figure 3 shows explicitly how the magnetic field components and $\theta(x)$ vary with distance, before they have been scaled by the factor B.

Equation (3) gives the behaviour of n_x^2 as a function of the other components of the refractive index and the plasma parameters. The behaviour of the n_y and n_z components is calculated using the parameters n and θ_0. n is the magnitude of the refractive index in the y-z plane, ie $n^2 = n_y^2 + n_z^2$; and θ_0 is the fixed angle n makes with the z-axis. The value of n is fixed by the antenna, but θ_0 can be varied by changing the angle the axis of the antenna

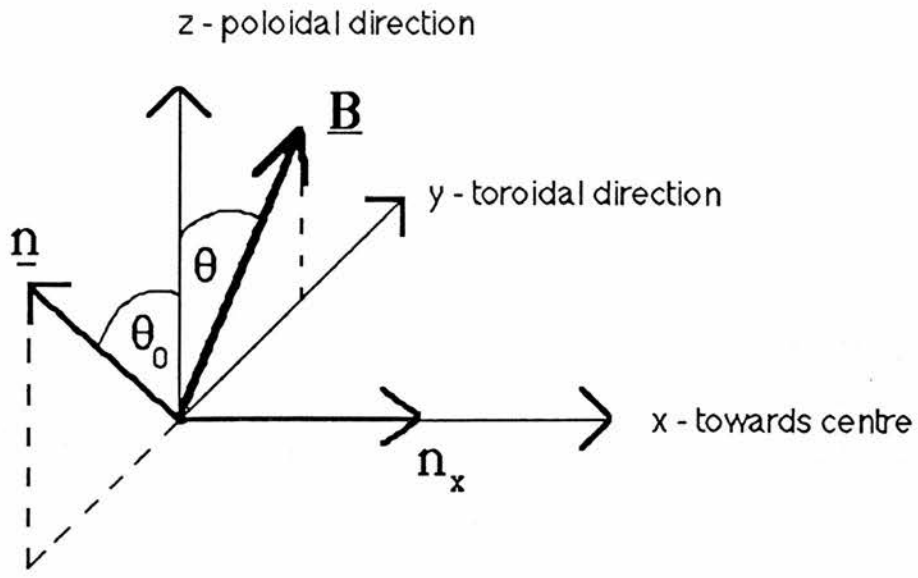

Fig 4.2 Coordinate system and variables to model RFP.

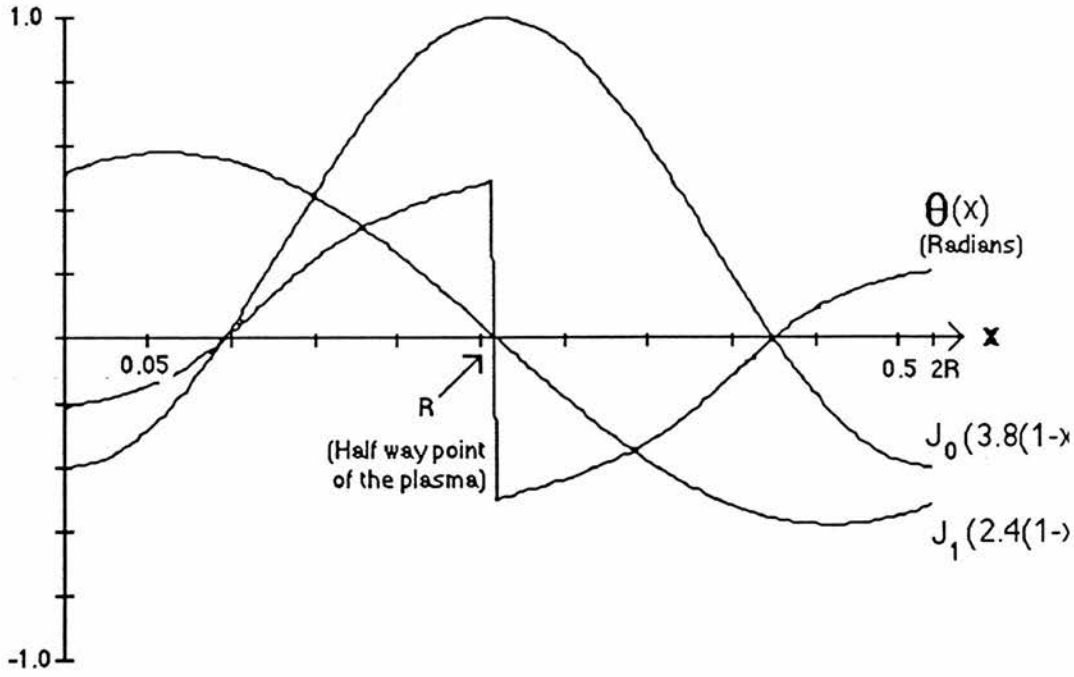

Fig 4.3 The magnetic fields in an RFP before they are scaled. The outer edge of the plasma is at x=0.

makes with the vertical. θ_0 is an important parameter in determining where wave energy will be deposited in the plasma, and will be discussed later.

When equation (3) was solved numerically on a computer n and θ_0 were treated as parameters which could be varied, along with the external frequency ω.

Finally, to solve equation (3) it is also necessary to specify the density profile of the plasma. This was taken to be parabolic, with its maximum at the centre of the plasma. In all the cases considered below the maximum density is 3×10^{19} m^{-3}.

4.2.2 Discussion of results

Parameters used in figures 4.1 to 6.7.

This section gives details of parameters used in the production of figures 4.1 to 6.7 by program CUTOFFS.

The radius of the torus is taken to be 0.26m, which is the minor radius of the HBTX1A RFP at Culham. The plasma is therefore treated as a slab of double this thickness. However, in any run of the program the x coordinate extend from the edge of the plasma to its centre at 0.26m because the aim of the program is to find parameters which allow energy to be deposited near the field reversal point, instead of 'bouncing' around the plasma.

In the graphs displayed here the values of x extend from 0 to the number called 'max x' at the bottom of each figure. Similarly the number 'max n_x^2 '

shows the maximum value of n_x^2 on each graph in a figure.

All the graphs show how the square of the refractive index in the x-direction varies with distance into the plasma. The full line is a plot of n_x^2 from equation (3) using the upper '+' sign and the dashed line the same plot using the lower '-' sign. The two branches meet where the argument of the square root becomes zero, and for higher values of x, n_x^2 becomes complex. In program CUTOFFS the value of x calculated for the second cutoff (ie where the two branches meet) is very slightly less than the true value to avoid trying to take the square root of a negative number. As a result the two branches of n_x^2 do not meet in the graphs shown here.

In any run of the program $\theta(x)$ and $\mathbf{B}(x)$ vary with position but are not affected by the values chosen for the other parameters. The scaling factor B has the constant value 0.3T in these diagrams.

Both θ_0 and θ are measured in radians. All the frequencies associated with the plasma are measured in units of gigaradians per second (G rad s^{-1}), as is ω, the angular frequency of the wave sent into the plasma.

Figures 4.1 and 4.2 show the effect of changing the frequency of the applied waves on the values of n_x^2 for a fixed value of n and varying values of θ_0. Comparison of the two sets of graphs shows that they are very similar apart from the n_x^2 scale. Changing the frequency from 0.5 G rad /s to 3.5 G rad /s

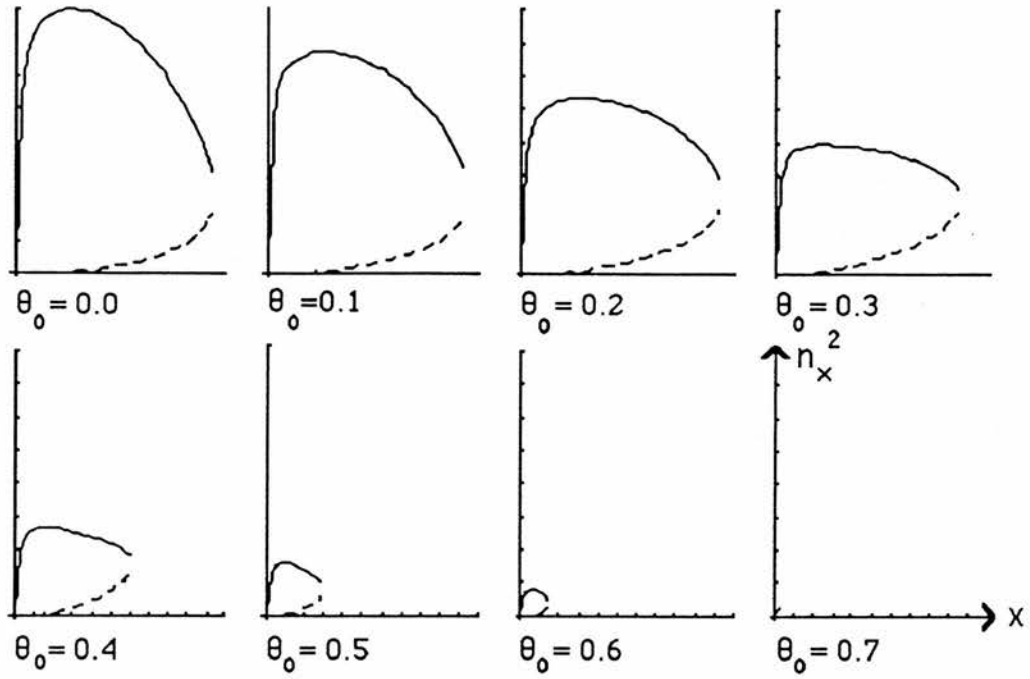

max n_x^2 = 801 000 max x = 0.11

Fig 4.4.1 Graph of n_x^2 v x for ω = 0.5 and n = 17

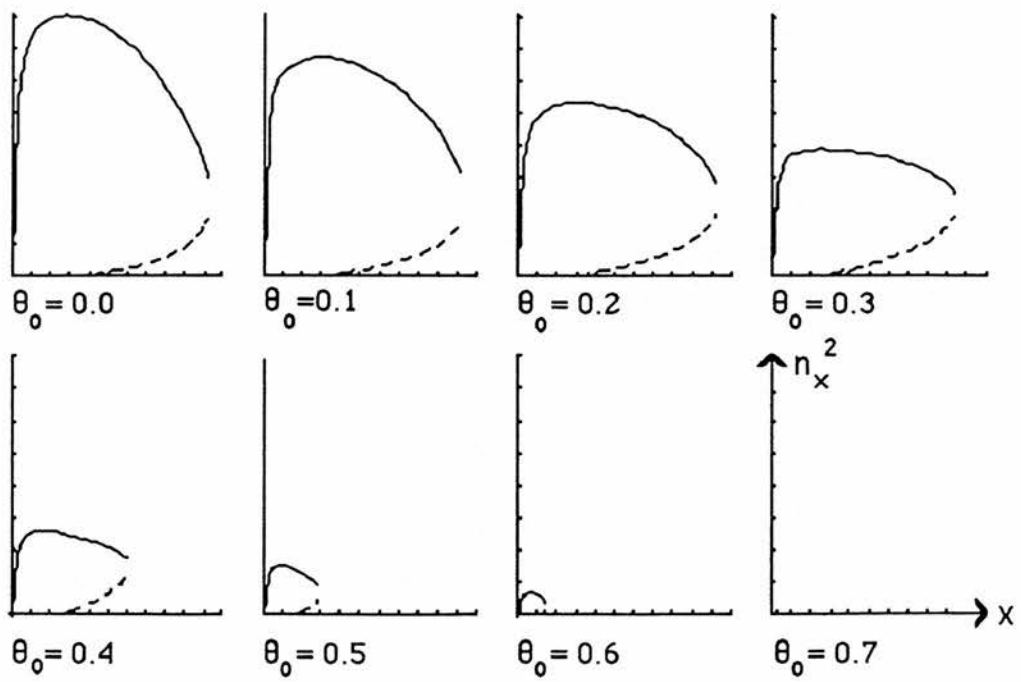

max n_x^2 = 16 100 max x = 0.11

Fig 4.4.2 Graph of n_x^2 v x for ω = 3.5 and n = 17

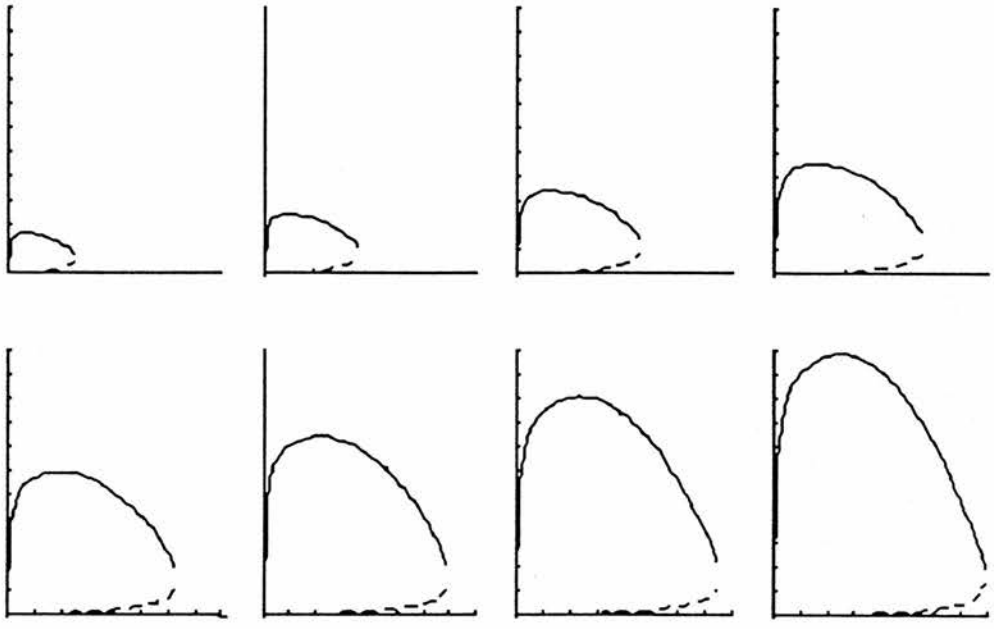

max n_x^2 = 2 200 000 max x = 0.16

Fig 4.5.1 Graph of n_x^2 v x for $\omega = 0.5$ and $\theta_0 = 0.0$

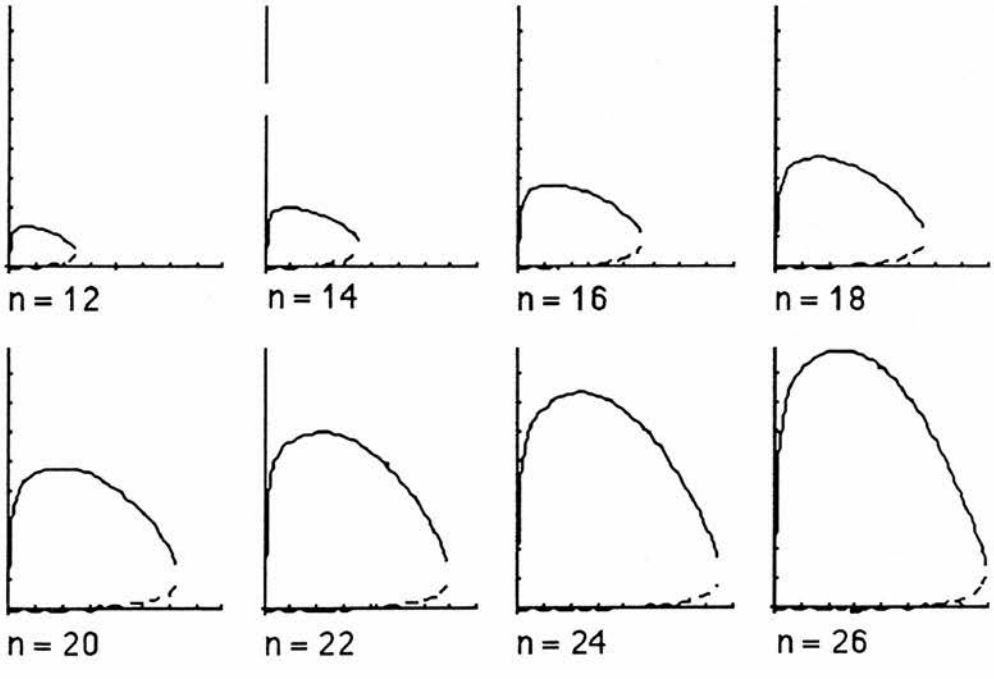

max n_x^2 = 44 000 max x = 0.16

Fig 4.5.2 Graph of n_x^2 v x for $\omega = 3.5$ and $\theta_0 = 0.0$

reduces the scale by a factor of about 50, which suggests that n_x^2 scales as $1/\omega^2$.

Now considering either set of graphs, we can see that θ_0 has a considerable effect on the shape of the graphs. As θ_0 increases the size of the graphs decreases and the second cutoff occurs nearer to the origin.

Figures 5.1 and 5.2 are complementary to 4.1 and 4.2. They again show the effects of changing the frequency of the waves, but they show how n_x^2 changes with n for a fixed value of θ_0. Again n_x^2 scales as $1/\omega^2$. The effect of increasing n is to increase the maximum value of n_x^2 and the distance of the second cutoff from the edge of the plasma.

Figures 6.1 to 6.7 follow on from figure 5.2 In all these figures the value of ω is 3.5 G rad s^{-1}. Within each set of graphs n increases from 12 to 26 in steps of 2. But each set of graphs has a higher value of θ_0 than the one before. It can be seen that θ_0 has a complicated effect on the behaviour of n_x^2.

Increasing θ_0 pushes the second cutoff further from the edge of the plasma, but at a certain value of θ_0 this changes and the second cutoff, instead of being at the centre of the plasma suddenly moves to within a few centimetres of the edge.

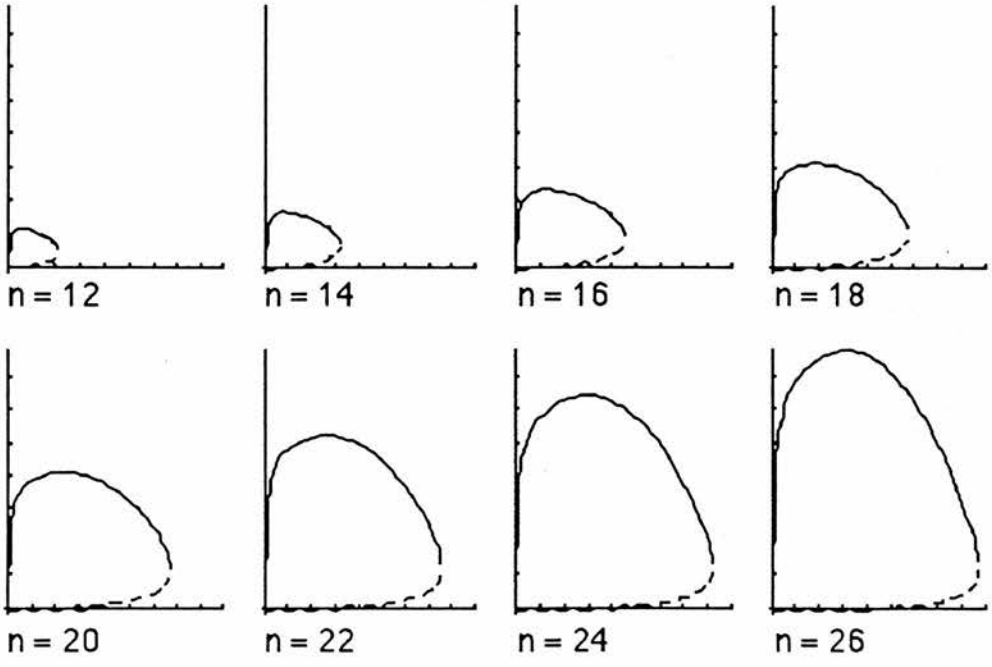

max n_x^2 = 39 000 max x = 0.18

Fig 4.6.1 n_x^2 v x for $\omega = 3.5$ $\theta_0 = 0.1$

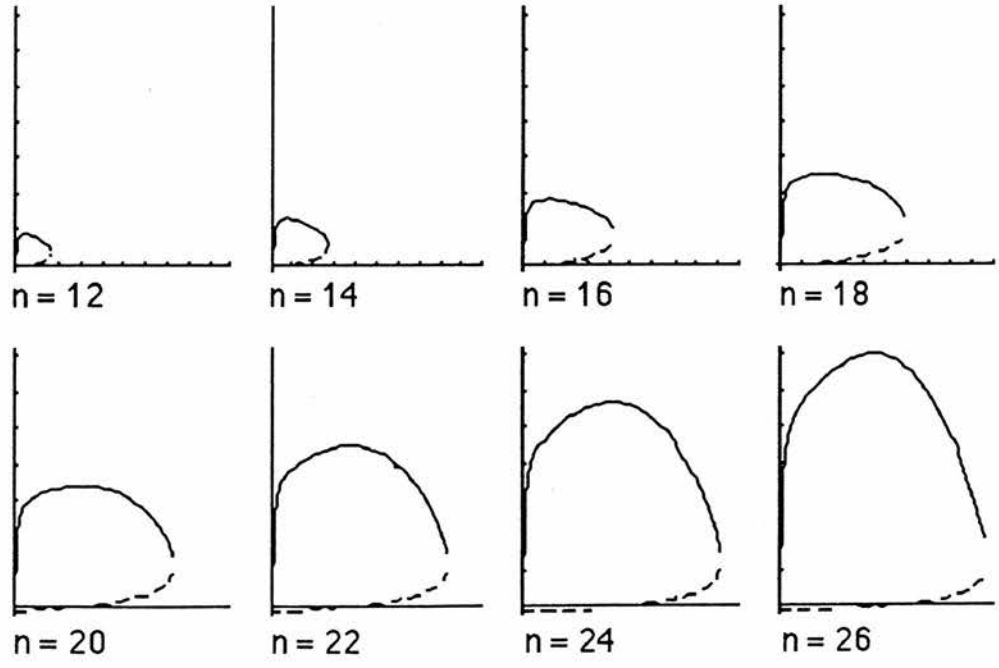

max n_x^2 = 36 000 max x = 0.20

Fig 4.6.2 n_x^2 v x for $\omega = 3.5$ $\theta_0 = 0.2$

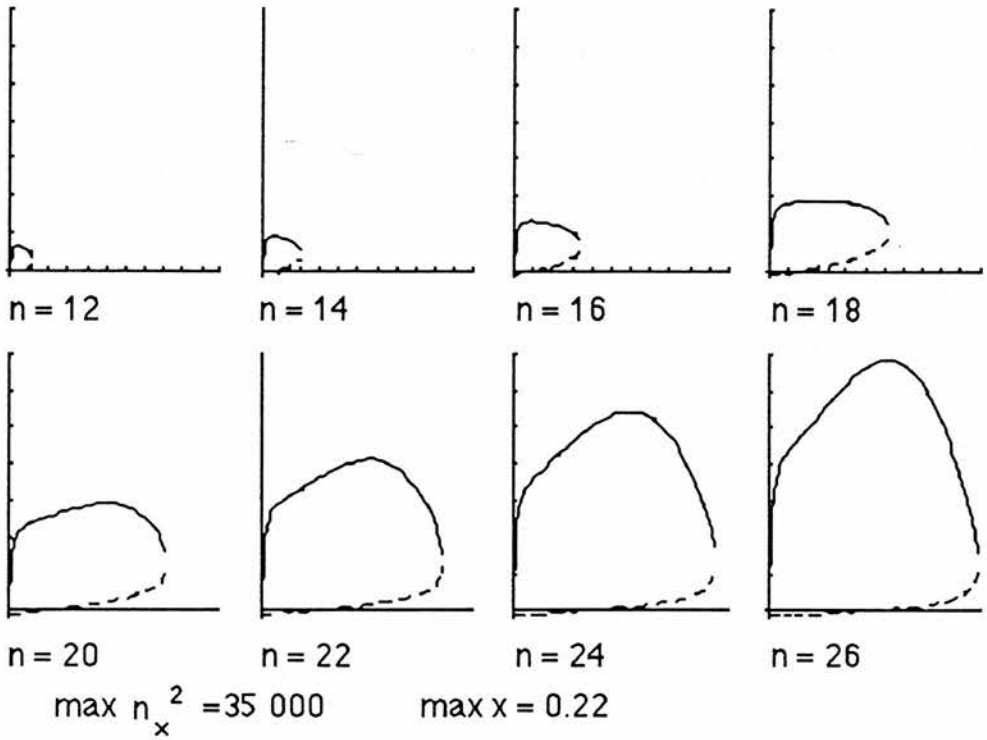

Fig 4.6.3 Graph of n_x^2 v x for $\omega = 3.5$ and $\theta_0 = 0.3$

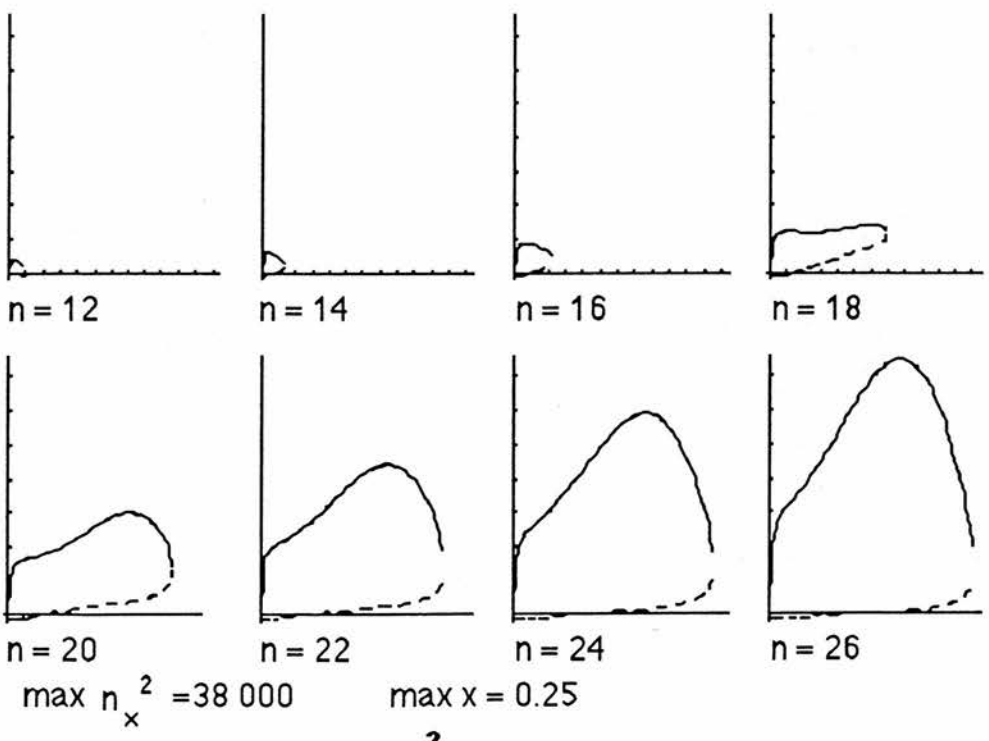

Fig 4.6.4 Graph of n_x^2 v x for $\omega = 3.5$ and $\theta_0 = 0.4$

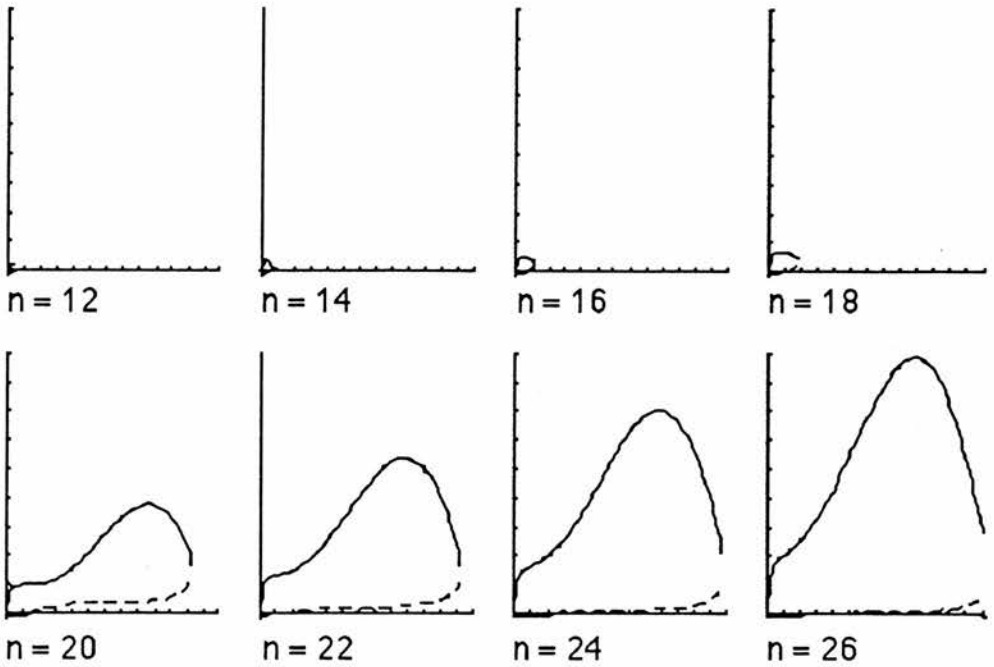

max n_x^2 = 45 000 max x = 0.26

Fig 4.6.5 Graphs of n_x^2 v x with $\omega = 3.5$ and $\theta_0 = 0.5$

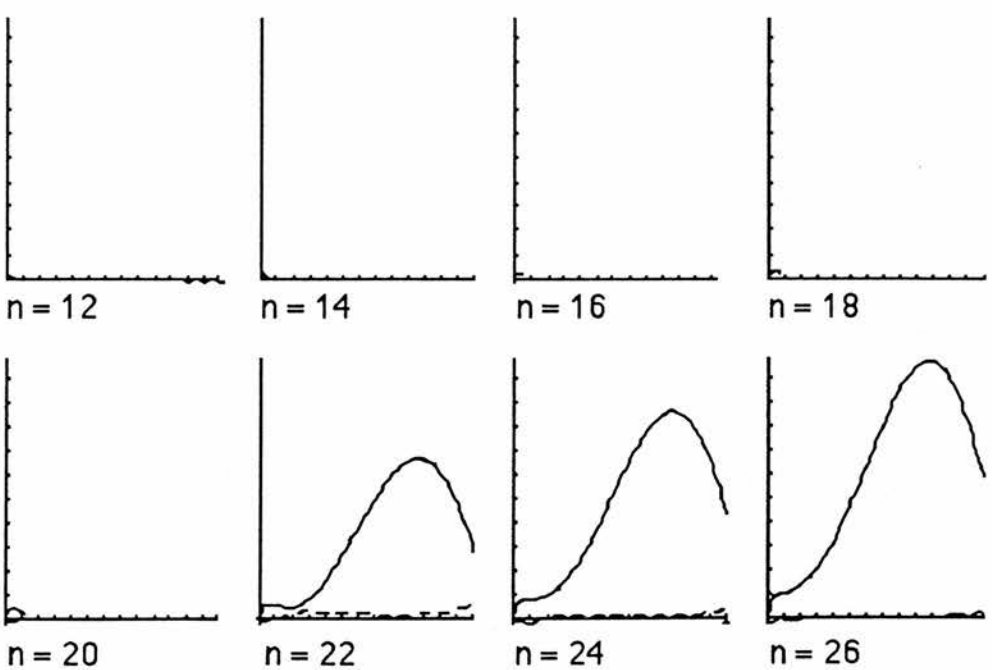

max n_x^2 = 54 000 max x = 0.26

Fig 4.6.6 Graphs of n_x^2 v x with $\omega = 3.5$ and $\theta_0 = 0.6$

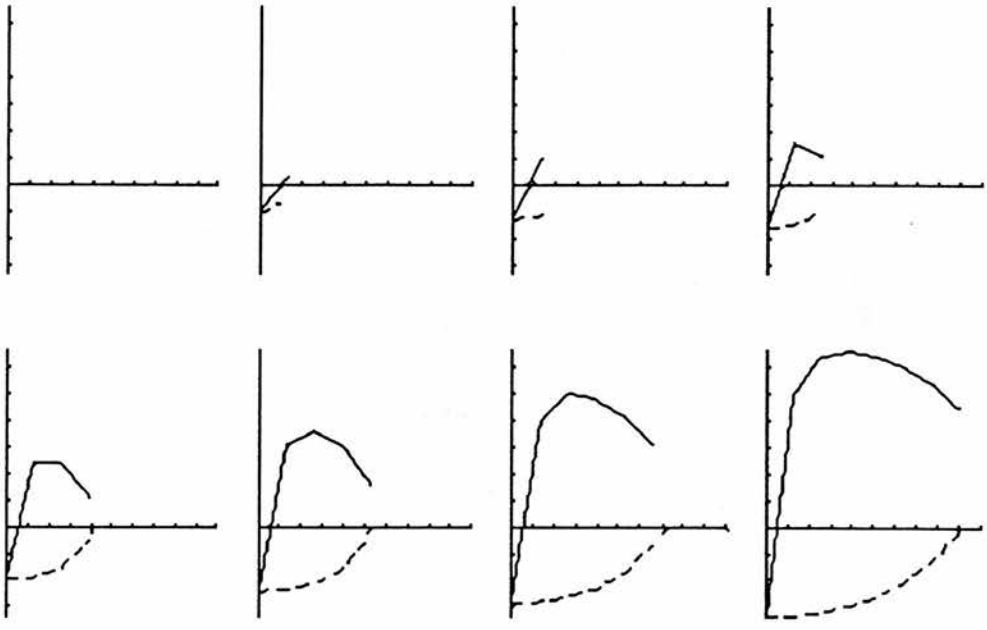

max n = 1 325 max x = 0.02

Fig 4.6.7 Graphs of n_x^2 v x for $\omega = 3.5$ and $\theta_0 = 0.7$

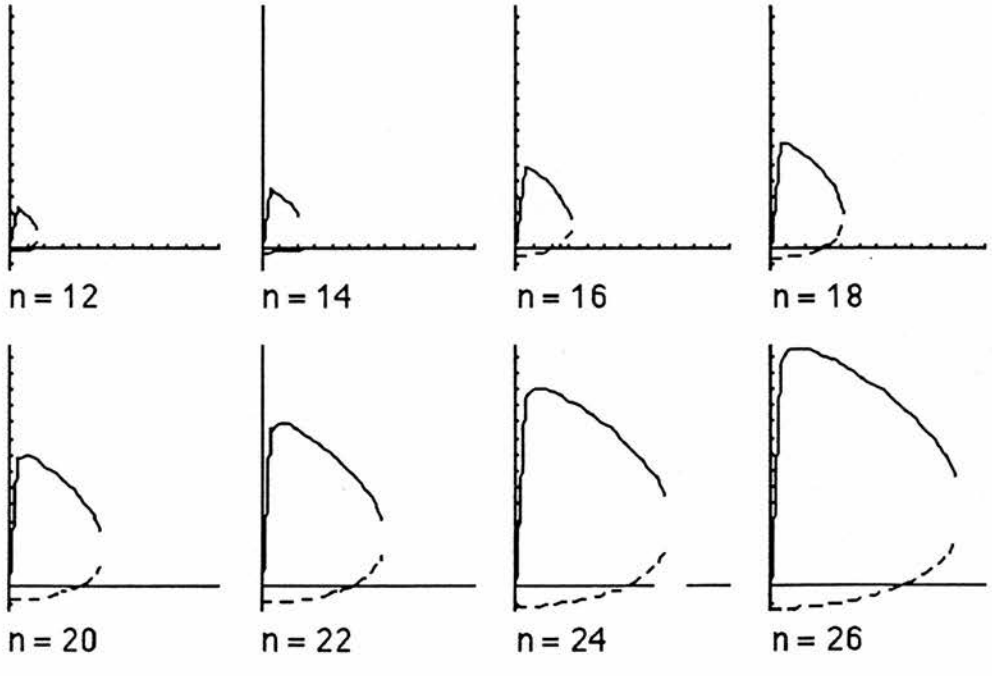

max n_x^2 = 7 300 max x = 0.06 m

Fig 4.7 Graph of n_x^2 v x for $\omega = 3.5$ and $\theta_0 = 0.1$, but with B = 0.15T.

4.2.3 Explanation of the results

The exact equation for n_x^2 is:- $n_x^2 = 0.5\,A - n_y^2 \pm 0.5\sqrt{(A^2 - 4B)}$. The expressions for A and B are given after equation (3). This section makes approximations for the values of the cold plasma dielectric tensor elements to try and explain the behaviour of the graphs discussed in the previous section.

One of the assumptions made in deriving equation (3) from cold plasma theory is that $\omega << \Omega_e$. To be able to make approximations in equation (3) it is also necessary to know the relative magnitude of the plasma frequency, ω_p. The number density of electrons in the slab of plasma is given by

$$n(x) = \frac{n_0 \, x \, (2R - x)}{R^2} \qquad (4.4)$$

and $n_0 = 3.10^{19}$ m^{-3} is the maximum density. With R = 0.26m the plasma frequency one centimetre from the edge of the plasma is 85 G rad s^{-1}, and at the centre of the plasma is 1 187 G rad s^{-1}. By comparison, the maximum value of the electron cyclotron frequency is 53 G rad s^{-1} at the centre of the plasma and less elsewhere.

Therefore it is assumed that $\omega << \Omega_e << \omega_p$ is the correct ordering of these three frequencies. Using this to find approximations for the dielectric tensor elements gives

$$\varepsilon_{\parallel} = 1 - X \approx -X = -\frac{\omega_p^2}{\omega^2}$$

$$\varepsilon_{\perp} = 1 - \frac{X}{1 - Y^2} \approx \frac{\omega_p^2}{\Omega_e^2} \qquad (4.5)$$

$$\varepsilon_{xy} = \frac{XY}{1 - Y^2} \approx -\frac{XY}{Y^2} = -\frac{\omega_p^2}{\omega\Omega_e}$$

The last equation also implies that, in this approximation

$$\varepsilon_{xy}{}^2 \approx -\varepsilon_{\parallel}\,\varepsilon_{\perp} \qquad (4.6)$$

The previous equations give the ordering of the tensor elements as

$$|\,\varepsilon_{\parallel}\,| >> |\,\varepsilon_{xy}\,| >> \varepsilon_{\perp} \qquad (4.7)$$

This means that $\varepsilon_{\perp}$ can be neglected compared to $\varepsilon_{\parallel}$ and ε_{xy}.

Using these approximations in the expression for A gives

$$\varepsilon_{\perp} A \approx \varepsilon_{\parallel}(\varepsilon_{\perp} - n_z^2) - \varepsilon_{xy}{}^2 = 2\varepsilon_{\parallel}\,\varepsilon_{\perp} - \varepsilon_{\parallel} n_z^2$$ which

finally gives

$$A \approx \frac{\Omega_e^2 (n_z^2 - 2\varepsilon_{\perp})}{\omega^2} \qquad (4.8)$$

It is difficult to proceed further than this because the relative sizes of n_z^2 and $\varepsilon_{\perp}$ vary as x increases.

Now consider an approximation for A^2 -4B, using the exact expression for A, not the approximation in equation (8).

Then

$$\varepsilon_\perp{}^2 (A^2 - 4B) = (\varepsilon_\perp - n_z{}^2)^2 \, (\varepsilon_\perp - \varepsilon_{||})^2 \; - \; 3 (\varepsilon_\perp \varepsilon_{||})^2 \; +$$

$$2 \varepsilon_\perp \varepsilon_{||} (\varepsilon_\perp - n_z{}^2) (\varepsilon_\perp + \varepsilon_{||})$$

Neglecting $\varepsilon_\perp$ in the terms of the form $(\varepsilon_\perp \pm \varepsilon_{||})$ gives finally

$$(A^2 \; - \; 4B) \;\; = \;\; \frac{\Omega^2 \, n_z \, (n_z^2 \; - \; 4\varepsilon_\perp)^{1/2}}{\omega^2} \qquad (4.9)$$

Assuming that the n_y term is also small compared to the terms kept, the approximation for $n_x{}^2$ is

$$n_x^2 \;\; \approx \;\; \frac{\Omega^2 \, [\, n_z^2 \; - \; 2\varepsilon_\perp \; \pm \; n_z \, (n_z^2 \; - \; 4\varepsilon_\perp)^{1/2} \,]}{2\omega^2} \qquad (4.10)$$

This does show a one over ω^2 dependence as predicted earlier, because the terms in the square bracket are independent of ω. Equation (10) also appears to show that $n_x{}^2$ is proportional to Ω^2. This is not the case because $\varepsilon_\perp$ is inversely proportional to Ω^2, so $n_x{}^2$ does not change as quickly with changes in the magnetic field as would appear at first sight. Figure 7 is drawn

with the same parameters as figure 6.1 except that the scaling factor for the magnetic field is 0.15T not 0.3T. Comparison of the two does show a decrease in the values of n_x^2 when the magnetic field is decreased, but not by a factor of 4.

Again it would be difficult to simplify (10) because of the relative sizes of n_z^2 and $\varepsilon_\perp$. It is not possible to use (10) to see if n_x^2 is proportional to a power of θ_0 because the only dependence on θ_0 left is in the n_z terms.

4.2.4 The position of the Cutoffs

Figures 4.8.1-5 show how the position of the first cutoff varies as a function of θ_0, for B = 0.3T. (At x_1 the wave begins to propagate in the plasma.) In the graphs each dashed line uses ω, the frequency of the wave, as a parameter. In going from 4.8.1 to 4.8.5 the value of n changes from 20 to 28. These high values of n were used because they are the ones which give substantial (> 30%) absorption of the incident wave.

From the graphs we see that the position of the first cutoff changes by a small amount as n increases, but depends strongly on θ_0 and the frequency of the wave. The thickness of the evanescent layer can be minimised by using low frequency waves and keeping the angle the perpendicular component of the wave makes with the z-axis small.

Figure 4.9 is the corresponding diagram for the second cutoff, the point

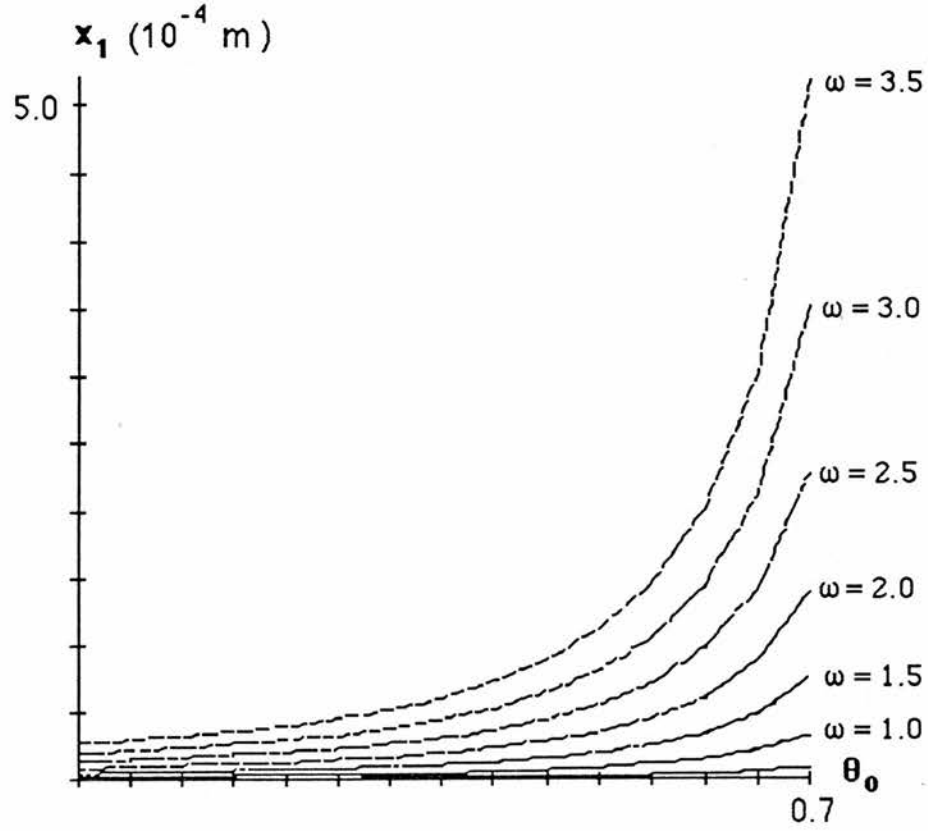

Fig 4.8.3 Graph of first cutoff v twist, for n = 24.

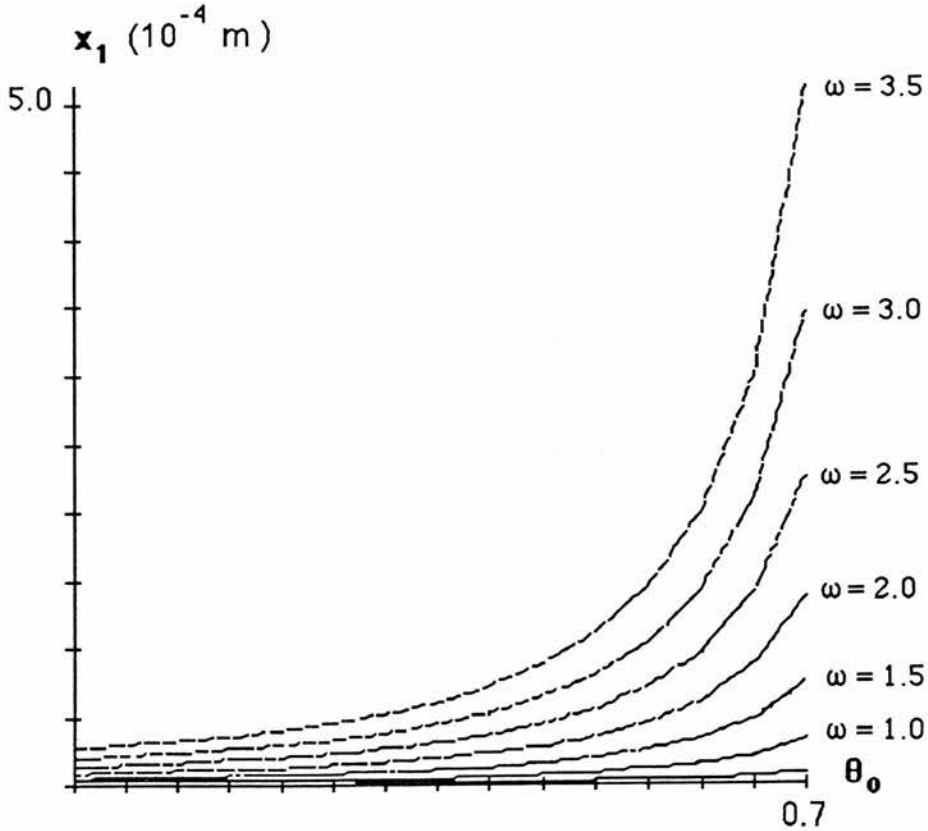

Fig 4.8.4 Graph of first cutoff v twist, for n = 26.

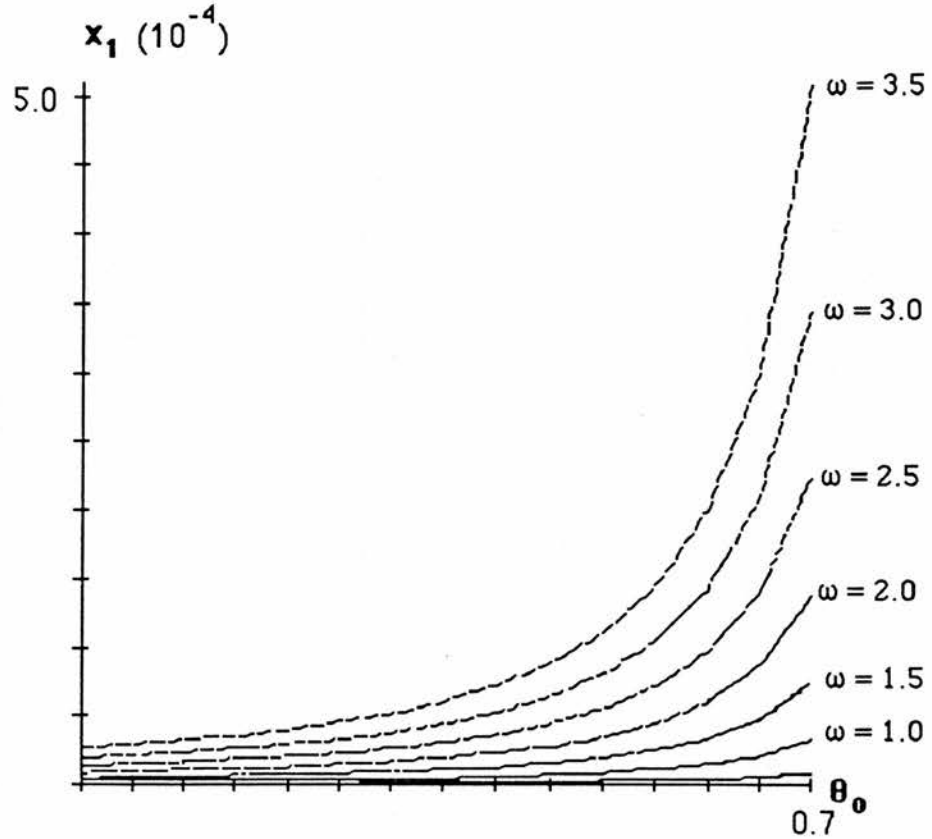

Fig 4.8.5 Graph of first cutoff v twist, for n = 28.

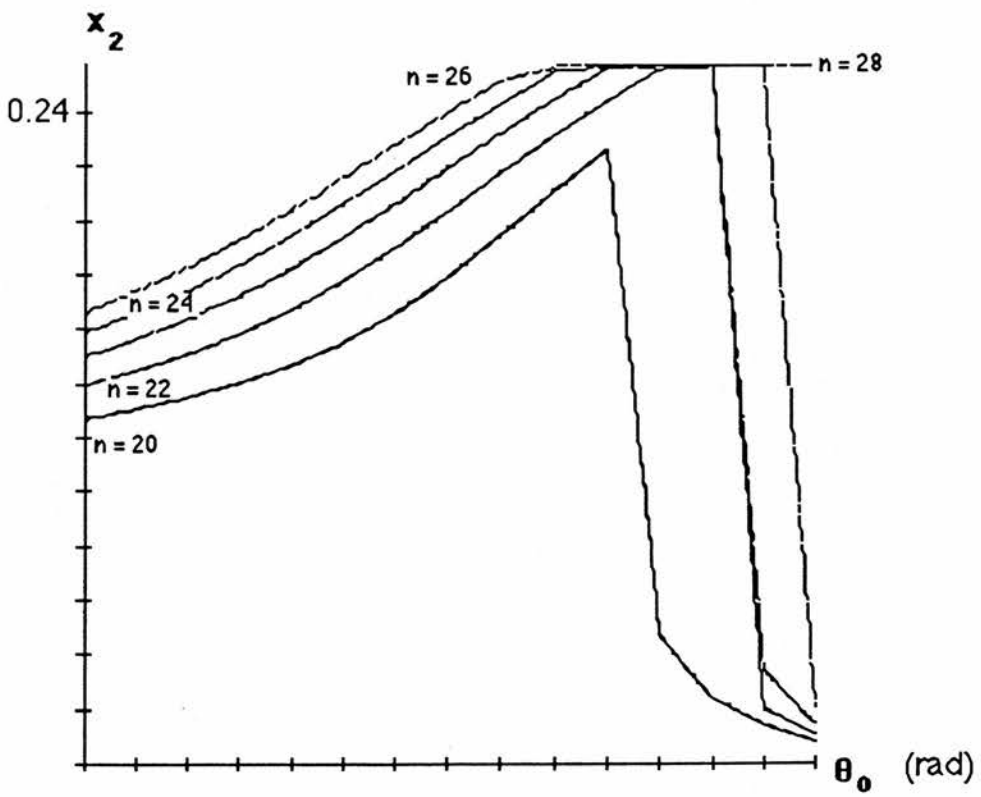

Fig 4.9 Graph of second cutoff v twist, for ω=3.5.

where n_x^2 becomes complex and the wave is strongly damped. The main difference between the two diagrams is that the frequency plays a less important part in determining the frequency of the second cutoff. The variation in the position of x_2 is comparable to that of x_1, but is swamped by the greater size of x_2.

The value of the perpendicular component of the refractive index, n, plays an important part in determining the position of the second cutoff.

The flat part at the top of the graph when n changes from 22 to 28 indicates that the second cutoff had not been reached when the program stopped calculating at the centre of the plasma.

The abrupt change in x_2 for large values of θ_0 can be seen by comparing figures 6.6 and 6.7. For the values of n comparable with those in figure 4.9 the second cutoff suddenly moves almost to the edge of the plasma as θ_0 changes from 0.6 rad to 0.7 rad.

4.3 ABSORPTION OF WAVES IN PLASMA

4.3.1 Behaviour near the edge of the plasma

Examination of the graphs in the previous section shows that at the edge of the plasma the upper branch of the square of the refractive index in the x direction changes rapidly from the value $1-n^2 < 0$ to a large positive value. This means that the waves are evanescent in a small region at the edge of the plasma. The change in n_x^2 is so rapid near the edge of the plasma that its behaviour can be approximated by a straight line.

The change in intensity of the wave in the edge region can be found by calculating the slope of the upper branch of n_x^2 ($\mu\, k_x^2$) at x=0 and using the fact that near the edge $k_x^2 = \lambda(x - x_1)$ in the equation

$$\frac{d^2 E}{dx^2} + k_x^2 E = 0 \qquad (4.11)$$

x_1 is the point where the wave stops being evanescent and begins to propagate, ie the first cutoff. The value of λ is given by the first derivative of k_x^2 at x = 0.

$$\left.\frac{d k_x^2}{dx}\right|_{x=0} = \frac{ne^2 \left[Y^2 (1 - n_z^2) - 2 - Y^2 \{(n_z^2 - 1)^2 + \frac{4n_z^2}{Y^2} \}^{1/2} \right]}{\varepsilon_0 mc^2 R (1 - Y^2)} \qquad (4.12)$$

In equation (12) R is the radius of the torus and $\lambda = d\, k_x^2 / dx$ at x=0.

Although R stands for the radius of the torus it is still relevant here because it is the half width of the slab, and is used to calculate the values of X (the square of the ratio of the plasma and external frequencies.) The relevant solution of equation (11) is the Bi Airy function because this is the one that decays in the plasma.

4.3.2 Warm Plasma Corrections

In the cold plasma approximation there is no absorption of energy in the plasma. One way to see how much energy is absorbed in the plasma is to use the warm plasma corrections to the cold plasma dispersion relation. This means that the wave looses energy by Landau damping. (It is shown in chapter 2 that the effect of Landau damping is to introduce a small imaginary component in the frequency of the wave.) At sufficiently low temperatures the only change is in the $\varepsilon_{||}$ term which becomes

$$\varepsilon_{||} \Rightarrow \varepsilon_{||} + i\delta\varepsilon_{||} \tag{4.13}$$

with $$\delta\varepsilon_{||} = 2\sqrt{\pi}\, X\, u_0^3 \exp(-u_0^2) \tag{4.14a}$$

and

$$u_0 = \frac{c}{2^{1/2} n_z v_{te}} \tag{4.14b}$$

where v_{te} is the electron thermal velocity and u_0 is the ratio of the phase velocity of the wave to the thermal velocity of the electrons.

Substituting $\varepsilon_{\parallel} + i\delta\varepsilon_{\parallel}$ into equation (3), with the assumption that n_x can be replaced by $n_x + i\delta n_x$ gives

$$\delta n_x = \frac{i\,\delta\varepsilon_{\parallel}\{(n_x^2 + n^2 - \varepsilon_{\perp})(\varepsilon_{\perp} - n_z^2) + \varepsilon_{xy}^2\}}{\varepsilon_{\perp} n_x\{4n_x^2 + 2(2n_y^2 - A)\}} \qquad (4.15)$$

assuming that terms $O(\delta^2)$ are neglected.

Equation (15) then gives an expression for δk_x, which is used to find where the energy is deposited in the plasma.

Substituting $k_x + i\,\delta k_x$ for k_x in the expression $\exp i(k_x x - \omega t)$ gives the attenuating factor as $\exp(-\int \delta k_x\, dx)$. However, the group velocity of the wave is negative, so the attenuation of the wave is given by $\exp(\int \delta k_x\, dx)$.

4.3.3 Absorption of the wave in the plasma

In program CUTOFFS the integral $\int \delta k_x\, dx$ was calculated using the trapezium rule. The range of integration was from the first cutoff to the second. The range was divided into one hundred steps, each of which could be subdivided into NINC substeps. The intensity of the wave is still plotted at the end of the larger steps, not at the substeps within them. In addition the intensity of the wave is normalised to one at the edge of the plasma.

In figures 10.1 to 12 NINC was set to one and the value of B is 0.3T.

The diagrams in figures 10.1 to 10.5 show how the amount of energy left in the wave at the first cutoff varies for different values of twist. The most

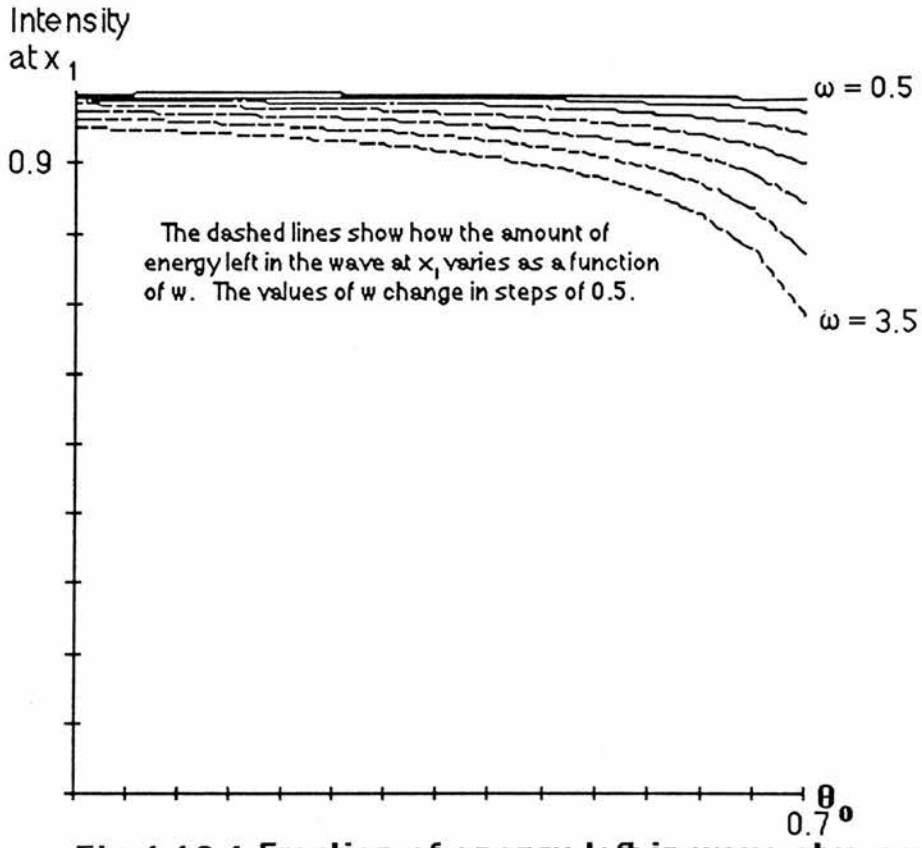

Fig 4.10.1 Fraction of energy left in wave at x_1 as a function of twist, for n = 20.

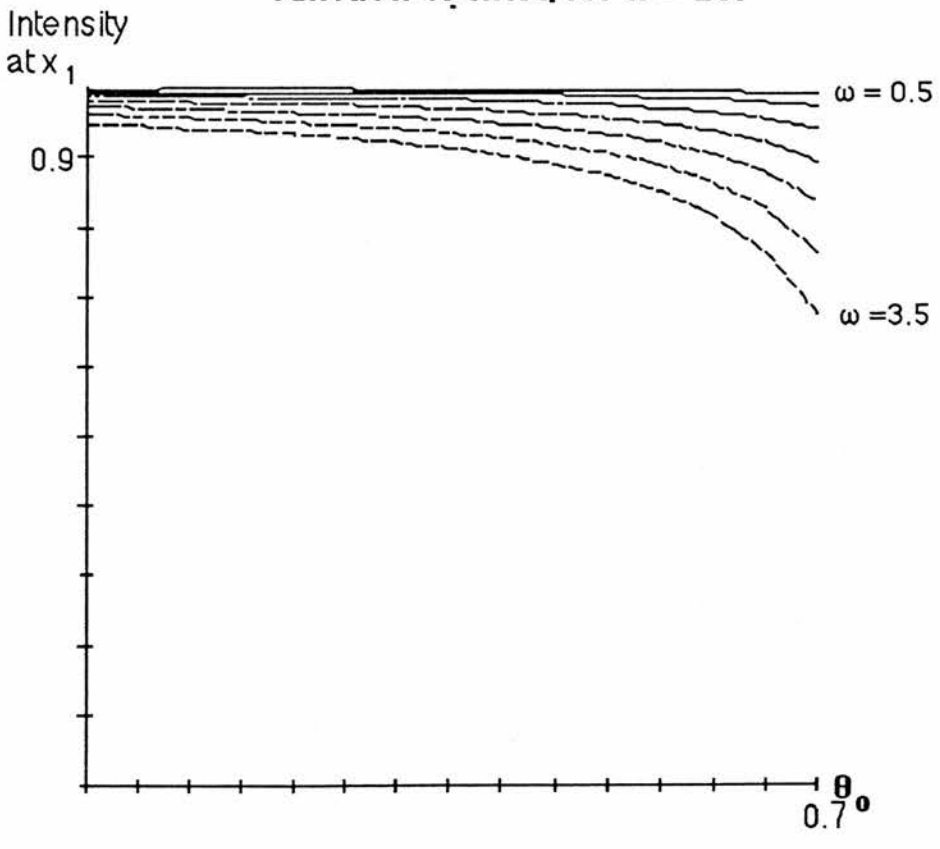

Fig 4.10.2 Fraction of energy left in wave at x_1 as a function of twist, for n = 22.

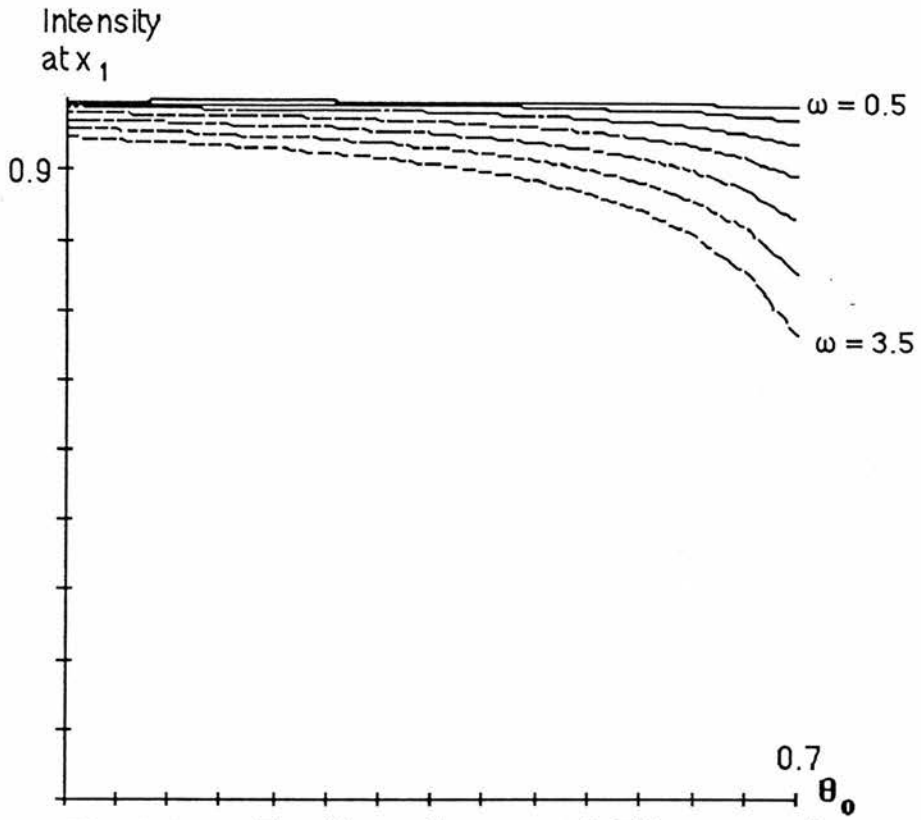

Fig 4.10.3 Fraction of energy left in wave at x_1 as a function of twist, for n = 24.

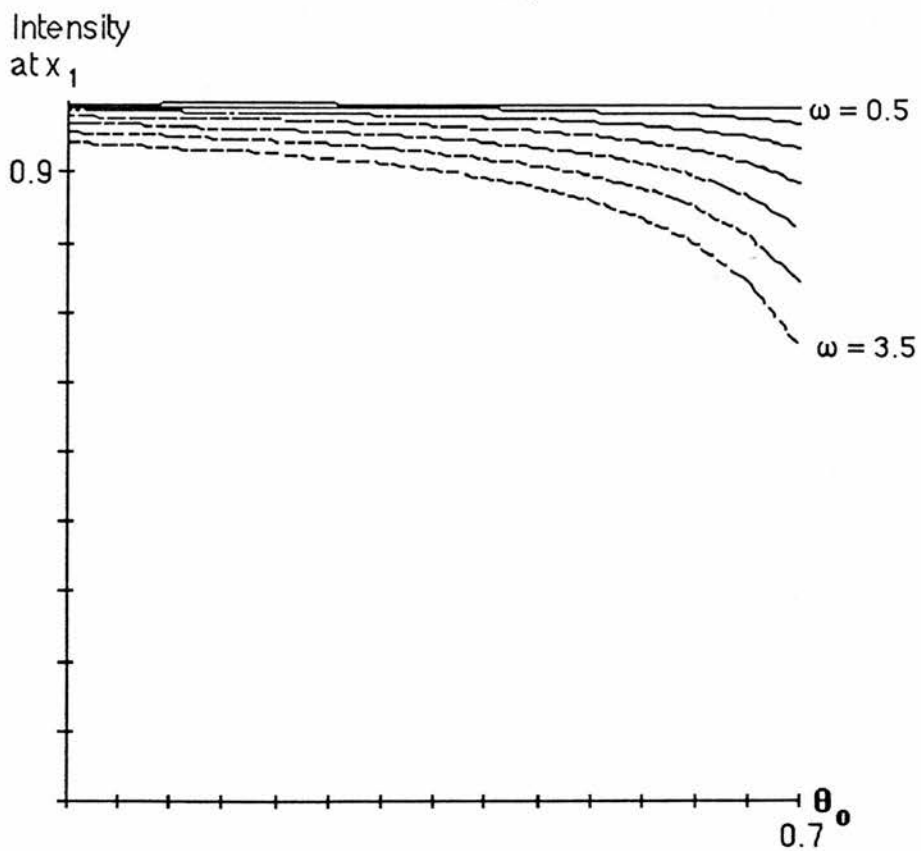

Fig 4.10.4 Fraction of energy left in wave at x_1 as a function of twist, for n = 26.

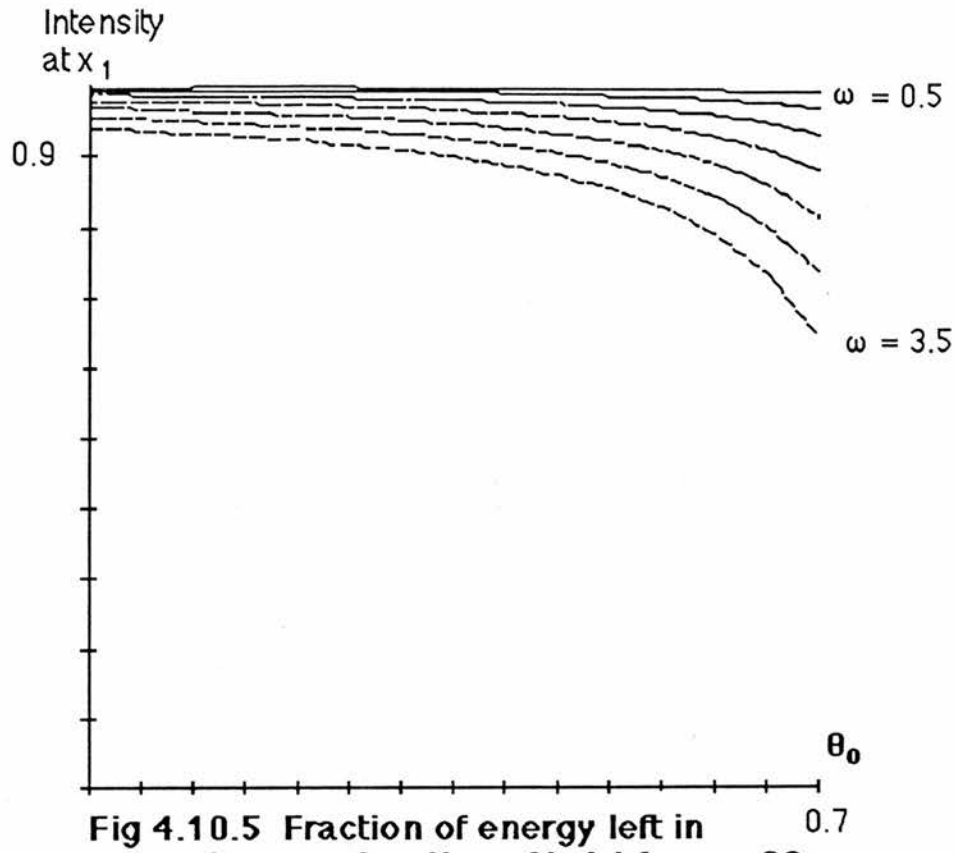

Fig 4.10.5 Fraction of energy left in wave at x_1 as a function of twist for n = 28.

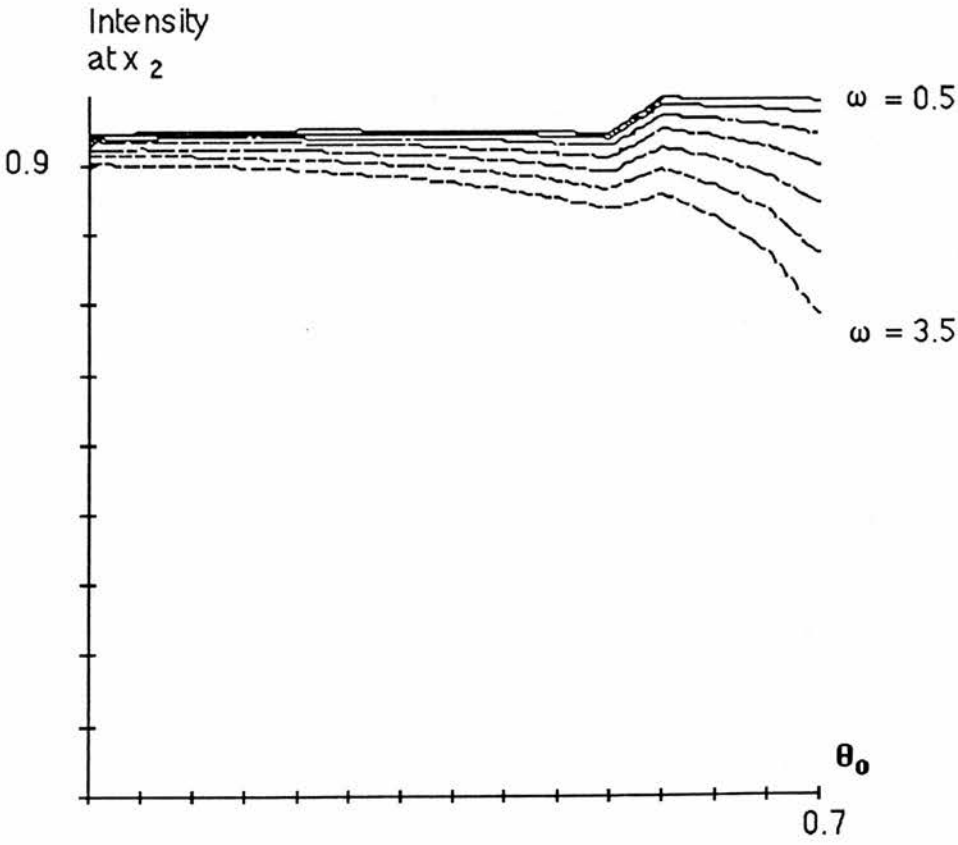

Fig 4.11.1 Fraction of energy left in wave at x_2 as a function of twist for n = 20.

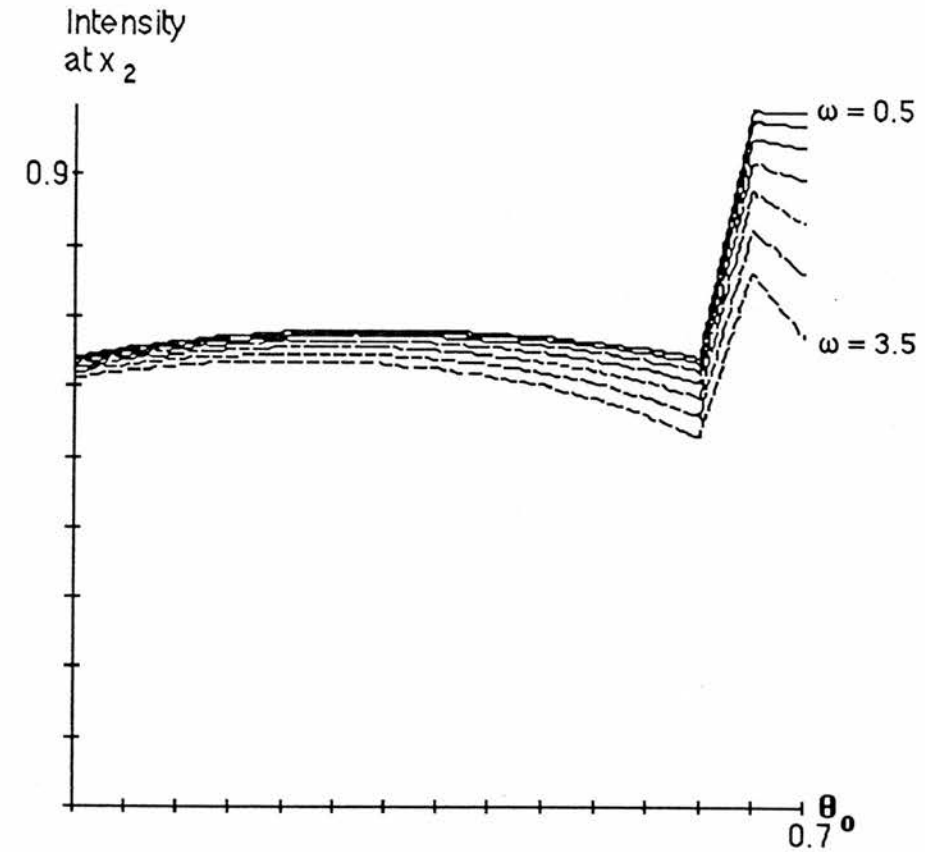

Fig 4.11.2 Fraction of energy left in wave at x_2 as a function of twist, for n = 24.

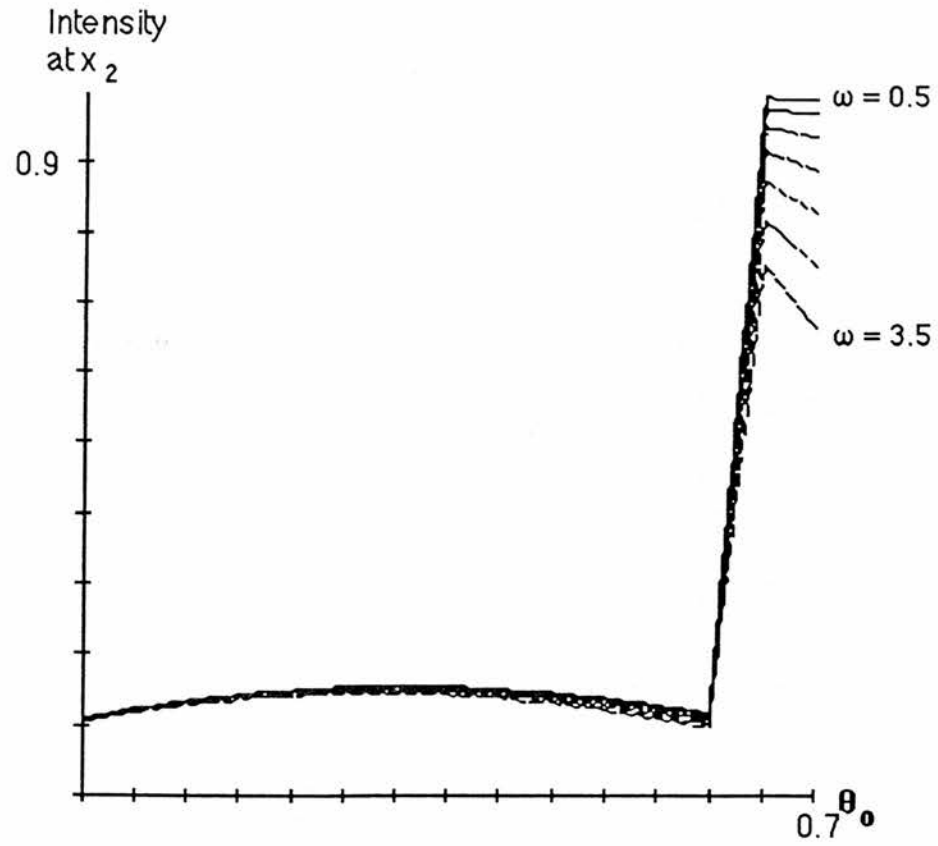

Fig 4.11.3 Fraction of energy left in wave at x_2 as a function of twist, for n = 26.

obvious point is that the higher the frequency the less energy penetrates to the bulk of the plasma, so this suggests choosing low values for the frequency of the wave. This is partly explained by looking at figs 8.1 - 8.5 which show how the width of the evanescent layer increases as ω increases.

The second point is that the fraction of energy in the wave tunnelling into the plasma is reduced as the twist increases. This means that more energy is reflected by the evanescent layer as the angle the perpendicular component of the propagation vector makes with the magnetic field at the edge of the plasma increases. There is little change in the amount of energy transmitted to the plasma as n increases.

Figures 11.1 - 3 show how the amount of energy reaching the second cutoff varies as n increases. The graphs for n = 26 and n = 28 are not present because all the energy has been absorbed by the second cutoff. Once again the amount of energy left in the wave at the second cutoff decreases as ω increases. The higher absorption of energy is desirable in this case because it means that more of the energy has been deposited in the plasma. As n increases more of the energy is absorbed.

Figure 12 plots the fraction of energy transmitted through the first cutoff which has been absorbed by the second cutoff. Figure 12 is plotted for ω = 3.5, but the results are similar for all the values of ω.

Figures 13.1 - 6 show how the fraction of energy left in the wave is reduced as it propagates into the plasma. The full line shows the fraction of energy left in the wave and the dashed line shows where the energy has been

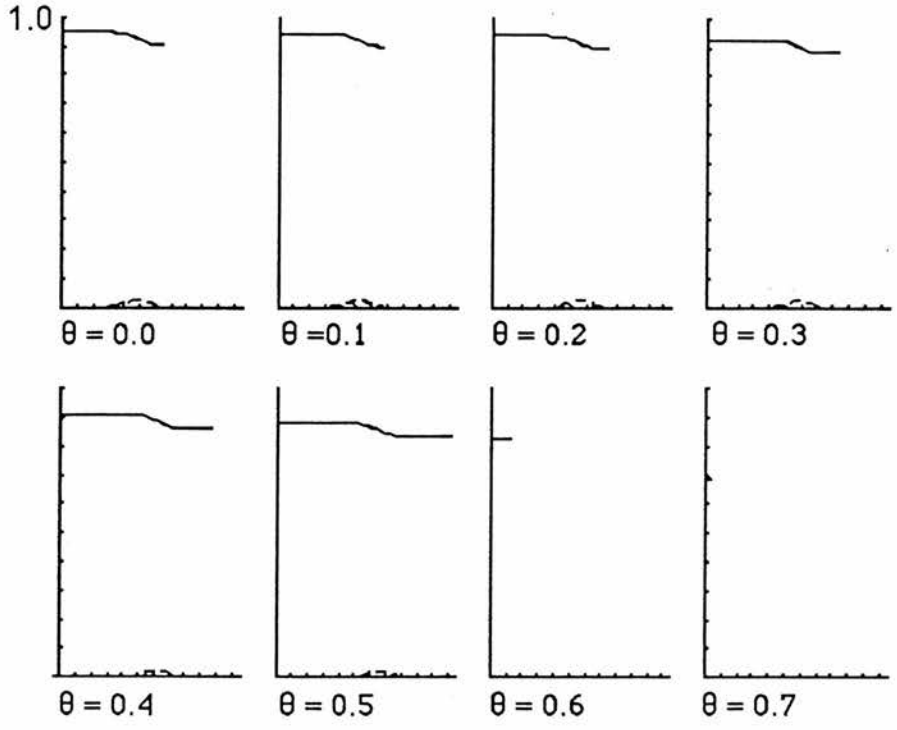

Fig 4.13.1 Relative intensity v x, for n = 20, ω= 3.5. max x = 0.23

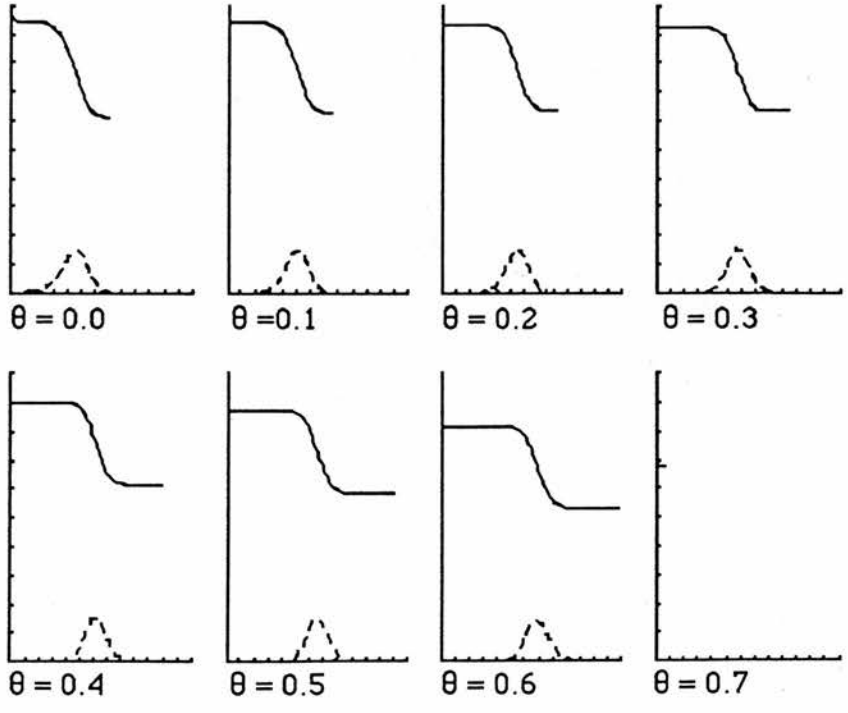

Fig 4.13.2 Relative intensity v x, for n = 22, ω= 3.5. max x = 0.26

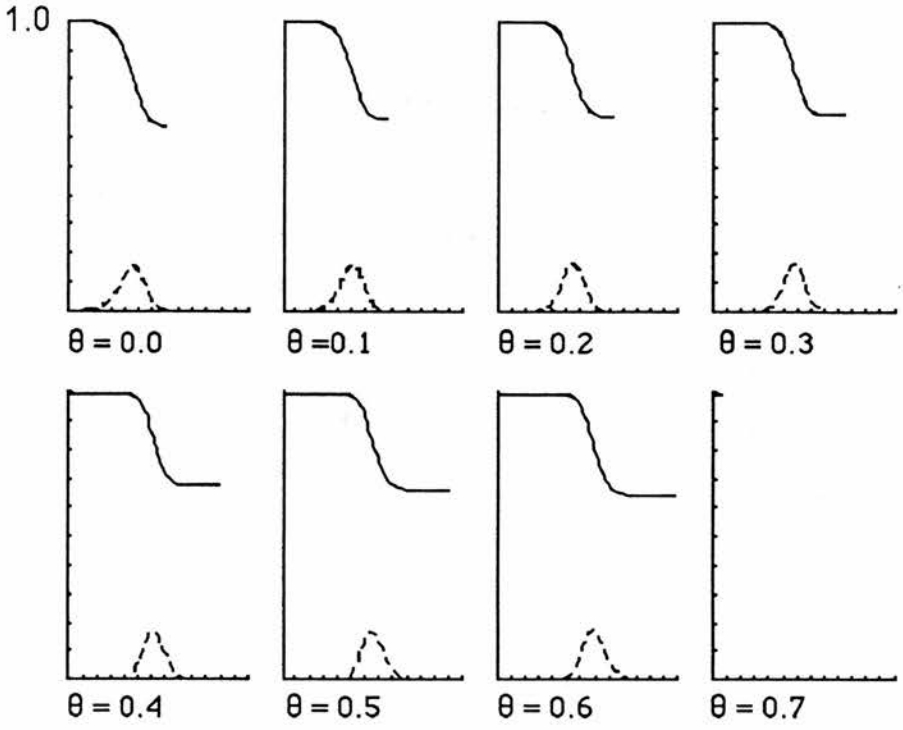

Fig 4.13.3 Relative intensity v x, for n = 22, ω= 0.5. max x = 0.26

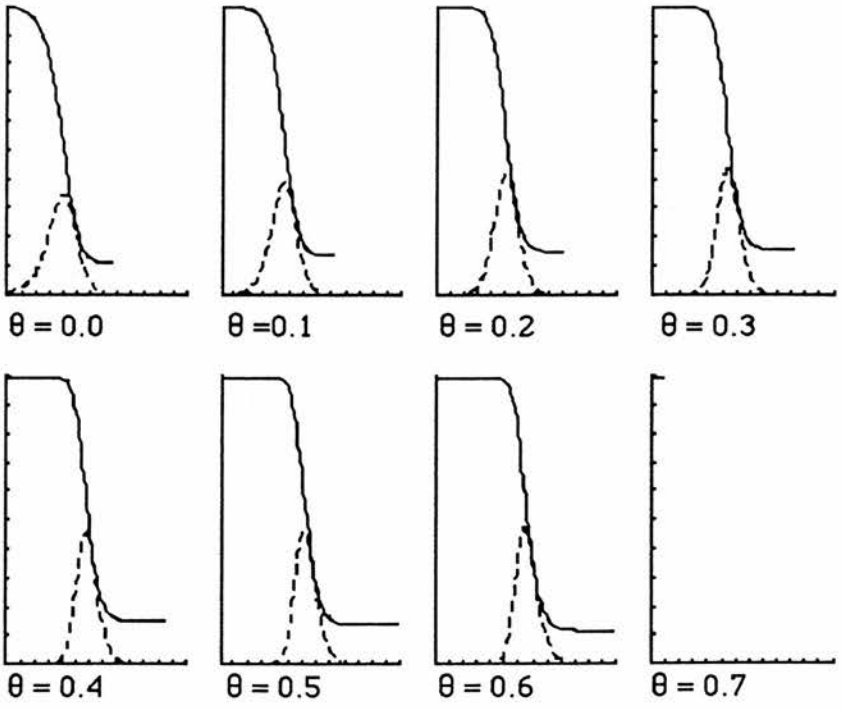

Fig 4.13.4 Relative intensity v x, for n = 24, ω= 0.5. max x = 0.26

θ = 0.0 θ =0.1 θ = 0.2 θ = 0.3

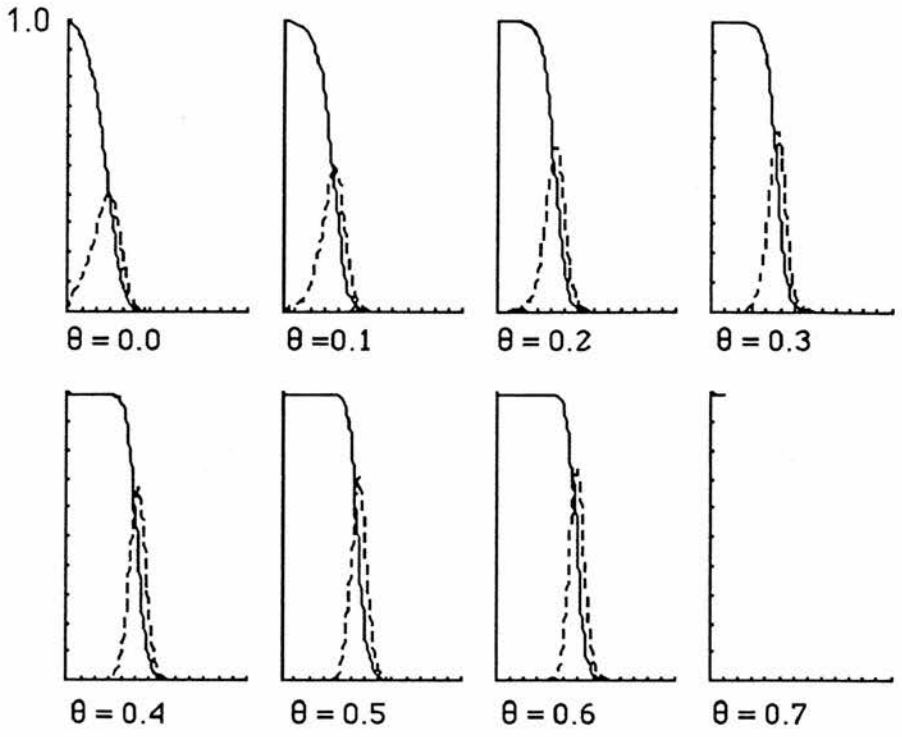

Fig 4.13.5 Relative intensity v x, for n = 26, ω= 0.5. max x = 0.26

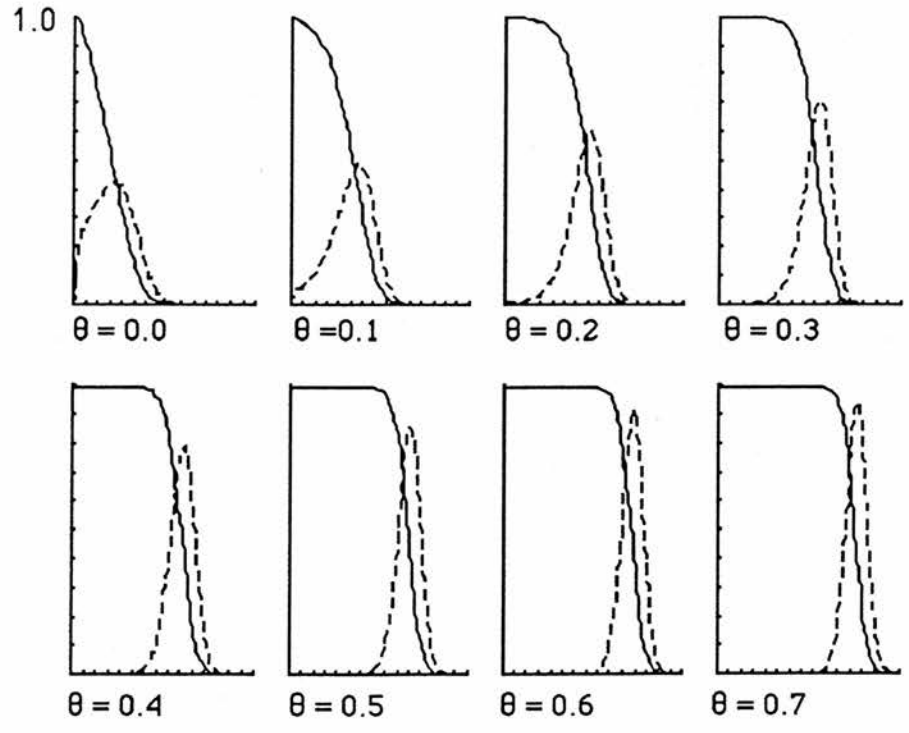

Fig 4.13.6 Relative intensity v x, for n = 28, ω= 0.5. max x = 0.15

absorbed. These graphs were based on those in figure 11 which show the fraction of energy left in the wave at the second cutoff. The results from figure 11 were used to determine which sets of parameters should be plotted in figure 13.

Again the graphs show that for the lower values of ω most of the energy gets through the evanescent layer. In addition all this energy is absorbed in the plasma for $n \geq 26$, while most of the energy is absorbed for $n = 24$.

The position of the maxima of the dashed curves show where most energy is absorbed. This position can be changed by adjusting the parameters. One thing which may affect the choice of parameters is the width of the area energy is absorbed over.

CHAPTER 5 FURTHER DEVELOPMENTS

There are two ways that the work in chapter 4 could be taken further. The first is to refine the model, for example by changing to cylindrical polar coordinates, or introducing changes in the way some variables are handled. For example, it would be good to introduce a temperature profile instead of assuming a constant temperature, since the temperature near the edge is less than at the centre for RFPs, which would probably change the position where the wave is absorbed; and to introduce the effects of pressure.

Less major changes would include investigating changes in the magnitude and profile of the magnetic field and the density. One of the major characteristics of RFPs is that there are large (~ 2%) fluctuations in the magnetic field, and these could also be significant.

Another change in the way the program operates would be to use a spectrum of wave numbers in the y-z plane, instead of only considering a monochromatic wave. This is discussed in section 5.1.

The second way forward is to solve Maxwell's equations directly in two regions. The first region is the vacuum at the edge of the plasma, which can be treated in a straightforward way; while the second region is the plasma itself. The presence of the plasma means that Maxwell's equations have to be modified. This is potentially very complicated, but section 5.2 gives a method for reducing the full Maxwell equations in the plasma to a set of coupled ordinary differential equations, and suggests how this work could be carried on.

SECTION 5.1 THE WAVE SPECTRUM

The previous chapter looked at the behaviour of whistler waves in a reversed field pinch. It was assumed that the waves could be generated with parameters such that they would be absorbed in the wave, but no account was taken of the wave spectrum.

One way to produce a spectrum of waves is to consider an antenna consisting of N parallel conductors, each of width 2w, separated by a distance s -2w, see figure 1. The current in each is assumed to be uniform across and along the strip, and to oscillate with frequency ω. There is also a constant phase difference ϕ between each strip in the antenna. The wave spectrum in the plane of the antenna is then found by Fourier transforming the antenna in the y-direction, ie along the direction in which the structure is periodic.

The amplitude of the contribution from the mth element is given by

$$A_m \propto e^{im\phi} \int_{ms-w}^{ms+w} e^{ik_{yz}\phi}\, d\phi \qquad (5.1)$$

and so the amplitude due to all N elements is

$$A \propto \sum_{m=0}^{m=N-1} e^{im\phi} \int_{ms-w}^{ms+w} e^{ik_{yz}\phi}\, d\phi \qquad (5.2)$$

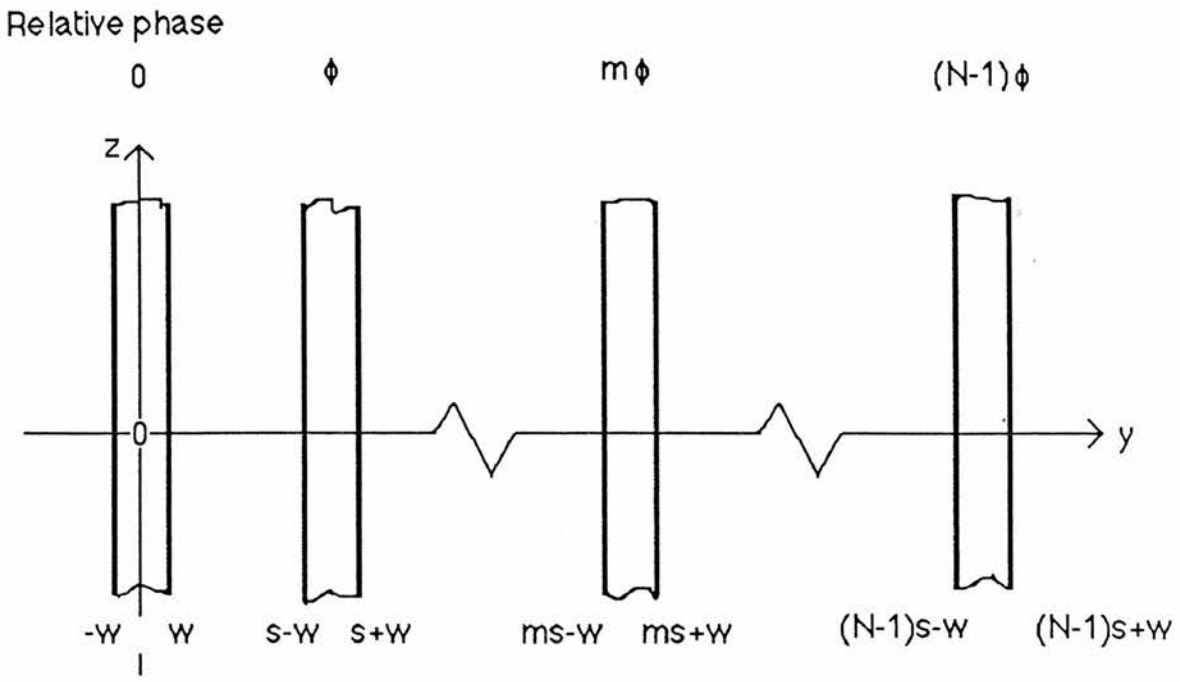

Fig 5.1 Array of N strips of width 2w, separated by a distance s, for use as an antenna to control the wave spectrum.

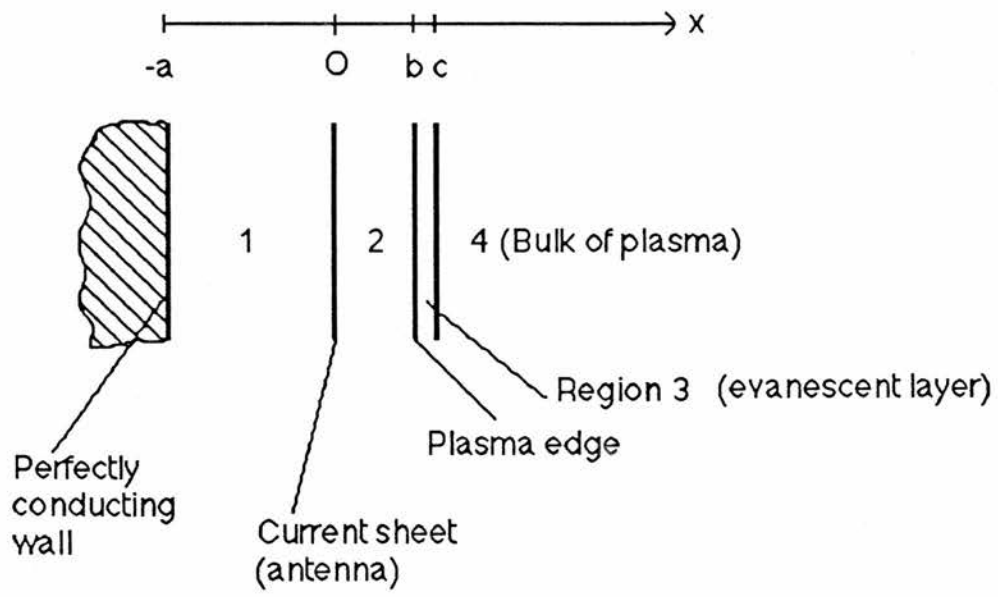

Fig 5.2 Coordinate system for antenna development.

Working out the integral gives

$$\int_{ms - w}^{ms + w} e^{ik_{yz}\phi}\, d\phi = 2\, e^{imsk_{yz}}\, \frac{\sin k_{yz} w}{k_{yz}} \qquad (5.3)$$

which means that

$$A \propto \frac{2w \sin k_{yz} w}{k_{yz} w} \sum_{m=0}^{m=N-1} e^{im(\phi + sk_{yz})} \qquad (5.4)$$

The summation in equation (4) is the sum to N terms of a geometric series, so finally

$$A \propto \frac{2w \sin k_{yz} w}{k_{yz} w} \frac{1 - e^{iN(\phi + sk_{yz})}}{1 - e^{i(\phi + sk_{yz})}} \qquad (5.5)$$

The intensity of the wave spectrum is the square of the amplitude, so

$$I \propto \frac{4 w^2 \sin^2 k_{yz} w}{w^2 k_{yz}^2} \frac{\sin^2 N\left(\frac{\phi + sk_{yz}}{2}\right)}{\sin^2\left(\frac{\phi + sk_{yz}}{2}\right)} \qquad (5.6)$$

This has the same form as the intensity of light falling on a screen after

passing through a diffraction grating. Treating the intensity as a function of k_{yz} means that the k_{yz} spectrum can be controlled by changing the phase difference between each element. More control is possible the higher the number of strips there are.

In terms of chapter 4 this means that the k-spectrum is fixed in the y-z plane by the width of the strips, their spacing and phasing, while the propagation properties perpendicular to this plane are fixed by the frequency at which the current oscillates.

In the frequency range considered in the previous chapter, 0.5 - 3.5 G rad s^{-1}, the vacuum wavelength of the waves varies from 54 cm to 3.77m. However, because the wavenumber perpendicular to the direction of propagation has to have values greater than 20 to absorb the wave, the wavelength in the plasma is reduced to a few centimeters even at the lower frequencies. This means that it is feasible to launch whistler waves using the strip antenna system described above.x

One way to generalise this result would be to consider the wave spectrum produced by a 2-D array of rectangles, which would involve Fourier transforming in two directions instead of one, and possibly calculating the self-consistent current distribution in each element.

There is a considerable literature describing various methods for calculating the behaviour of different kinds of antennae and how they couple to plasmas for ion cyclotron, lower hybrid and electron cyclotron waves. This would provide a good starting place for further work.

5.2 SOLUTION OF MAXWELL'S EQUATIONS IN PLASMA AS A SET OF COUPLED ODES.

Figure 2 shows how an antenna and a toroidal confinement system can be modelled in slab geometry. (See for example Adam's paper.) The wall of the torus is assumed to be perfectly conducting, and is situated at x=-a. Moving towards the centre regions 1 and 2 are assumed to be vacua separated by the antenna at x=0. The antenna itself is assumed to be a current sheet. The plasma edge is at x=b. Region 3 is the evanescent layer at the edge of the plasma. The wave can propagate in the plasma for x≥c, so region 4 is the bulk of the plasma.

To proceed transform Maxwell's equations by changing the variables from **E** and **B** to

$$\mathbf{L} = k_0 \mathbf{E} \quad \text{and} \quad \mathbf{P} = \omega \mathbf{B} \tag{5.7}$$

to get

$$\nabla \times \mathbf{L} = i\, k_0 \mathbf{P} \quad \text{and} \quad \nabla \times \mathbf{P} = -i k_0\, \underline{\varepsilon} \cdot \mathbf{L} \tag{5.8}$$

$$\underline{\varepsilon} = \begin{bmatrix} 1-a & iaY_z & -iaY_y \\ -iaY_z & 1-a(1-Y_y^2) & aY_yY_z \\ iaY_y & aY_yY_z & 1-a(1-Y_z^2) \end{bmatrix} \tag{5.9}$$

$\underline{\varepsilon}$ is the cold plasma dielectric tensor in the case when $\mathbf{B} = (0, B_y, B_z)$. The Y_is are the electron cyclotron frequency for the corresponding components of $\underline{\mathbf{B}}$.

$a = X / (1-Y_y^2 - Y_z^2)$, where X is the square of the plasma frequency divided by the square of the applied frequency. [Also let $Y^2 = Y_y^2 + Y_z^2$.]

Now, if ∇ can be replaced by $(d/dx, i k_y, i k_z)$ this gives

$$ik_yP_z - ik_zP_y = -ik_0 \left[(1-a)L_x + i aY_zL_y - iaY_yL_z \right] \quad (5.10.1)$$

$$ik_zP_x - dP_z/dx = -ik_0 \left[- iaY_zL_x + (1-a(1-Y_y^2)) + aY_yY_z L_z \right] \quad (5.10.2)$$

$$dP_y/dx - ik_yP_x = -ik_0 \left[iaY_yL_x + aY_yY_z L_y + (1-a(1-Y_z^2)) \right] \quad (5.10.3)$$

$$ik_yL_z - ik_zL_y = ik_0 P_x \quad (5.11.1)$$

$$ik_zL_x - dL_z/dx = ik_0 P_y \quad (5.11.2)$$

$$dL_y/dx - ik_yL_x = ik_0 P_z \quad (5.11.3)$$

Solving the set of simultaneous equations 10.1 - 11.3 gives

$$P_x = (k_yL_z - k_zL_y) / k_0 \quad (5.12.1)$$

$$L_x = (k_zP_y - k_yP_z - iaY_zk_0L_y + iaY_yk_0L_z) \quad (5.12.2)$$

and the matrix equation

$$d\,\mathbf{A} / dx = \underline{\mathbf{d}} \,.\, \mathbf{A} \quad (5.12.3)$$

with $\mathbf{A} = (Ly, Pz, Lz, Py)$ (5.13)

and equation (14) for $\underline{\mathbf{d}}$ and equation (15) giving expressions for some of the matrix compoments of $\underline{\mathbf{d}}$:-

$$\underline{\mathbf{d}} = \begin{bmatrix} -iak_0k_yY_z & (k_0^2\,(1-a) - k_y^2) & iak_0k_yY_y & k_yk_z \\ d_{2,1} & iak_0k_yY_z & d_{2,3} & -iak_0k_zY_z \\ -iak_0k_z & k_yk_z & iak_0k_zY_y & (k_z^2 - k_0^2\,(1-a)) \\ d_{4,1} & iak_0k_yY_y & d_{4,3} & -iak_0k_zY_y \end{bmatrix} \qquad (5.14)$$

where
$$d_{2,1} = (1-a)\,[\,k_0^2\,(1-a\,(1-Y_y^2)) - k_z^2\,] - a^2\,k_0^2\,Y_z^2 \qquad (5.15)$$

$$d_{2,3} = (1-a)\,(\,k_yk_z + a\,k_0^2\,Y_y\,Y_z\,) + a^2\,k_0^2\,Y_y\,Y_z$$

$$d_{4,1} = -[\,(1-a)\,(\,k_yk_z + a\,k_0^2\,Y_y\,Y_z\,) + a^2\,k_0^2\,Y_y\,Y_z\,]$$

$$d_{4,3} = (1-a)\,[\;k_y^2 - k_0^2\,(1-a\,(1-Y_z^2))\,] + a^2\,k_0^2\,Y_z^2$$

In the plasma equation (13) has to be solved numerically. This can be done by using NAG routines which provide the solutions of ordinary differential equations, which involves splitting the equation into its real and imaginary parts.

One way to check that the encoding has been done correctly is to solve the equations in the case of a current sheet in a vacuum. The system is assumed to be infinite in the y- and z-directions and only to vary in the x-direction. In this case with an infinite current sheet and assuming that the boundary conditions are given by perfectly conducting walls the solution is known to be that the normal components of the electric field are zero at the wall, while the x-component falls to zero. The normal component of the magnetic field is zero at the walls and the other two components are arbitrary.

The solution in the presence of the plasma probably has to be divided up

into four regions illustrated in figure 2. In region 1 the fields should behave as decribed in the previous paragraph. In the region between the current sheet and the plasma there will be a mixture of incoming and reflected waves. In the evanescent layer, region 3, there will again be an incoming and a reflected wave. To deal with the bulk of the plasma, region 4, the first approximation would be assume that the wave is absorbed or propagates to infinity, before considering the more complicated case in which energy would be reflected from cutoffs in the plasma.

APPENDIX PROGRAM CUTOFFS

A.1 PRINT OUT OF PROGRAM CUTOFFS

The following long program, CUTOFFS, is the main program used to produce the results discussed in this thesis. CUTOFFS is the name of the file containing the entire program and also the name of the main program within the file. The rest of the program is written as several subroutines and functions which can be called by changing the main part of the program within do loops 1-3. These do loops are important because they give the values of n (called nz in this program), ω (called EXFREQ) and θ_0 (called TWIST).

The most fundamental part of the program is the function NXP2. This function calculates X and Y and from them the dielectic tensor elements. NXP2 is basic to the operation of the program and is called by many of the subroutines.

```
      PROGRAM CUTOFFS
C  Changed values of tworpi, cdevel and magsize 14/1/88.
C  PROGram calculates the intensity of a wave at xpCUT2
       IMPLICIT NONE
       DOUBLE PRECISION XPOS,XINC,NINC,NZMIN,NZMAX,NZINC,MINFRQ,
      1MAXFRQ,INCFRQ,MINTWT,MAXTWT,INCTWT,NZ,EXFREQ,TWIST,YTEST,
      2XPCUT1,XPCUT2,NXP2,XMAX,RADIUS,DUMMY1,DUMMY2,DELKX,
      3DELNX,TWORPI,DEVEL,U0,NX2,INTENS
       WRITE(6,1001)
 1001 FORMAT(' ENTER XPOS AS F6.3 AND NO INCREMENTS AS F7.1',/,
      1' XX.XXX YYYY.Y')
       read(5,1002) XMAX,NINC
 1002 FORMAT(F6.3,F7.1)
       read(7,1003) NZMIN,NZMAX,NZINC,MINFRQ,MAXFRQ,INCFRQ,MINTWT,
      1MAXTWT,INCTWT
 1003 FORMAT(3F7.3,/,3F7.3,/,2f7.3,f7.3)
```

```
      WRITE(5,1111) NZMIN,NZMAX,NZINC,MINFRQ,MAXFRQ,INCFRQ,MINTWT,
     1MAXTWT,INCTWT
 1111 FORMAT(3F6.2,/,3F6.2,/,2f6.2,f7.3)
      RADIUS=0.26D0
      IF (XMAX.EQ.RADIUS) THEN
       XMAX=XMAX-1.0D-5*RADIUS
      END IF
      WRITE(10,999) NINC,XMAX
 999  FORMAT(' PROGRAM CUTOFFS    B0=0.15T   NINC=',F8.1,'  XMAX='
     1,F8.4)
      WRITE(10,997)
 997  FORMAT(6X,'NZ  EXFREQ   TWIST',9X,'XPCUT1',9X,'XPCUT2')
c    1,12x,'MAX',9X,'INTENS')
      DO 1 NZ=NZMIN,NZMAX,NZINC
      DO 2 EXFREQ=MINFRQ,MAXFRQ,INCFRQ
      DO 3 TWIST=MINTWT,MAXTWT,INCTWT

c      CALL CUTOFF(NZ,EXFREQ,TWIST,XMAX,XPCUT1,XPCUT2)
c      caLL ABSORB(NZ,EXFREQ,TWIST,NINC,XPCUT1,XPCUT2,INTENS)
C      CALL ABSOUT(NZ,EXFREQ,TWIST,XMAX,NINC)
C      CALL CUTOUT(NZ,EXFREQ,TWIST,XMAX)
       CALL REFRAC(NZ,EXFREQ,TWIST,XMAX)
C      CALL TRIAL(NZ,EXFREQ,TWIST,XMAX,NINC)

 3    CONTINUE
 2    CONTINUE
 1    CONTINUE
      STOP
      END


      FUNCTION NXP2(NZ,EXFREQ,TWIST,XPOS,YTEST,DELKX,
                                                NXM2,U0,A2M4B)
      IMPLICIT NONE
C     CALCULATE THE BASIC QUANTITIES
      DOUBLE PRECISION NXP2,NZ,EXFREQ,TWIST,XPOS,XMAX,XINC,X,Y,
     1ANGLE,BETA,COS2,SIN2,A,B,EXY2,EPERP,EPAR,
     2 A2M4B,S17AEF,S17AFF,J0Z,J1W,XCONST,YCONST,bfield,RADIUS,M,
     3 ARG,YTEST,DELKX,TWORPI,CDEVEL,U0,DEPAR,DELNX,NXM2,magsize
C magsize is a factor to multiply the basic magnetic field strength
C of 0.3T.   Ie bfield=magsize*0.3T*(form factor)

      M=1D0
      RADIUS=0.26D0
      tworpi=2.5066283d0
      magsize=1.0D0
C     CDEVEL = c/(sqrt(2) * Vth)
C     m*Vth**2 = kT = 100eV
       cdevel=71.537d0
```

```
C    YCONST=e*B0/(Me*1E9*EXFREQ)
C    B0=0.3T  e=1.6E-19  Me=9.11E-31  PERM=8.85E-12
C    RHOMAX=3E19  TWORPI=SQRT(2*PI)
     CDEVEL=C/(VTHERMAL*SQRT(2))
C    VTHERMAL=ELECTRON VELOCITY= 100 eV
C    XCONST=N0*E*E/(PERM*ME*(EXFREQ*1E9*RADIUS)**2)
     YCONST=magsize*52.689352D0/EXFREQ
     XCONST=95257.586D0/(RADIUS*RADIUS*EXFREQ*EXFREQ)
     ARG=1.0D0-XPOS/RADIUS
     J0Z=S17AEF((3.8*ARG),M)
     J1W=S17AFF((2.4*ARG),M)
     bfield=DSQRT(J0Z*J0Z+J1W*J1W)
     ANGLE=DATAN(J0Z/J1W)
     Y=bfield*YCONST
     X=XCONST*XPOS*(2.0D0*RADIUS-XPOS)
     BETA=ANGLE-TWIST
     YTEST=Y*DCOS(BETA)
     SIN2=(NZ*DSIN(BETA))**2.0D0
     COS2=(NZ*DCOS(BETA))**2.0D0
     EPAR=1.0D0-X
     EPERP=1.0D0-X/(1.0D0-Y*Y)
     EXY2=(X*Y/(1.0D0-Y*Y))**2.0D0
     A=((EPERP-COS2)*(EPERP+EPAR)-EXY2)/EPERP
     B=((EPERP-COS2)**2.0D0-EXY2)*EPAR/EPERP
     A2M4B=A*A-4.0D0*B
     IF (A2M4B.GE.0.0D0) THEN
      NXP2=0.5D0*A-SIN2+0.5D0*DSQRT(A2M4B)
      NXM2=NXP2-DSQRT(A2M4B)
     ELSE
      NXP2=-1.0D0
      NXM2=-1.0D0
     END IF

      CALCULATION OF delKx
      IF (NXP2.GE.0.0) THEN
       U0=CDEVEL/(NZ*DCOS(BETA))
       DEPAR=X*TWORPI*U0*U0*U0*DEXP(-1.0D0*U0*U0)
       DELNX=DEPAR*((EPERP-COS2)*(NXP2+NZ*NZ-EPERP)+EXY2)/
    1  (2.0D0*EPERP*DSQRT(NXP2)*(2.0D0*NXP2-A+2.0D0*SIN2))
       DELKX=DELNX*3.335557D0*EXFREQ
      ELSE
       U0=-1.0D0
       DELKX=-1.0D0
     END IF

      return
     END
```

```
      SUBROUTINE CUTOFF(NZ,EXFREQ,TWIST,XMAX,XPCUT1,XPCUT2)
C     Calculates the value of the CUTOFFs INDEPENDENTLY of ninc.
      IMPLICIT NONE
C     CALCULATES THE CUTOFFS
      DOUBLE PRECISION NZ,EXFREQ,TWIST,XMAX,XPCUT1,XPCUT2,
     1MAX,XPOS,XINC,PREV,NX2,NXP2,EST2,YTEST,DELKX,XMIN,NXM2,U0,
     2CUT,A2M4B

C     CALCULATION OF XPCUT1
      MAX=6.5D-3
CCCCC Change the value of XINC from 10-5 to 10-6
      XINC=1.0D-6
C  nx*nx=1-nz*nz at x=0, but when nz=0 prev=0
      PREV=1.0d0-nz*nz
      XPCUT1=-1.0D0
      DO 200 XPOS=0.0,MAX,XINC
       NX2=NXP2(NZ,EXFREQ,TWIST,XPOS,YTEST,DELKX,NXM2,U0,A2M4B)
       IF ((PREV.LE.0.0).AND.(NX2.GT.0.0)) THEN
        XPCUT1=XPOS
        GO TO 201
       ELSE
        PREV=NX2
       END IF
  200  CONTINUE
  201  CONTINUE
      IF (XPCUT1.le.0.0D0) THEN
       XPCUT2=-1.0D0
       RETURN
      END IF

C     New method to estimate xpCUT2, independent of ninc.
      XINC=(XMAX-XPCUT1)/1.0D2
C  Changed 15/1/88.  Accounts for case when xpcut1=0
      DO 202 XPOS=(XPCUT1+xinc),XMAX,XINC
C     Take the previous value of xpos
       CUT=XPOS-XINC
       NX2=NXP2(NZ,EXFREQ,TWIST,XPOS,YTEST,DELKX,NXM2,U0,A2M4B)
       IF ((A2M4B.LE.0.0D0).OR.(NX2.LT.0.0D0)) THEN
        GO TO 203
       END IF
  202  CONTINUE
  203  CONTINUE

      IF (CUT.GT.(XMAX-1.5D0*XINC)) THEN
C      ie reached end of region considered, so xpCUT2= this value
       XPCUT2=CUT
      ELSE
C      estimate xpCUT2 more accurately
       MAX=CUT+XINC
```

```
      XINC=XINC/1.0D3
      DO 204 XPOS=CUT,MAX,XINC
       XPCUT2=XPOS-XINC
       NX2=NXP2(NZ,EXFREQ,TWIST,XPOS,YTEST,DELKX,NXM2,U0,A2M4B)
       IF ((A2M4B.LE.0.0D0).OR.(NX2.LT.0.0D0)) THEN
       RETURN
      END IF
204   CONTINUE
     END IF

     END


     SUBROUTINE CUTOUT(NZ,EXFREQ,TWIST,XMAX)
C     This SUBROUTINE only WRITEs out the values of the CUTOFFs.
     IMPLICIT NONE
     DOUBLE PRECISION NZ,EXFREQ,TWIST,XMAX,NINC,XPCUT1,XPCUT2
     CALL CUTOFF(NZ,EXFREQ,TWIST,XMAX,XPCUT1,XPCUT2)
     WRITE(10,4000) NZ,EXFREQ,TWIST,XPCUT1,XPCUT2
4000 FORMAT(3F8.2,2F15.6)
     END


     SUBROUTINE
ABSORB(NZ,EXFREQ,TWIST,NINC,XPCUT1,XPCUT2,INTENS)
C     CALCULATES THE AMOUNT OF ABSORPTION BETWEEN CUTOFFS
     IMPLICIT NONE
     DOUBLE PRECISION NZ,EXFREQ,TWIST,NINC,XPCUT1,XPCUT2,XPOS,
    1XINC,NXP2,NX2,YTEST,DELKX,SUM,PREV,INTENS,DEPOST,NXM2,U0,
    2WEEMIN,WEEMAX,WEEINC,WEEXPS,MAX,PREVII,A2M4B,REDUCE,M,N
    3,THIRD,LAMBDA,LTHIRD,BIZERO,BIX1,S17AHF,NEXTX,ZERO,ONE,
    4R75,R50,R25,N75,N50,N25,U075,U050,U025,X75,X50,X25,NX
    5,u0atmax,prevdepost,xdepost,idepost
C     DEPOST IS THE ENERGY DEPOSITED BY THE WAVE IN AN INTERVAL

C     If XPCUT1 is less than ZERO DO not procede.
     IF (XPCUT1.LE.0.0D0) THEN
      RETURN
     END IF

C.....C
C     Now calculate the reduction in intensity in evanescent region.
C     Solving Airy's equn. in terms of xi = lthird*(x-x1).  When
C     x=0, xi=-x1*lthird; but this gives evanescent region on the
C     right, so for Bi(0) the arg. is -xi.   At x=x1, xi=0 exactly.

     ZERO=0.0D0
     ONE=1.0D0
     M=1D0
```

```
      THIRD=1.0D0/3.0D0
      LTHIRD=(LAMBDA(NZ,EXFREQ,TWIST))**THIRD
      BIZERO=S17AHF((LTHIRD*XPCUT1),M)
      BIX1=S17AHF(0.0D0,M)
      REDUCE=(BIX1/BIZERO)**2.0D0
c     Rate at which energy deposited between 0 and xpcut1
      R75=0.75D0*REDUCE
      R50=0.5D0*REDUCE
      R25=0.25D0*REDUCE
C Ie points at which intensity in plasma falls below f*REDUCE
C     write(10,3001) ZERO,ONE,ZERO,XPCUT1,REDUCE,ZERO
C3001 FORMAT(3F20.6,/,3F20.6)
C.....C

      XINC=(XPCUT2-XPCUT1)/1.0D2
      WEEINC=XINC/NINC
C     See energy.for for the change in the next IINE.
      MAX=(XPCUT2-XINC)+0.5D0*WEEINC
C     Makes sure point XPCUT2 is included, but points beyond excluded.
      X75=ZERO
      X50=ZERO
      X25=ZERO
      U075=ZERO
      U050=ZERO
      U025=ZERO
      N75=ZERO
      N50=ZERO
      N25=ZERO
      PREVII=REDUCE

C     Set up initial conditions for trapezium rule.

     NX2=NXP2(NZ,EXFREQ,TWIST,XPCUT1,YTEST,DELKX,NXM2,U0,A2M4B)
      SUM=-1.0D0*DELKX
      PREV=0.0D0

c This value of n is the one used in the FORMula x=x1+n*XINC
      N=-1D0
      prevdepost=0.0d0
      xdepost=0.0d0
      u0atmax=0.0d0
      idepost=0.0d0
      DO 300 XPOS=XPCUT1,MAX,XINC
       N=N+1D0
       WEEMIN=XPOS
       WEEMAX=XPOS+XINC+0.1D0*WEEINC
C      Again makes sure that xpos+XINC is included.
       IF (WEEMAX.GT.XPCUT2) THEN
C       Imaginary square root.
```

```
      GO TO 300
     END IF

     DO 301 WEEXPS=WEEMIN,WEEMAX,WEEINC

NX2=NXP2(NZ,EXFREQ,TWIST,WEEXPS,YTEST,DELKX,NXM2,U0,A2M4B)
C      Trapezium Rule
      SUM=SUM+PREV+DELKX
      PREV=DELKX
      INTENS=REDUCE*DEXP(SUM*WEEINC)
 301   CONTINUE

C.....C
C   Points where intensity falls below 75%, 50%, 25% with
C   associated parameters.
     IF ((PREVII.GT.R75).AND.(INTENS.LE.R75)) THEN
      X75=NEXTX
      N75=N
      U075=U0
     ELSE IF ((PREVII.GT.R50).AND.(INTENS.LE.R50)) THEN
      X50=NEXTX
      N50=N
      U050=U0
     ELSE IF ((PREVII.GT.R25).AND.(INTENS.LE.R25)) THEN
      X25=NEXTX
      N25=N
      U025=U0
     END IF
C.....C

CCCCCCCCCC Changed d-6 to d-4.  This might produce results more
CCCCCCCCCC quickly.
     IF (INTENS.LT.1.0D-4) THEN
      GO TO 333
     ELSE
c  DEPOST is the amount of energy in an interval per unit length
c  and in fact is the derivitive of the intensity.
      depost=2.0D-2*(previi-intens)/XINC
c      DEPOST=1.0D-2*(PREVII-INTENS)/XINC
      PREVII=INTENS
c  Plot results at end of interval not at the beginning.
      NEXTX=XPOS+XINC
       if (depost.gt.prevdepost) then
        prevdepost=depost
        u0atmax=u0
        xdepost=nextx
        idepost=intens
        nx=dsqrt(nx2)
       end if
```

```
C      write(10,3000) N,NEXTX,INTENS,DEPOST
C      write(10,3000) NEXTX,INTENS,DEPOST
C3000  FORMAT(4F20.6)
       END IF

 300  CONTINUE

 333  CONTINUE
c     write(10,2345) NZ,EXFREQ,TWIST,X75,X50,X25,N75,N50,N25,
c    1            U075,U050,U025
c2345 FORMAT(3F8.2,3F10.6,3F8.2,3F10.4)
C     write(10,2346) nz,exfreq,twist,xdepost,idepost,prevdepost,
C    1u0atmax,intens
C     write(10,2346) nz,exfreq,twist,xdepost,intens
C2346 FORMat(3f7.3,5f11.6)

C  Print out intensity at x1 and x2, or max x to show how changes overall.
       write(10,3003) NZ,exfreq,twist,xpcut1,REDUCE,xpcut2,xpos,
     1  intens
 3003  FORMat(3f6.2,5f10.6)

      END


      SUBROUTINE ABSOUT(NZ,EXFREQ,TWIST,XMAX,NINC)
      IMPLICIT NONE
C     This SUBROUTINE prints out the contents of SUBROUTINE absorb.
      DOUBLE PRECISION
NZ,EXFREQ,TWIST,XMAX,NINC,XPCUT1,XPCUT2,TEMP
     1,INTENS
      CALL CUTOFF(NZ,EXFREQ,TWIST,XMAX,XPCUT1,XPCUT2)
      IF (XPCUT1.LT.0.0D0) THEN
       RETURN
      ELSE
       write(10,5002) NZ,EXFREQ,TWIST,XPCUT1,XPCUT2,XMAX,NINC
 5002  FORMAT(' NZ',5X,F13.2,/,' EXFREQ ',F13.2,/,' TWIST  ',F13.2,/,
     1 ' XPCUT1 ',F13.6,/,' XPCUT2 ',F13.6,/,' XMAX   ',F13.6,/,
     2 ' NINC   ',F13.1)
       CALL ABSORB(NZ,EXFREQ,TWIST,NINC,XPCUT1,XPCUT2,INTENS)
       TEMP=-1.0D0
       write(10,5003) TEMP
 5003  FORMAT(F20.6)
      END IF
      END


      FUNCTION LAMBDA(NZ,EXFREQ,TWIST)
C     Calculates lambda:-  kx2=lambda*(x-xpcut1) near xpcut1.
      IMPLICIT NONE
```

```
      DOUBLE PRECISION NZ,EXFREQ,TWIST,LAMBDA,M,J0Z,J1W,S17AEF,
     1S17AFF,ANGLE,NPAR02,XCONST,YCONST,ARG,Y2,magsize
C.....C
C  Analytic expression for the gradient at x=0
      M=1D0
      magsize=1.0D0
      YCONST=magsize*2.7761679D3/(EXFREQ*EXFREQ)
C     YCONST= (e*B0/m*1e9)**2, B=0.3T, freqency in GHz.
      XCONST=1.4091359D6/(EXFREQ*EXFREQ)
C     XCONST=n0*e*e/(epsilon0*m*R*R*1e18)    n0=3e19
      ARG=1.0D0-0.0D0/0.26D0
      J0Z=S17AEF((3.8D0*ARG),M)
      J1W=S17AFF((2.4D0*ARG),M)
      ANGLE=DATAN(J0Z/J1W)
      NPAR02=(NZ*DCOS(ANGLE-TWIST))**2.0D0
      Y2=YCONST*(J0Z*J0Z+J1W*J1W)
      LAMBDA=4.076D6*(Y2*(1.0D0-NPAR02)-2.0D0-
     1Y2*DSQRT((NPAR02-1.0D0)**2.0D0+4.0D0*NPAR02/Y2))/(1.0D0-Y2)
C     4.076d0=(n0*e*e/epsilon0*m*w*w*R)*(w*w/c*c)   Lambda is
C     d(kx2)/dx and the w*w/c*c converts d(nx2)/dx to this.  See
C     notes.
C NB NB NB   Lambda is the gradient of kx2.
C.....C
      RETURN
      END


      SUBROUTINE REFRAC(NZ,EXFREQ,TWIST,XMAX)
C     Prints out values of nx2.
      IMPLICIT NONE
      DOUBLE PRECISION
NZ,EXFREQ,TWIST,XMAX,NXP2,XPOS,YTEST,DELKX,
     1NXM2,U0,A2M4B,XINC,NX2,XPCUT1,XPCUT2,NINC,TEMP

      XPCUT1=0.0D0
      XPCUT2=1.0D0
      NINC=1.0D0
      write(10,6000) NZ,EXFREQ,TWIST,XPCUT1,XPCUT2,XMAX,NINC
 6000 FORMAT(' NZ',5X,F13.2,/,' EXFREQ ',F13.2,/,' TWIST  ',F13.2,/,
     1' XPCUT1 ',F13.6,/,' XPCUT2 ',F13.6,/,' XMAX   ',F13.6,/,
     2' NINC   ',F13.1)
      XINC=XMAX/100.0D0
      TEMP=-1.0D0
      DO 600 XPOS=0.0D0,XMAX,XINC
       NX2=NXP2(NZ,EXFREQ,TWIST,XPOS,YTEST,DELKX,NXM2,U0,A2M4B)
       IF (NX2.NE.-1.0D0) THEN
        write(10,6001) XPOS,NX2,NXM2
 6001   FORMAT(3F20.6)
       ELSE
```

```
      GO TO 6003
     END IF
600  CONTINUE
6003 CONTINUE
     write(10,6002) TEMP
6002  FORMAT(F20.6)

    RETURN
    END


    SUBROUTINE TRIAL(NZ,EXFREQ,TWIST,XMAX,NINC)
    IMPLICIT NONE
C     This SUBROUTINE prints out the contents of SUBROUTINE absorb.
    DOUBLE PRECISION
NZ,EXFREQ,TWIST,XMAX,NINC,XPCUT1,XPCUT2,TEMP
   1,INTENS
    CALL CUTOFF(NZ,EXFREQ,TWIST,XMAX,XPCUT1,XPCUT2)
    IF (XPCUT1.LT.0.0D0) THEN
     RETURN
    ELSE
     CALL ABSORB(NZ,EXFREQ,TWIST,NINC,XPCUT1,XPCUT2,INTENS)
    END IF
    END
```

A.2 COMMENTS ABOUT PROGRAM CUTOFFS

A.2.1 The Main Program

The main part of the program is straighforward. It reads in the range and the step size of the parameters to be investigated: the value of the component of the refractive index vector in the plane of the magnetic field, called NZ; the angular frequency of the wave ω, measured in units of G rad s^{-1}, which is the variable EXFREQ; and lastly the range which the angle the refractive index vector makes with the magnetic field at the edge of the plasma; this corresponds to θ_0 in chapter 4, and is called TWIST in the program.

At this stage the distance the wave propagation will be followed into the plasma, XMAX, is also input, along with the number of increments to be used in other parts of the program, NINC.

The main part of the program is then contained in three do-loops, controlled by the values of NZ, EXFREQ and TWIST. Various subroutines are called within these do-loops depending on the information required.

A.2.2 Function NXP2

This function is the calculational heart of the program, since it calculates the values of the two branches of the square of the refractive index in the x-direction in slab geometry, as given in equation (4.3).

As explained in chapter 4 the plasma density varies in the x-direction and the magnetic field is in the y-z plane. The magnetic field components are found using NAG routines S17AEF and S17AFF to calculate the values of the

J_0 and J_0 Bessel functions. The factors 3.8 and 2.4 in the Bessel function arguments make them a better fit to published data on the magnetic fields.

The last section of the function calculates the imaginary part of the propagation vector, so that it can be used to calculate the amount of damping.

A.2.3 Subroutine CUTOFF

This subroutine uses information on the value of NXP2 and the point where the two branches of the refractive index coincide to calculate the point where n_x^2 changes from negative to positive and the wave can propagate in the plasma. This value is called XPCUT1. It is usually small and determines the width of the evanescent layer. If the value of XPCUT1 is too large the program stops at this point.

If the two branches of the refractive index are not coincident when the maximum distance into the plasma is reached this is the value given to the variable XPCUT2. If the two branches are concident before this point the last incremental step in the x-direction is subdivided into one thousand substeps and the value of XPCUT2 is then calculated.

The subsiduary subroutine CUTOUT prints out the values of XPCUT1 and XPCUT2 along with the values of NZ, EXFREQ and TWIST.

A.2.4 Function LAMBDA

At the edge of the plasma the upper branch of n_x^2 changes very rapidly from being negative to positive, so it is possible to approximate n_x^2 as a straight

line in this region. The slope of this line can be found at x = 0 and converted to give the slope of k_x^2 at this point, which is then called λ, LAMBDA. (See equation (4.12).) This value of LAMBDA is then used in Airy's equation in subroutine ABSORB to calculate the attenuation.

A.2.5 Subroutine ABSORB

As the name suggests this subroutine calculates the amount of absorption of the wave in the plasma.

First it uses the value XPCUT1 previously established to see if the evansecent region is too large to continue. If it is not it calculates the amount of energy which tunnels through by solving Airy's equation, with I given by the function LAMBDA. The amount of energy tunnelling through is given by the square of the ratio of the Bi Airy function at XPCUT1 to that of the Bi function at the edge of the plasma, assuming that the wave intensity is normalised to 1 at the edge of the plasma.

It then uses the trapezium rule and the value of δk_x calculated by CUTOFF to calculate the amount of absorption. The interval between XPCUT1 and XPCUT2 is divided into 100 intervals, each of which can be further subdivided into NINC further subintervals.

Subroutine ABSOUT is used to group subroutines CUTOFF and ABSORB and then to print out the results, so that only one subroutine needs to be called in the main program. Subroutine TRIAL also has this function.

Subroutine REFRAC is used to print out the values of the two branches of the square of the refractive index if this is required.

BIBLIOGRAPHY

Abramowitz M. & I.A. Stegun Handbook of Mathematical Functions. Dover Publications, Inc. New York (1972)

Adam J. Chauffage Cyclotronique Impedace d'Antenne en Presence d'un Mecanisme de Forte Absorption. EUR-CEA-FC-1004 (1979)

Ando A. *et al Physical Review Letters* **56**, 2180 (1986) Plasma Current Generation and Sustainment by Electron Cyclotron Waves in the WT-2 Tokamak.

Arfken G. Mathematical Methods for Physicists (2nd ed.) Academic Press, Inc. New York (1970)

Balfour A. & D.H. Marwick Programming in Standard FORTRAN 77. Heinemann Educational Books. London (1979)

Behn R. *et al Plasma Physics and Controlled Fusion* **26**, 173 (1984) Recent Alfven Wave Heating Results on the TCA Tokamak.

Bekefei G. Radiation Processes in Plasmas. John Wiley and Sons, Inc. New York (1966)

Bickerton R.J. *et al Plasma Physics and Controlled Fusion* **28**, 1943 (1986) Confinement and Heating of Plasmas in the JET Tokamak.

Bodin H.A.B. *Nuclear Instruments and Methods* **207**, 1 (1983) Reversed Field Pinches.

Bodin H.A.B. and Newton *Nuclear Fusion* **20**, (1980) Reversed-field- pinch Research.

Bornatici M. *Plasma Physics* **24**, 629 (1982) Theory of Electron Cyclotron Absorption of Magnetised Plasmas.

Bornatici M *et al. Nuclear Fusion* **23**, 1153 (1983) Electron Cyclotron Emission and Absorption in Fusion Plasmas.

Boyd T.J.M. and J.J. Sanderson Plasma Dynamics. Nelson. London (1969)

Brambilla M. *Nuclear Fusion* **16**, 47 (1976) Slow-wave Launching at the Lower Hybrid Frequency using a Phased Waveguide Array.

Budden K.G. The Propagation of Radio Waves. Cambridge University Press. Cambridge (1985)

Cairns R.A. Plasma Physics. Blackie & Son Ltd. Glasgow (1985)

Clemmow P.C. & J.P. Dougherty Electrodyamics of Particles and Plasmas. Addison-Wesley Publishing Company, Inc. Reading (Mass) (1969)

Cowling T.G. Magnetohydrodynamics. Adam Hilger Ltd. Bristol (1976)

Dawson J. *Physics of Fluids* **4**, 869 (1961) On Landau Damping.

Fisch N.J. *Physical Review Letters* **41**, 873 (1978) Confining a Tokamak Plasma with rf-driven Currents.

Fisch N.J. *Reviews of Modern Physics* **59**, 175 (1987) Theory of Current Drive in Plasmas.

Fisch N.J. & A.H. Boozer *Physical Review Letters* **45**, 720 (1980) Creating an Asymmetric Plasma Resisitivity with Waves.

Gill R.D. (ed) Plasma Physics and Nuclear Fusion Research. Academic Press. London (1981)

Golant V.E. *Soviet Physics - Technical Physics* **16**, 1980 (1972) Plasma Penetration near the Lower Hybrid Frequency.

Hasegawa A. *Nuclear Fusion* **20**, 1158 (1980) Toroidal Current Production by Kinetic Alfven Waves.

Hooke W. *Plasma Physics and Controlled Fusion* **26**, 133 (1984) Review of Experiments on Current Drive in Tokamaks by Means of RF Waves.

Jobes F.C. *et al Physical Review Letters* **55**, 1295 (1985) Current Rampup by Lower-Hybrid Waves in the PLT Tokamak.

Lashmore-Davies C.N. *5th International Workshop on Electron Cyclotron Emission and Electron Cyclotron Heating.* San Diego, November 1985, p264. On the Application of Whistler Waves to Toroidal Discharges.

Muskhelishvili N.I. Singular Integral Equations. P. Noordhoff Ltd. Holland (1953)

Robertson S. and p Schmid *Nuclear Fusion* **27**, 267 (1987) Instability of a Reversed Field Pinch Without a Conducting Shell.

Stix T.H. *Physics of Fluids* **3**, 19 (1960) Absorption of Plasma Waves.

Stix T.H. The Theory of Plasma Waves. McGraw-Hill Book Company Inc. New York (1962)

Stix T.H. *Physical Review Letters* **15**, 878 (1965) Radiation and Absorption via Mode Conversion in an Inhomogeneous Collision-free Plasma.

Taylor J.B. *Physical Review Letters* **33**, 1139 (1974) Relaxation of Toroidal Plasma and Generation of Reverse Magnetic Fields.

Taylor J.B. *Reviews of Modern Physics* **58**, 741 (1986) Relaxation and Magnetic Reconnection in Plasmas.

Wesson J. Tokamaks. Clarendon Press. Oxford (1987)

Weynants R.R. *et al.* ICRH Antenna Design and Coupling Optimization Studies. Proceedings of the 2nd Joint Grenoble-Varenna International Symposium (1980)

Whittaker E.T. & G.N. Watson A Course of Modern Analysis, (4th ed.) Cambridge University Press (1927)

Woltjer L. *Proceedings of the National Academy of Sciences* **44**, 489 (1958) A Theorem on Force-free Magnetic Fields.

Wort D.J.H. *Plasma Physics* **13**, 258 (1971) The peristaltic Tokamak.